TURUN YLIOPISTO

Portable X-ray diffraction and clustering method as a tool in mineral exploration

Joonas Rinne

Geologia (kallioperägeologia)
Pro gradu -tutkielma
Laajuus: 30 op

Ohjaajat:
Esa Heilimo
Irmeli Huovinen

18.6.2026
Turku

Pro gradu -tutkielma

Pääaine: Geologia
Tekijä: Joonas Rinne
Otsikko: Portable X-ray diffraction and clustering method as a tool in mineral exploration
Ohjaajat: Esa Heilimo, Irmeli Huovinen
Sivumäärä: 104 sivua + liitteet 8 sivua
Päivämäärä: 18.6.2026

Kaivosteollisuus tarvitsee jatkuvasti uusia malminetsintämenetelmiä, jotka ovat tehokkaampia ja kykeneväisempiä löytämään aiemmin havaitsematta jääneitä esiintymiä perinteisiin menetelmiin verrattuna. Tässä tutkielmassa selvitetään kannettavan röntgendiffraktiolaitteen (pXRD) ja klusteroinnin hyödyllisyyttä malminetsinnässä. Tutkielman aineisto on otettu neljästä kairasydämestä Metsämontun vulkaanisesta massiivisesta sulfidiesiintymästä (VMS), joka sijaitsee Etelä-Suomessa. Esiintymä sisältää hydrotermisesti muuttuneita amfiboliittifasieksen kiviä.

XRD-menetelmä antaa tietoa mineraalien kiderakenteesta. XRD-menetelmä perustuu röntgensäteiden heijastumiseen kiteiden atomitasosta Braggin lain mukaisesti. Kannettava XRD toimii samalla periaatteella kuin laboratoriossa käytettävä XRD, mutta sitä voidaan käyttää kenttäolosuhteissa ja se on halvempi ja vähemmän aikaa vievä kuin perinteinen laboratorio-XRD. Tässä tutkimuksessa käytetyt pXRD-mittaukset tehtiin Geologian tutkimuskeskuksen (GTK) toimesta Olympus Portable Onsite XRD Terra-542 -laitteella.

Tutkimusaineistoa analysoitiin DIFRRAC.EVA ohjelmistolla. Näytteet klusteroitiin ohjelmiston klusterointityökalulla, jonka jälkeen jokaiselle näytteelle tehtiin mineraloginen analyysi. Analyysituloksia verrattiin GTK:n loggausraportin havaintoihin analyysitulosten paikkaansapitävyyden selvittämiseksi.

Tulosten perusteella klusterointimenetelmä pystyy pääosin erottamaan sulfidimineraaleja ja indikaattorimineraaleja sisältävät näytteet sivukivistä. Menetelmä ei kuitenkaan vaikuta kykenevän erottamaan erilaisia muuttumisvyöhykkeitä toisistaan erittäin muuttuneessa ja deformoituneessa esiintymässä, jota tämän tutkimuksen aineisto edustaa. Kannettava röntgendiffraktioanalyysi pystyy havaitsemaan erilaisia mineraaliryhmiä, jotka toimivat indikaattorimineraaleina VMS-esiintymässä, mutta se ei useimmiten pysty määrittämään mineraalien koostumusta mineraaliryhmien sisällä. Ohjelmisto ei myöskään havainnut kordieriittia, joka on tärkeä VMS-esiintymien indikaattorimineraali, kaikissa kordieriittipitoisissa näytteissä. Lähes kaikki loggausraportin mukaan kordieriittia sisältävät näytteet klusteroituivat kuitenkin yhteen, vaikka mineralogisessa analyysissä ei olisi havaittu kordieriittia. Joillakin sulfideja sisältävillä näytteillä oli korkeampi tai piikikäs diffraktogrammitausta, mikä teki näytteen mineralogisesta analyysistä haastavaa.

Kannettavalla XRD- ja klusterointimenetelmällä on selkeä potentiaali kairasydännäytteiden tehokkaaseen ja nopeaan analysointiin malminetsintäprojektien alkuvaiheissa. Vaikka niillä ei ole laboratoriopohjaisten analyysien luotettavuutta ja tarkkuutta, suurten näytemäärien kohdalla pXRD- ja klusterointianalyysiä voidaan hyödyntää määrittämään, mitkä näytteet kannattaa tutkia yksityiskohtaisemmin.

Avainsanat: Metsämonttu, VMS, pXRD, klusterointi, mineraali

Master's thesis

Subject: Geology
Author: Joonas Rinne
Title: Portable X-ray diffraction and clustering method as a tool in mineral exploration
Supervisors: Esa Heilimo, Irmeli Huovinen
Number of pages: 104 pages + appendices 8 pages
Date: 18.6.2026

The mineral exploration industry is in constant need of new exploration methods to make the process more efficient and to find deposits not detected by traditional methods. This study researches the usability of a portable X-ray diffraction (pXRD) and effectiveness of clustering in mineral exploration. The study focuses on samples from four drill cores taken from a volcanogenic massive sulphide (VMS) deposit of Metsämonttu, southwestern Finland. The deposit contains hydrothermally altered amphibolite facies metamorphic rocks.

The XRD method provides information on the crystal structure of minerals. The XRD method is based on the reflection of x-rays at the atomic plane of crystals according to the Bragg's law. Portable XRD is fundamentally same as laboratory based XRD but can be used in field environment and is cheaper and less time consuming than traditional laboratory XRD. The pXRD analyses in this study were made with Olympus Portable Onsite XRD Terra-542 device by Geological survey of Finland (GTK).

The data was analyzed with DIFFRAC.EVA software. The samples were clustered using the software's clustering tool, and then a mineralogical analysis was made for each of the samples. Analysis results were compared with information from the logging report made by GTK to see how well the analysis results match with observations.

It was found out that the clustering method is mostly able to separate samples containing sulphide minerals and indicator minerals from barren samples. However, the method does not seem to be capable of distinguishing various alteration zones from each other on a highly altered and deformed deposit like in this study. Portable XRD analysis can detect various mineral groups that work as indicator minerals for the VMS deposit, but it is mostly unable to determine composition of minerals in the groups. It was also not possible to detect cordierite in all of the samples that contain cordierite, which is important indicator mineral in VMS deposits. However, almost all of the samples containing cordierite according to the logging report were clustered together by the software even if cordierite was not detected in the mineralogical analysis. Some of the samples with sulphides had higher or spiky diffractogram background, which made the sample mineralogical analysis challenging.

The pXRD and clustering methods have clear potential for effective and quick analysis of drill cores in earlier phases of mineral exploration projects. While it lacks the reliability and accuracy of laboratory-based analyses, with large number of samples the pXRD and clustering analysis can be used to determine which samples should be studied in more detail.

Key words: Metsämonttu, VMS, pXRD, clustering, mineral

Table of contents

1 Introduction

There is an increasing need for the exploration and exploitation of mineral deposits, especially for critical minerals. New types of minerals and elements are needed for future technologies including batteries and AI technology. There is a need to find new types of mineral deposits and deposits of constantly decreasing ore grades. This leads to larger exploration areas. Therefore, new methods and tools are needed to make the exploration of minerals more efficient and effective (Koskinen 2018; Sarala et al. 2019; COM 2023). A portable X-ray diffraction (pXRD) tool is one of the potential methods that could be useful in the search for new ore deposits by detecting specific mineral groups that are typical indicators for specific deposit types.

XRD has been researched since 1930 s and has been widely used in analyzing materials that are capable of scattering X-rays, including ore geology (Etter & Dinnebier 2014; Lavina et al. 2014). However, XRD analyses have previously mainly been done with laboratory equipment, which requires laborious sample preparations and sending samples to suitable laboratories. This takes time and can be expensive. Portable XRD equipment could be used in a field environment, making analyzing the samples a much faster and more efficient process. Portable XRD measurements are not as accurate or reliable as full laboratory XRD measurements, but preparing the samples requires much less time. It could potentially be used to analyze large number of samples in earlier phases of mineral exploration. Portable version of the XRD has been developed since early 2000 s, but only little research has been done on the suitability of using it in ore geology and mineral exploration (Sarrazin et al. 2005; Sarala & Koskinen 2018).

This thesis aims to research the usability of pXRD in mineral exploration. The main focus is on clustering of the samples that is done with DIFFRAC.EVA software and pXRD data from Geological Survey of Finland. The samples have been taken from Precambrian bedrock drill cores from the area of old Metsämonttu mine in Kisko in Southern Finland. The area contains volcanogenic massive sulphide (VMS) deposits, and the main commodities of the mine were zinc, lead and copper with some gold and silver (Latvalahti 1979). The focus is on data from 4 drill cores in the area which were measured by the pXRD instrument in approximately 10 m intervals. The goal is to see if the clustering method is able to group samples in a useful way for mineral exploration in the specific deposit type and if it is possible to detect sulphides or specific minerals or mineral groups that are typical indicators for VMS ores in the area.

2 X-ray diffraction

2.1 Theory of X-rays and diffraction

X-ray diffraction (XRD) is a well-established method in identifying minerals and crystal structures (Burkett 2018). XRD is based on crystal constructive interference of monochromatic X-rays and Bragg's law. XRD is best suited for detection of fine-grained minerals such as clays and powdered crystalline rock (Sarala & Koskinen 2018). X-ray diffraction was discovered in 1912 in an experiment conducted by Max von Laue, Walter Friedrich and Paul Knipping. The first classification system for powder diffraction patterns was published in 1936, and further major development was made in the 1960s (Etter & Dinnebier, 2014). Since then, the XRD method has been widely used in geosciences and there has been continuous development in making XRD method more capable of analyzing different types of material. XRD was first used exclusively for structurally well-arranged crystalline materials but can now be used for almost any material scattering X-rays (Lavina et al., 2014).

Electromagnetic radiation, including X-rays, can be described as both waves and particles called photons. X-rays are electromagnetic waves with a wavelength range of 0,01–1 nm in the electromagnetic spectrum (Figure 1b). Electromagnetic waves can be explained as a variation in the amplitude of energy in time and they can be classified by the speed with which they fluctuate over time. Wavelength (Figure 1a) is the time taken by a wave to complete a full sequence. As the wave oscillates faster, the wavelength decreases and frequency increases (Cervantes 2016). The speed of the wave can be calculated from equation (1):

$$v = \lambda f \tag{1}$$

where v = the speed of the wave, λ = wavelength and f = frequency.

Electromagnetic waves like X-rays can travel in vacuum space unlike other types of waves like sound. In vacuum the speed of electromagnetic wave equals the speed of light. If electromagnetic wave travels through a medium, the speed of the wave decreases compared to the speed in vacuum. The speed of the wave in a medium can be calculated from equation (2):

$$v = \frac{c}{n} \tag{2}$$

where c = the speed of light and n = index of refraction.

The wavelength of an electromagnetic wave is inversely proportional to its energy. This is evident from the equation (3):

$$E = hf = \frac{hc}{\lambda} \quad (3)$$

Where h = the Planck's constant (Ermrich & Opper 2011).

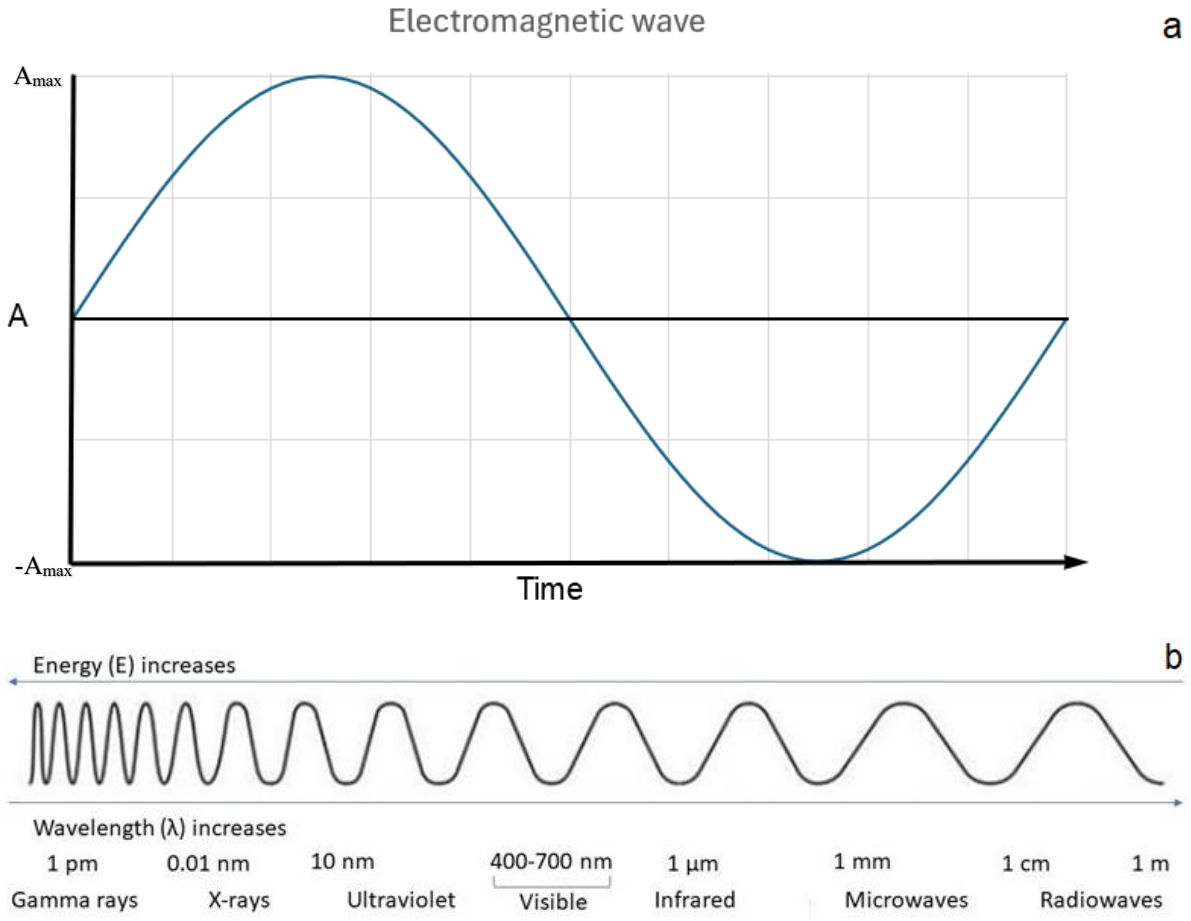

Figure 1a & 1b. (a) A simplified graph of an electromagnetic wave with one full wavelength sequence where the maximum amplitude is A_{max}. (b) The electromagnetic spectrum (Siira 2021, modified from Booysen et al. 2021).

Electromagnetic waves travel in a straight line in vacuum or homogeneous material. If there is a substance with different index of refraction in the path of the waves, they may be subject to various effects. These include reflection, refraction, scattering and diffraction. X-rays are also attenuated and absorbed. When photons enter a substance like mineral, some of them may be

reflected from the grain surface. Some photons pass the grain and might be refracted, and some may be absorbed. Photons that are reflected or refracted by the substance are said to be scattered (Ermrich & Opper 2011).

There are two types of scattering, coherent and incoherent. Coherent (Rayleigh) scattering is the elastic scattering that happens when incoming photons hit electrons of the inner shell of atom. The energy of the photon is preserved, and the wavelength remains constant. This type of scattering is the most important for X-ray diffraction. In incoherent scattering the energy of the photon decreases, and wavelength increases. There are two types of incoherent scattering, Compton scattering and fluorescence. If the incoming photon has high energy, it can eject an electron from the inner shell of the atom. This creates a void in the inner shell, and it is filled by an electron from one of the outer shells. The movement of the electron creates an X-ray photon that is emitted from the atom. This effect can be used in X-ray fluorescence (XRF) method but is unwanted in XRD. If the energy of the incoming photon is lower, it only pushes an electron to an excited state, and this is called Compton scattering. This type of incoherent scattering can be ignored in XRD (Ermrich & Opper 2011).

When X-rays with certain intensity (I_0) and wavelength (λ) pass through substance with certain attenuation coefficient (μ, also known as absorption coefficient), the transmitted intensity can be calculated from Equation (4):

$$I = I_0 e^{-\mu d} \tag{4}$$

Where d is the length of the travel through the substance (Ermrich & Opper 2011).

Diffraction and interference of X-rays was described by Bragg (1913) as reflections at the atomic plane of the crystal lattice (Figure 2). Their positions can be calculated using Bragg's law:

$$2d\ sin\theta\ =\ n\lambda \tag{5}$$

Where d = the interplanar spacing, θ = the Bragg angle, n = order of the interference and λ = the wavelength. The interplanar spacing (d) between the lattice planes can be explained with the Miller indices. The intensity of the reflections is affected by the symmetry of the crystal, positions of the atoms in the unit cell, number of electrons of the atoms, the amount of material and the absorption in the material. In materials with a high symmetry, certain reflections might not be visible due to destructive interference (Ermrich & Opper 2011).

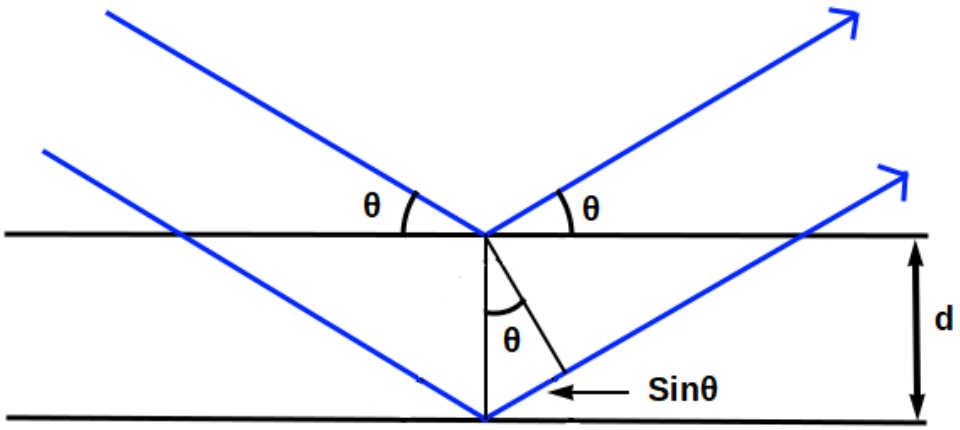

Figure 2. Reflection of ray of light according to Bragg's law. The lines with arrows describe rays of light. d is the interplanar spacing. Θ is the Bragg angle. Figure adapted from Ermrich & Opper 2011.

2.2 XRD analysis method

2.2.1 Production of X-rays

X-rays with sufficient intensity for XRD analysis can be produced by multiple methods. There are two common methods for producing X-rays. The first is by using an electromagnetic field to deflect high-energy electrons, which results in X-rays being emitted. This is done with synchrotrons, which are very large and expensive instruments which limits their usage to huge research centers. The second method is using sealed X-ray tubes. With this method the X-rays are obtained by bombing a suitable anode material with focused electron beam. The maximum usable power affects the achievable maximum intensity of the X-rays and is limited by the cooling system requirements for the anode. The X-ray tubes are more suitable for smaller laboratories and are widely used in XRD systems (Ermrich & Opper 2011).

In a sealed X-ray tube (Figure 3), the electrons are transmitted by cathode which consists of heated filament, which is typically tungsten. There is a high voltage difference between the cathode and the anode, which accelerates the electrons towards the anode. The electrons reach certain kinetic energy, which is then converted to radiation and heat as the electron decelerates. Only about 1 % of the energy is converted to radiation and 99 % to heat, which is why a cooling system is required for the anode. The X-rays are emitted from the tube anode through a thin window of suitable material like beryllium. This window makes the tube sealed but it lets the X-rays pass through. The X-ray is then aimed at the sample through specific optical components.

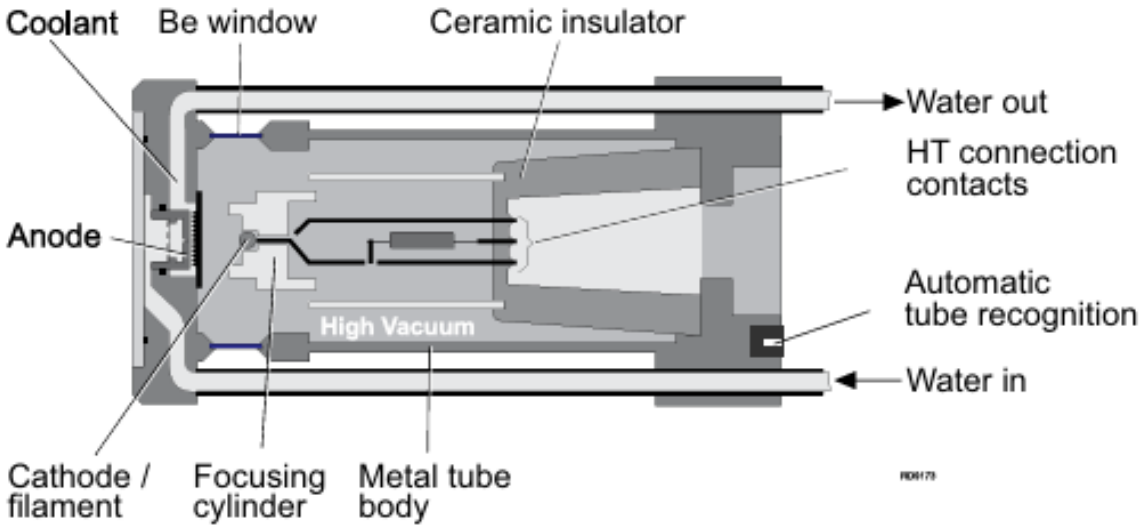

Figure 3. An illustration of sealed ceramic X-ray tube of X´Pert type (Ermrich & Opper 2011).

Two types of radiation are emitted when accelerated electrons interact with the anode, white radiation and the characteristic X-ray radiation. White radiation is caused by the loss of energy, which emits X-rays in continuous spectrum. White radiation is mostly unwanted for X-ray diffraction experiments. Observing the monochromatic characteristic X-ray radiation is in the focus when studying crystal structures. Bohr's atomic "shell" mode can be used to explain the principles of characteristic X-ray radiation. According to Bohr's model, the nucleus of the atom consists of positively charged protons and neutrons without charge. There are negatively charged electrons grouped in shells around the nucleus. Each shell outwards from the nucleus can hold an increasing number of electrons. The shell and the proton number affect the energy of a specific electron in the atom, and the energy generally increases outwards from the nucleus (Ermrich & Opper 2011).

When high-energy radiation like X-rays irradiates the atom, it can expel an electron from the atom if the binding energy of the electron in a specific shell is lower than the energy of the radiation. Incoming X-ray radiation is absorbed and scattered. If the energy of the incoming X-ray radiation is too high, most of the photons pass the atom, interacting with it only occasionally. Expelling an electron results in a void in the shell and puts the atom in an excited state with higher energy. This excess energy will then be released by transferring an electron from a higher-energy outer shell to lower-energy inner shell with the void, emitting an X-ray photon. Each atom has specific energy levels and emits monochromatic characteristic X-ray radiation. Wavelenght of the emitted photon/X-ray wave is related to the atomic number (Z) based on the Moseley law:

$$\frac{1}{\lambda} = Z^2 \tag{6}$$

The optimal voltage for producing characteristic X-ray radiation is specific for each anode material. If the voltage is too small, the characteristic radiation is hard to detect. If the voltage is too high, the amount of white radiation is too great compared to the characteristic radiation (Ermrich & Opper 2011).

2.2.2 XRD method setups

XRD setups consist of X-ray tube, optical components, the sample and a detector. X-rays produced by the tube pass through optical components and hit the sample. X-rays are diffracted by the sample and then pass through new set of optical components and enter the detector. Two main methods can be used to study samples using XRD; reflection geometry and transmission geometry. In reflection geometry the sample is a flat surface that scatters the X-rays. This is also called Bragg-Brentano geometry. This geometry is the most used method for laboratory phase analysis. In this setup (Figure 4) the focal spot of the X-ray tube, the sample surface and the detector slit form a so-called focusing circle. The X-ray tube and the detector slit also form the so-called measurement circle, where the sample surface is the center of the circle. There are some advantages to this method. This method can be used even at high angles and with spinning as there will not be powder spillage. The sample is often spun for improved particle statistics. This method can also be used for liquid samples, and very large samples (Ermrich & Opper 2011).

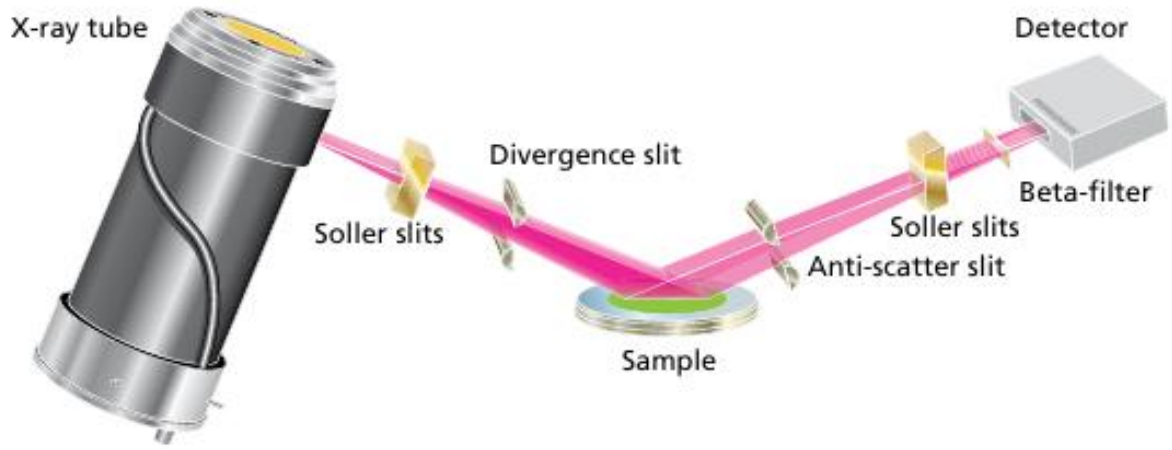

Figure 4. Bragg-Brentano setup for powder diffractometer with components for reflection measurements (Ermrich & Opper 2011).

In transmission geometry the X-rays pass through an X-ray transparent sample. In this method the sample could be between foils, or in glass capillary or it could be a thin solid sample transparent for X-rays. An additional focusing component between the X-ray source and the sample is required in this method. In foil samples the absorption of the material is an important factor. Highly absorbing samples could only be several micrometers thick, while maximum thickness for samples with lower absorption could be around 4 mm. The capillary method is typical for samples that consists of material sensitive to moisture or texture effects. The powdered material is loosely inserted into the capillary. The sample can be diluted with X-ray transparent substance like cork flour or glass to improve the transparency of the sample (Ermrich & Opper 2011).

2.2.3 The detector

The detector is used to detect and count the photons diffracted by the sample. There are three types of X-ray detectors: point (0D), line (1D) and area (2D) detectors. Point detectors count all photons but are not position sensitive. The advantages of point detectors include high dynamic range, low background noise and cost-effectiveness (Ermrich & Opper 2011). Line detectors are also called position-sensitive detectors. Line detectors cover a certain angular range. A line detector resembles multiple adjacent point detectors and is much faster than point detectors. Advantages of the line detectors include very fast measurement, being able to investigate small sample amounts and having good angular resolution. Area detectors are somewhat similar to line detectors. They are typically used for special applications like

texture analysis and micro-diffraction. Advantages of area detectors include fast measurement, ability to analyze small spots and quantity samples and improved analysis of highly textured samples (Ermrich & Opper 2011).

2.2.4 Diffractograms

X-rays are diffracted from the sample and are detected by the detector. The detector measures the diffracted angles of the X-rays and their intensities. Based on Bragg's law (formula 5), the data is used to make diffractograms. Diffractogram consists of diffraction angle on the x-axis and intensity on the y-axis. Diffractogram (Figure 5) consists of peaks and a background. The peak patterns can be used to determine the mineral composition of the sample. This includes locations, shapes and intensities of the peaks.

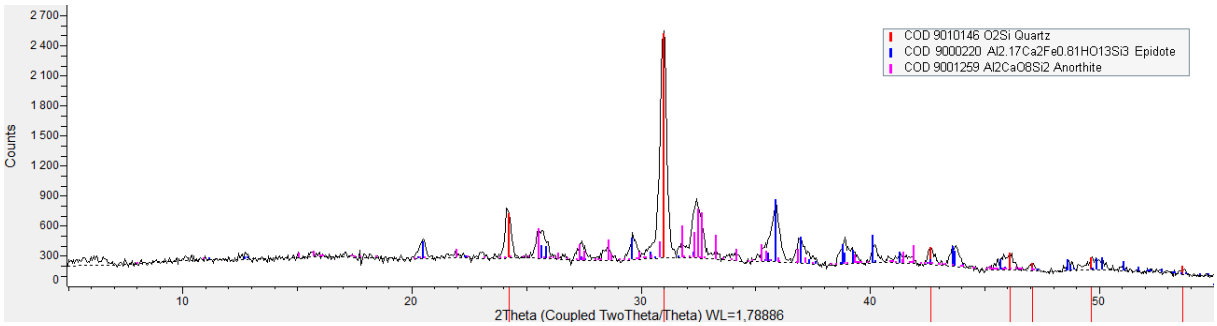

Figure 5. An example of a diffractogram from the sample MM_241_95. Intensity is depicted on the y-axis and diffraction angle (2 Theta) on the x-axis. Colored bars present the minerals detected based on the peak patterns.

Various effects can affect the quality and accuracy of the diffractograms. For example, the evaporation of tungsten filament in the X-ray tube and deposition on the anode and the window leads to decreasing intensity of the X-rays over time. This can cause additional lines to appear on the diffractogram and make the interpretation harder. Also, certain minerals like sulphides can decrease the quality of the background. Effects and causes that can affect the quality and accuracy of the diffractograms are explained in more detail by Ermrich & Opper (2011) and Siira (2021).

2.3 Portable X-ray diffraction

The pXRD is a portable X-ray powder diffraction device that is suitable for field usage. It was originally developed for field deployment on Mars in the early 2000s. The first commercial pXRD was CheMin and it used a charge-coupled device (CCD) camera. It was funded by NASA for the Mars research project. Other main parts of the device are the X-ray tube and

the sample holder. The device can be used as both portable X-ray diffraction and X-ray fluorescence (pXRF) (Sarrazin et al. 2005; Sarala & Koskinen 2018). The pXRD was designed to be lightweight (about 15 kg) and small enough to fit in a car. It is battery powered and controlled by a laptop. All the data collection and analysis can be done on-site. The sample preparation and measurement times are relatively quick compared to laboratory XRD (Sarrazin et al. 2005).

The pXRD uses transmission geometry (Figure 6) and the X-rays are directed through the powder sample, and the CCD detector is on the opposite side of the sample. The X-rays are generated with X-ray tube that typically contains cobalt, producing Co radiation. The X-rays are collimated with a collimator so that the rays are parallel and have minimum spreading. The pXRD does not need as fine-grained powder sample as laboratory XRD. For the pXRD the sample material only needs to be crushed and sieved to grain size of <150 µm. Overized grains cause a bad diffraction pattern. The grain size must remain coarse enough so that the particles can move properly and not get stuck to each other or the sample holder. In laboratory XRD the sample is typically spun during the measurement, but in pXRD there is only a sample vibration system that aims to move crystals into random orientation. The lack of moving parts is advantageous for field usage (Sarrazin et al. 2005; Sarala & Koskinen 2018). pXRD can detect the common rock forming minerals including albite, amphiboles, feldspars, magnetite, muscovite and quartz. pXRD can also detect heavy and indicator minerals including apatite, biotite, chlorite, hematite, zircon and others. More details on pXRD's ability to detect specific minerals and comparison between pXRD and laboratory XRD can be found on the study done by Sarala & Koskinen (2018).

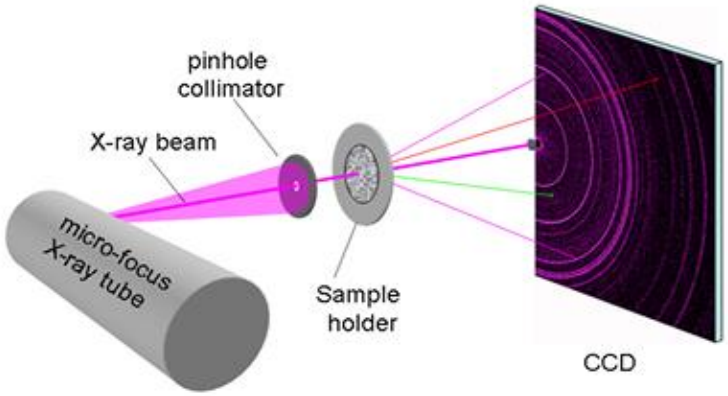

Figure 6. Transmission type geometry of the CheMin pXRD device with the main components (Sarrazin et al. 2005).

2.4 Portable XRD analysis softwares and clustering

The software used in this study is DIFFRAC.EVA by Bruker-AXS. Another available software is XPowder, but it was not utilized much in this study. DIFFRAC.EVA can be used to identify various components of solid samples. In addition, it can be used for other analytical purposes like clustering multiple samples into groups based on diffractogram peak patterns. The software is based on PolySNAP and SNAP-1D computer programs (Barr et al. 2004).

After the sample data is inserted into the software and a database is selected, it creates a diffractogram with a peak profile. The software creates an internal copy of the original data file and does not edit the original data. The software creates a list of components with potentially matching peak patterns based on the selected database and the peak profile of the sample. The user can manually pick the minerals that fit the peak profile. Geological knowledge is required to determine which minerals the sample can possibly contain as the software only gives a list of all possibly matching substances according to the database used (DIFFRAC.EVA Cluster Analysis Manual).

DIFFRAC.EVA can also be used for clustering multiple samples. When atleast 3 samples are inserted into the software, it can cluster them based on the peak profiles. Clustering can be done without using a database. The imported sample data can be pre-processed and controlled in various ways. For example, data can be checked for amorphous material, and wavelet

smoothening can be used to remove noise from a signal. Amorphous samples, if present, are treated separately. Once all samples are imported, each peak pattern is matched against every other pattern including itself. The software uses weighted mean of various correlation coefficients to make a cluster analysis of the samples (Barr et al. 2004; DIFFRAC.EVA Cluster Analysis Manual).

The cluster analysis results in a dendogram (Figure 7), a visual representation of the clustered peak patterns. In a dendrogram, all individual peak patterns are located at the bottom of the plot in separate box. These classes are then connected in stepwise fashion and are linked by horizontal tie bars based on the calculations made by the software. The height of the tie bars represents the dissimilarity of the peak patterns, meaning the closer the tie bars are, the more similar the patterns are. A cut level line is used to divide the sample peak profiles into clusters. The cut line can be moved manually, and the software changes the clusters based on the selected cut line height on the dendogram.

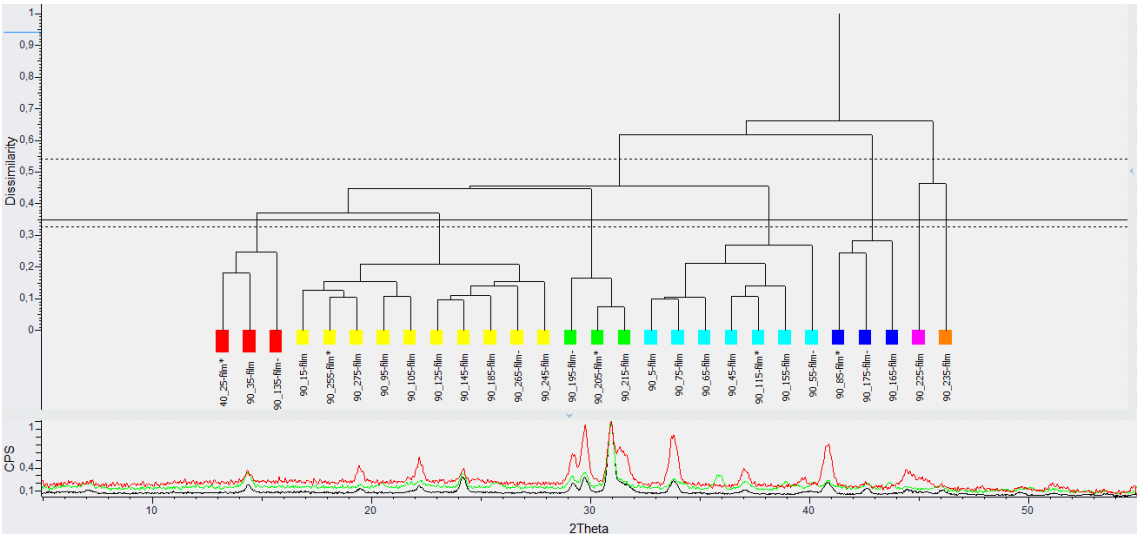

Figure 7. An example of a dendogram from the drill core MM190. Combined individual diffractograms of the selected cluster can be seen below the dendogram.

Dendograms and clustering can be done using multiple different methods, and the software automatically attempts to choose the most suitable method for the chosen sample set. It is possible to test different methods manually to confirm the most suitable method. In addition to dendograms, the clustered data can be displayed in other visual formats including well displays, pie charts and 3D representations (Barr et al. 2004; DIFFRAC.EVA Cluster Analysis Manual).

3 Volcanogenic massive sulphide deposits

3.1 Introduction to volcanogenic massive sulphide deposits

VMS deposits are base and precious metal concentrations that have been formed by hydrothermal fluids in submarine settings with active volcanism. VMS deposits have been found across the world, but they are concentrated on orogens that have had extensional periods. Hydrothermal fluids utilize the faults formed by extension and circulate the crust, leaching metals from the hot volcanic rocks and precipitate them near the colder seafloor. Most VMS deposits have formed during periods of major ocean closing and terrane accretion, including Late Archean, Paleoproterozoic, Paleozoic and Mesozoic (Galley et al. 2007).

VMS deposits vary in structure and mineralogy depending on the formation conditions and available metal sources. VMS deposits belong to the group of exhalative deposits, which also include sedimentary exhalative (SEDEX) deposits. They typically consist of sulfide mineral body, which is underlain by stockwork zone and often overlain by exhalative horizon. The stockwork zone works as a channelway for hydrothermal fluids that form the orebody. The host rock can be either volcanic or sedimentary or combination of both. They often contain economical amounts of copper, lead, zinc, gold, silver and possibly some trace elements. VMS deposits typically occur in clusters and form districts (Galley et al. 2007).

3.2 Genesis of volcanogenic massive sulphide deposits

VMS deposits typically form in extensional tectonic environments of variable scale. This includes mid-ocean ridges, back-arc basins, early arc formation phases and extension in post accretion arc settings. The most common settings for VMS deposits are various rifting environments where the extension causes crustal thinning. This results in mantle depressurization and generation of basaltic magma from partial melting of the mantle. These melts rise through the crust to subseafloor environment and form intrusion or a magma chamber (Galley et al. 2007). The volcanic intrusion usually forms around the depth of 2-5 km, and they are typically mafic and gabbro diorite-tonalite-trondhjemite in composition (Franklin et al. 2005).

The basaltic magma from the mantle may also underplate the crust (Figure 8). This can cause partial melting of the crust, which forms anhydrous, high temperature melts. This results in bimodal magmatism in many VMS deposits. The type of VMS depends on the time of

formation and the tectonic setting. VMS deposits in mid-ocean ridges are typically mafic, while island arc VMS deposits are more bimodal. (Galley et al. 2007; Franklin et al. 2005).

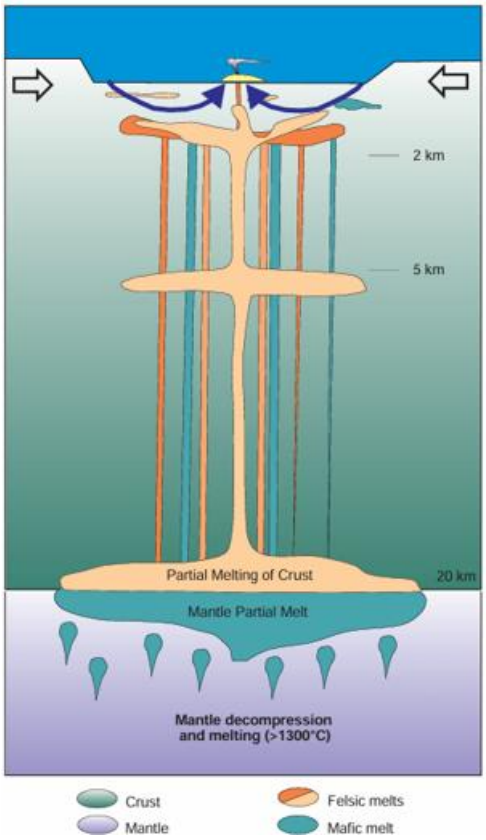

Figure 8. A typical VMS formation environment in a rifting setting. Partial melts of the mantle underplate the crust which causes partial melting of the crust. The melts rise upwards and form magma chambers. The heat from the magma chamber near the seafloor initiates and sustains thermal convection of hydrothermal fluids producing VMS deposits (Galley et al. 2007).

The heating from the intrusion causes and sustains convection of hydrothermal fluids below the seafloor, which can form VMS deposits (Galley et al. 2007). This hydrothermal convection must last atleast 100 to 10 000 years to start forming VMS deposits (Ohmoto 1995). The lifespan of the convection system is affected by the mass of the intrusion, temperature of the magma and permeability of the host rock (Franklin et al. 2005). VMS deposits also form in arc formations related to subduction and accretional settings. Crustal thickening in these settings can result in modification of the subduction angle or direction of the colliding plates or cessation of subduction along a section of plate boundary. This can form extensional domains like strike-slip basins and the magmatism in these domains can sustain hydrothermal convection for long enough to form VMS deposits (Galley et al. 2007, after Ziegler 1992 and Hamilton 1995).

When rising magma intrudes the crust and forms a magma chamber it starts heating the surrounding crust. This causes connate seawater in the porous rocks to heat up and become buoyant (Galley et al. 2007). The fluids get heated up to about 300-400°C. This heated water then rises through the cracks formed by the extension in the crust. At the same time cold sea water is drawn in the fault system above the cooling intrusion. The circulating heated fluids cause alterations to the host rocks and leach metals. The fluids then rise to or near the seafloor and precipitate the metals, forming the VMS deposit over time (Franklin et al. 2005). Magmatic fluids or gases can also be present in the fluid convection system, but their role is minor in most VMS systems (Ohmoto 1995).

To form VMS deposits, sulfate (SO_4^{2-}) in the circulating seawater needs to be reduced to dissolved sulfides (H_2S or HS^-). In this form S can react with metals and leach them from the rocks (Robb 2005). Sulfate can be reduced to sulfide in two ways. First is the reduction of sulfate to sulfide directly by bacterial reduction in euxinic basin environment, but this has likely only been possible during Archean time and not in Phanerozoic (Ohmoto 1995). The second way is that the seawater sulfate forms fine grained disseminated gypsum or anhydrite in the footwall rocks in temperatures below 150°C as the seawater percolates downwards. This gypsum or anhydrite could then be dissolved as the temperature rises and be partially reduced to H_2S (Ohmoto 1995).

The descending modified seawater reacts with higher-temperature volcanic rocks and leach metals from them. After the fluid temperature rises to around 300–400°C, the metal rich fluid becomes buoyant and starts circulating upwards. As the hot metal rich fluids rise, they contact and react with cooler rocks in the stockwork zone and cause alterations. Some metals precipitate and form stockwork ores, which are typically low grade. As the fluids rise further, they mix with the cold seawater within the unconsolidated sediments or seafloor. This causes precipitation of primitive ores that have high Pb + Zn and low Cu content. In later stages of the deposit formation there might be reactions between hotter hydrothermal fluids and the primitive ores. This forms more mature ores that are enriched in chalcopyrite and pyrite (Ohmoto 1995).

Often the hot hydrothermal fluids are released into the seawater through black smokers. Black smokers are chimney-like vents that are formed from the precipitating sulfides. The seafloor around the black smoker complex is covered by debris from collapsed black smokers (Hannington et al. 1998). There is often a thin exhalative layer on top of the VMS deposit that

forms by mixing of hydrothermal fluids with cold seawater mostly within unconsolidated sediments over wide area (Ohmoto 1995).

3.3 Classification of VMS deposits and geological and geographical settings

VMS districts can be divided into five lithostratigraphic types. These types are (1) bimodal mafic, (2) mafic, (3) pelitic-mafic, (4) bimodal-felsic and (5) siliciclastic-felsic. Types 1, 2 and 3 are usually formed in ocean-ocean subduction environments. Type 1 is mafic dominated but can contain up to 25% felsic volcanic strata. Type 1 is dominant in nascent arc rifting but is also related to Archean rifting environments with komatiites. Type 2 is dominated by MORB-boninite arc tholeiitic successions, pillow lavas and massive basaltic flows. This type is related to intra-oceanic back-arc environments and some ophiolite assemblages. Type 3 consists of subequal amount of basaltic and pelitic successions. Type 3 is also related to intra oceanic back-arcs but can also be found in mafic alkalic terranes related to seamount construction or late back-arc volcanism (Franklin et al. 2005).

Types 4 and 5 form in ocean-continent margin and continental back-arc environments. Type 4 contains 35 % to 70 % felsic components and 20 % to 50 % mafic components. This type forms in continental margin arcs and related back arcs. In type 5, siliciclastic strata constitute up to 80 % and felsic volcaniclastic rocks up to 25 %. Mafic components can constitute up to 10 %. Type 5 is typical for mature epicontinental back-arcs (Franklin et al. 2005). Continental back-arc basins contain some of the most economically important VMS deposits (Galley et al. 2007). The principal environments for each VMS district type related to the evolution of Earth’s crust are shown in Figure 9.

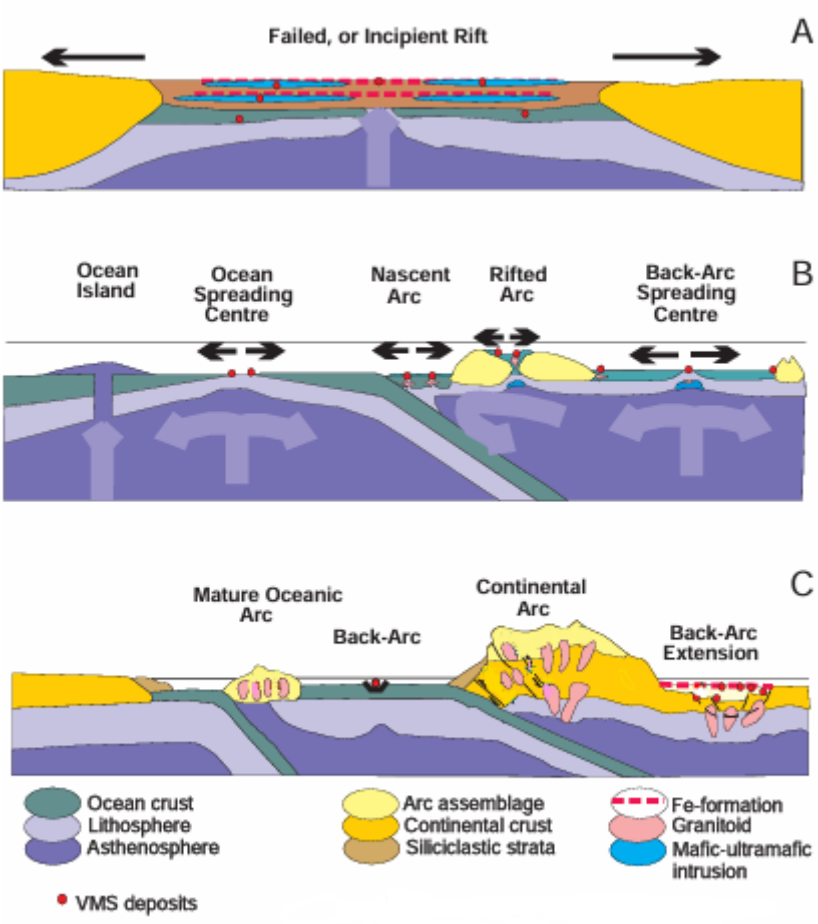

Figure 9. The major tectonic settings that have formed VMS deposits during the stages of the formation of Earth's crust. (A) Early Earth mantle plume activity formed rifting environments with basins characterized by early oceanic crust, primitive basalts, siliciclastic infill and associated Fe-formations. Similar rifting environments have formed during the Phanerozoic in back-arc basins. These typically host bimodal-mafic VMS deposits. (B) The formation of ocean spreading centers and oceanic basins which host mafic VMS deposits. Oceanic arc formations started to form with the development of subduction zones. These host bimodal mafic, bimodal felsic and mafic VMS deposits. (C) The formation of mature arc environments and subduction fronts. The resulting arc assemblages host most of the felsic-dominated and bimodal siliciclastic VMS deposits, which are typical in back-arc settings (After Galley et al. 2007, modified from Groves et al. 1998).

Modern VMS deposits mainly form in mid-ocean ridges and arc environments. VMS deposits preserved in the geological records are found mainly from rocks of varying kinds of arc environments because subduction has removed most of the ancient seafloor VMS deposits. Some ancient seafloor VMS deposits can be found in ophiolite suites. VMS deposits in Archean time formed mainly in rifting basins related to mantle plume activity and are typically found in greenstone belts. These deposits are characterized by early oceanic crust consisting of primitive basalts and komatiites, and deposition of siliciclastic sediments (Galley et al. 2007).

VMS deposits have been found in every major continent except Antarctica. Large portion of the known VMS deposits are in Canada in mainly Archean and early Proterozoic provinces. Australia is another country with vast amounts of VMS deposits in Archean areas (Galley et al. 2007). Japan has large number of Phanerozoic Besshi and Kuroko locality type VMS deposits (Galley et al. 2007; Franklin et al. 2005). The western coast of both North and South America contains large amounts of VMS deposits of the Mesozoic age. Other areas containing important VMS deposits include Iberia, coastal areas of the Red Sea, Urals and northern Europe. VMS deposits in Finland are mainly of Paleoproterozoic age (Franklin et al. 2005).

3.4 Mineralogy and structure of VMS deposits

VMS deposits are major sources of base metals Cu, Pb and Zn and precious metals Ag and Au. They can also contain significant amounts of rarer elements like Co, Sn, Se, Mn, Cd, In, Bi, Te, Ga and Ge (Galley et al. 2007). VMS deposits can be divided into two general types based on major metal content, Cu-Zn and Cu-Pb-Zn deposits. Cu-Zn deposits form when hydrothermal fluids react with basalts at maximum temperature of 350°C to 400°C. Cu-Zn deposits are predominant in the types (1), (2) and (3) of the lithostratigraphic classification. Cu-Pb-Zn deposits form when fluids react with sedimentary or felsic volcaniclastic strata in temperatures somewhat lower than in Cu-Zn deposits. Cu-Pb-Zn deposits are more predominant in the types (4) and (5) of the lithostratigraphic classification. The Au content of VMS deposits in any setting is controlled by multiple different factors, including temperature, water depth, precipitation mechanics and input from magmatic sources. The Ag content is higher in felsic dominated deposit types (Franklin et al. 2005).

The VMS ore body is typically lenticular in shape and contains 60 % or more sulfide minerals. The main sulfide minerals in VMS deposits are pyrite, pyrrhotite, chalcopyrite, galena and spharelite. Other common metallic minerals are magnetite, hematite and cassiterite. Gangue minerals are typically quarts, chlorite, barite, gypsum and carbonates (Lydon 1984). Cordierite and anthophyllite phases are typical indicators of nearby VMS deposit, but they only form in deposits that have metamorphosed to greenschist or higher metamorphic grades (Taylor et al. 1995). The lenticular ore body typically has metallic zonation patterns which are related to changes in temperature and fluid composition over time. The chalcopyrite / (spharelite + galena) ratio increases inwards from the hanging wall

contact to the core of the ore body. This means that the core is more Cu rich and Zn poor than the outer parts of the ore body (Lydon 1984).

In an idealized VMS deposit (Figure 10) the outermost zone of the massive sulfide lens contains Zn-Pb rich “black ore” which formed in early stage of the hydrothermal activity in temperatures of around 200°C to 300°C. This zone contains spharelite, galena, pyrite, baryte and anhydrite. The zone below the black ore zone contains the more mature “yellow ore”. The yellow ore formed as a replacement product of the black ore by Cu-rich minerals. This happened when the temperature of the hydrothermal fluids increased to about 280°C - 380°C during the thermal maximum stage. This zone contains spharelite, chalcopyrite, pyrite and occasionally galena. In the core of the massive sulfide lens there might be almost monomineralic pyrite zone (Lydon 1984; Ohmoto 1995). Other metallic minerals like pyrrhotite and magnetite tend to concentrate in the core area of the massive sulfide lens with highest Cu/Zn ratio (Lydon 1984). There is typically a thin exhalative or tuffaceous horizon on top of the massive sulfide lens that can cover a large area around the hydrothermal vent. This horizon is variable in composition and can contain pyrite, hematite and chert (Lydon 1984; Ohmoto 1995).

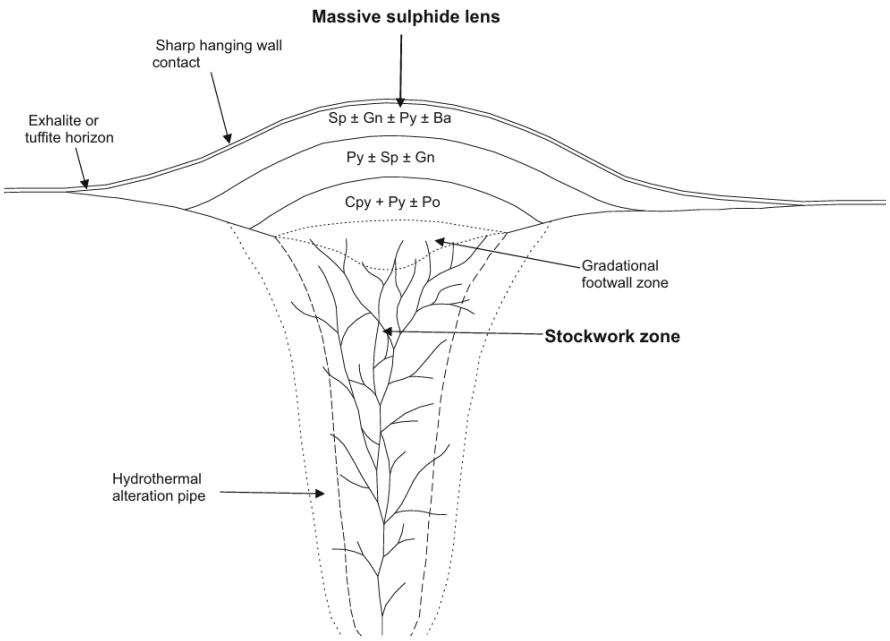

Figure 10. Conceptual VMS deposit structure. Abbrevations: Sp = sphalerite, Gn = galena, Py = pyrite, Ba = barite, Cpy = chalcopyrite, Po = pyrrhotite. After Lydon (1984).

There is usually an upwards widening pipe-shaped stockwork vein system or stringer zone under the massive sulfide lens. The stockwork system works as a channel way for the hydrothermal fluids. On average they are about 100m wide at the top and about 100m deep but can extend hundreds of meters in both directions (Ohmoto 1995; Galley et al. 2007). The stockwork zone contains disseminated sulfides and is characterized by distinctive metasomatic alteration halos that extend further away from the stockwork zone (Galley et al. 2007; Lydon 1984). The proximal zone of the stockwork zone typically contains chloritization, while the distal zone tends to have more sericitic alteration (Lydon 1984).

The core of the stockwork zone is typically Fe-chlorite + quartz + sulfide ± sericite ± talc in composition, with increasing quartz + sulfide content towards the lower contact of the massive sulfide lens. The core is surrounded by a wider, more sericitic zone with a composition of Fe-Mg-chlorite + sericite. The outermost zone is rich in sericite, phengite and Mg-chlorite and can contain albite, carbonate and barite. The outermost zone can also extend to the hanging-wall above the massive sulfide lens (Galley et al. 2007). As a result of destruction of the feldspar component of the original volcanic rock during chloritization, the chloritic stockwork core is depleted in calcium, sodium and silicon. The chloritic core is also enriched in iron and magnesium content. Potassium is usually depleted in the chloritic core but enriched in the seritic zones. Otherwise, the metasomatic changes in the sericitic zones are less intense gradational continuations of the ones in the chloritic core. The intensity of the metasomatism decreases outwards from the core of the stockwork system (Lydon 1984).

4 Geology

4.1 Regional geology

The bedrock of Finland is part of the Fennoscandian shield which is located in the northern Europe. The Fennoscandian shield extends from southern Norway to northwestern Russia. The Fennoscandian shield belongs to the larger East European craton, which extends from the Scandinavian Caledonides to the Ural Mountains in the east and the Black Sea in the south. The bedrock of Finland covers about 1/3 of the Fennoscandian shield. The bedrock of Finland can be divided into four tectonic provinces, Karelia, Lapland-Kola, Norrbotten and Svecofennia (Nironen 2017).

The oldest tectonic province in Finland is the Karelia province, which mostly consists of Archean basement that is partially covered by Palaeoproterozoic sequences. Majority of the Archean intrusive and volcanic rocks in Finland formed around 2,75–2,60 Ga, but some rocks in the Siurua complex have been dated up to 3,5 Ga (Lahtinen et al. 2005; Mutanen and Huhma 2003). Majority of the bedrock of Finland formed during the Palaeoproterozoic Svecofennian orogeny around 1,92–1,79 Ga (Lahtinen et al. 2005). This includes the Svecofennian province which can be divided into two subprovinces, Central and Southern Finland (Nironen 2017).

During the Svecofennian orogeny several microcontinents and volcanic arcs accreted to the older Karelia continental block (Nironen 2017). There are multiple theories on whether this consisted of continuous, retreating subduction (Bogdanova et al. 2015) or multiple orogenic stages (Lahtinen et al. 2005). The accretional events resulted in the growth of new juvenile crust in Central and Southern Finland. Island arc -type volcanic rocks formed within the continental margin and mafic to ultramafic intrusive rocks emplaced into the older turbiditic sequences. At the same time new sedimentary rocks accumulated on the seafloor (Nironen 2017).

The Svecofennian orogeny involved the accretion of multiple volcanic arcs in Southern Finland. The most important two are the Häme belt and the Uusimaa belt and these volcanic arcs accreted around 1,88–1,86 Ga. The volcanic rocks that formed in these volcanic arcs were diverse and contain rocks with the composition between rhyolites and basalts. The sedimentary rocks deposited in these arcs were mainly mudstones and greywackes but contain also some felsic supracrustal rocks and carbonates (Kähkönen 2005). Multiple VMS deposits

formed in the Uusimaa belt around 1895–1875 Ma and they are typically related to bimodal igneous rocks with calc-alkaline affinity (Eilu & Tontti 2012).

The collision of the protocontinent Volgo-Sarmatia with the Fennoscandian protocontinent marked the end of the Svecofennian orogeny at 1,80 Ga. This resulted in the new continent Baltica and caused transpressional deformation in Southern Finland. After the collision there was a time of crustal stabilization around 1.76–1.65 Ga. This is evidenced by the appearance of ultramature quart arenites and unconformity within sedimentary layers suggesting deep erosion (Nironen 2017). The last major event affecting the bedrock of Southern Finland was the rapakivi magmatism around 1.67–1.54 Ga. Rapakivi magmatism was bimodal containing both mafic and felsic rock types and it was caused by intracontinental rifting. Mafic dyke swarms are also associated with the rapakivi magmatism (Haapala et al. 2005).

4.2 Orijärvi formation

The Orijärvi formation belongs to the Uusimaa belt in southern Finland subprovince within the Fennoscandian shield. The Uusimaa belt is characterized by felsic supracrustal and volcanic rocks that formed around 1.90-1.88 Ga. The belt also contains a large number of mudstones, graywackes and sedimentary carbonates. Massive sulfide deposits and banded-iron formations are relatively common in the Uusimaa belt (Kähkönen 2005). The Orijärvi area contains four different formations which represent different phases of oceanic arc system evolution from early arc to back-arc basin. These formations are Orijärvi, Kisko, Salittu and Toija. The Orijärvi formation is the oldest and is characterized by bimodal magmatism and synvolcanic Orijärvi granodiorite. There is likely a correlation to the Bergslagen area in central Sweden (Väisänen & Mänttäri 2002).

The volcanic rocks in the area are mainly volcanoclastic but contain some units of lava origin as well. Volcanic rocks in the area are predominantly calc-alkalic in chemical composition, but there are also some basaltic layers with tholeiitic composition. The volcanic rocks are covered by argillaceous and arenitic sedimentary rocks. Rocks in the area are metamorphosed in lower-pressure amphibolite facies and have been folded in two phases (Latvalahti 1979).

There are multiple known VMS deposits in the Orijärvi formation and the earliest mining operation in the area started in 1757. The major mined deposits in the study area are Metsämonttu and Aijala. Aijala mine was active from 1949 to 1958 and Metsämonttu from 1952 to 1974. Aijala deposit was mined mainly for copper and Metsämonttu for zinc, lead and

silver. These deposits are stratabound. Aijala deposit occur near the contact of intermediate-basic pyroclastic volcanites and acidic volcanites. Another small deposit, Aurums-Aijala, was mined for Pb, Zn and gold (Latvalahti 1979).

4.3 Metsämonttu deposit

The Metsämonttu succession is a Paleoproterozoic Zn-Pb-Cu-Ag-Au VMS deposit in the Aijala member in southwestern part of Orijärvi formation (Hokka et al. 2024). It is located withing the Uusimaa belt in Fennoscandian shield. The Aijala member hosts almost all known sulfide and oxide deposits in the Orijärvi formation (Latvalahti 1979). The Metsämonttu deposit was discovered in 1946 by Suomen Malmi Oy. It was detected from ground electric anomalies during exploration in Aijala area and the deposit was confirmed with diamond drilling (Puustinen 2003). The mine in Metsämonttu was operational from 1952 to 1974 and the mining was done in two periods from 1952 to 1958 and from 1964 to 1974 (Warma 1975). The total of about 1.7 megatons of rock was mined of which 1.5 megatons was ore (Puustinen 2003). The ore grades were 3.51 % Zn, 0.79 % Pb, 0.27 % Cu, 25.02 g/t Ag and 1.4 g/t Au (Latvalahti 1979).

The Metsämonttu deposit (Figure 11) locates in the contact between intermediate-basic pyroclastic volcanites and acidic volcanite. The host rock is pyroclastic acidic volcanite that is interbedded with quartz and plagioclase phenocrysts and contains potassic tuffite interlayers. The acidic volcanite is stratigraphically overlain by the intermediate-basic volcanite which is composed of pyroclastic and tuffitic rocks. Altered rocks in the Metsämonttu deposit include dolomitic limestones and chlorite-bearing tremolite-diopside skarns. In addition, there are cordierite-anthophyllite rocks and cordierite mica gneisses that increase in abundance downward from the upper part of the deposit. There are also some narrow intralayers of iron formations (Latvalahti 1979).

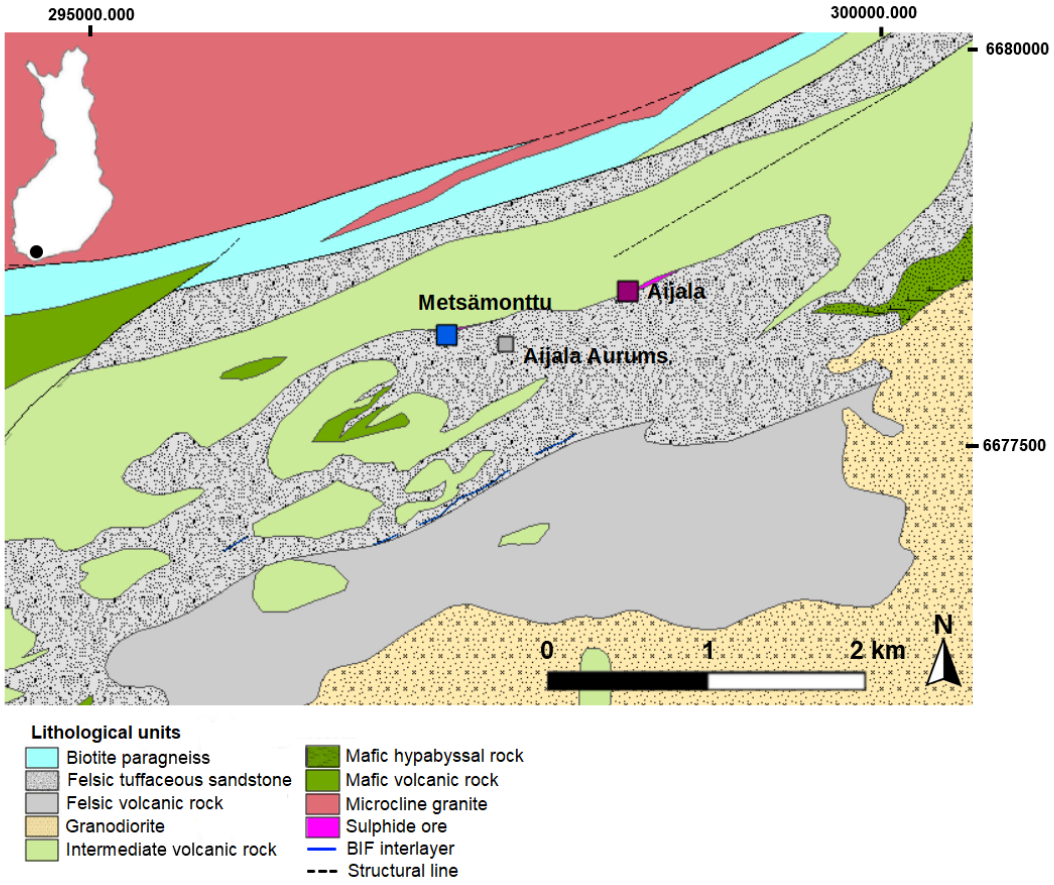

Figure 11. 1:200 000 Geological map of the study area. (Bedrock of Finland 200k, © Geological Survey of Finland [2026]).

4.4 Metsämonttu deposit ore mineralogy and structure

Ore in the Metsämonttu deposit (Figure 12) appears as multiple small orebodies that are strata bound and delimited to the alteration zone within the felsic rocks near the contact with mafic-intermediate volcanites. Ore bodies are elongated, vertical, almost parallel and have been strongly affected by metamorphosis and folding. Pyrrhotite, pyrite, chalcopyrite, spharelite and galena are the major ore minerals. The size of the orebodies and the zinc and lead content decrease downward in the deposit. The orebodies are generally less than 10m thick but are up to 20m thick in the dolomitic limestones and skarns. The length of the orebodies is typically 100 to 150 m. The Metsämonttu deposit is divided into two separate zones by large fault displacement, and the two zones have been named Old and New Metsämonttu (Latvalahti 1979; Leväniemi & Hokka 2021).

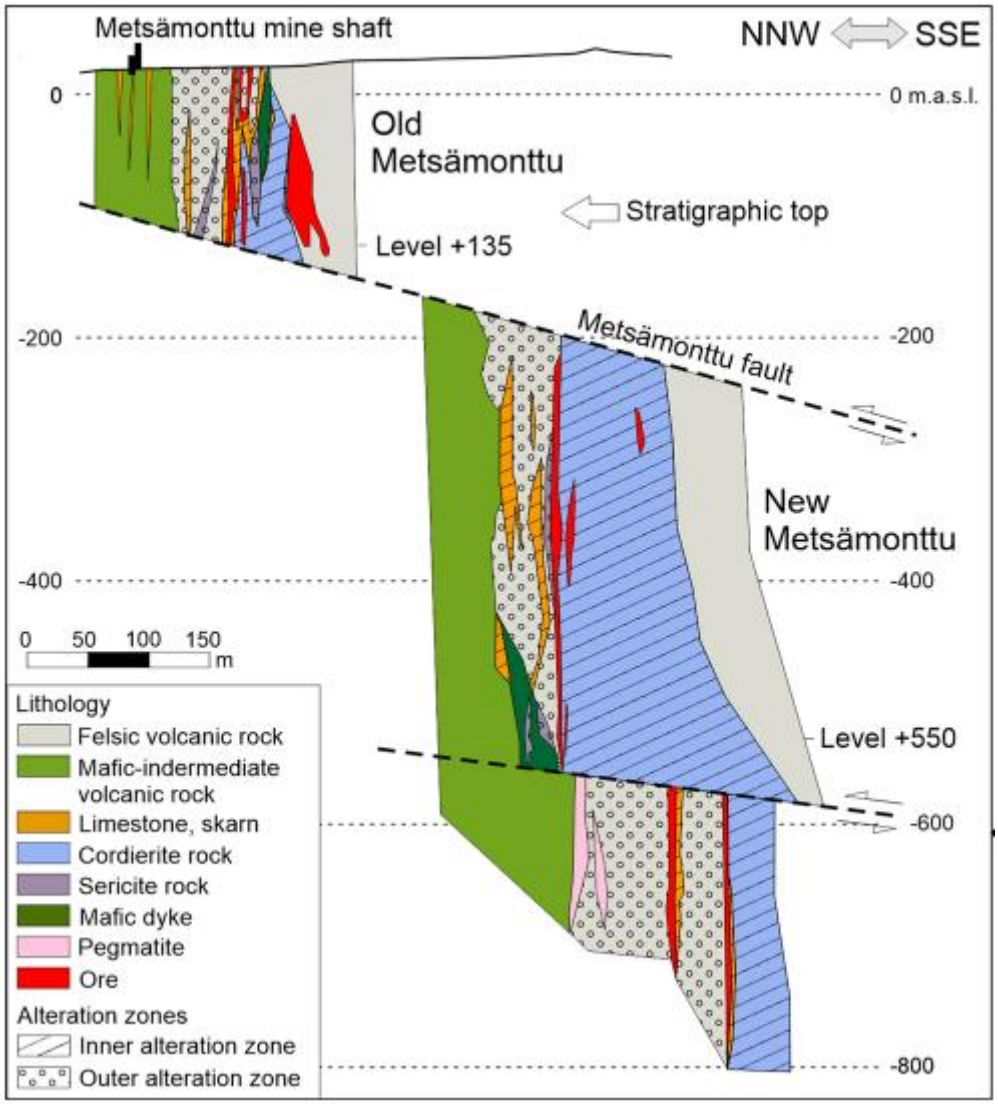

Figure 12. Schematic cross-section view of the central part of the Metsämonttu mine (Leväniemi & Hokka 2021, after Latvalahti 1979 and unpublished mine maps of Outokumpu Oy).

Structurally the ores in the Metsämonttu deposit appear as disseminated sulfides, breccia ores and occasionally as massive sulfide veins. Breccia ores are economically the most important ore types. Breccia ores conform with bedding and in detail they cut and replace the wall rocks. The contacts with breccia ores and wall rocks are sharp in both structure and metal content. Breccia ores are submassive and generally appear in chlorite-rich tremolite-diopside skarns, dolomite limestones and occasionally in quartz rocks. Lead and silver contents are greater in breccia ores within skarns and dolomitic limestones than in other ore types. Quartz rock and cordierite mica gneiss hosted breccia ores are iron sulfide predominant. Massive sulfide veins are typically a few centimeters to several meters in width and pyrrhotite and pyrite are the main sulfide minerals. The veins cut wall rocks with sharp contacts. Disseminated ores are typically associated with breccia ores and replace amphibole and

pyroxene grains. Disseminated iron sulfides in cordierite-anthophyllite rocks contain pyrrhotite and pyrite, and in sericite or muscovite gneisses only pyrite is present. Chlorite-bearing shears are typically filled with remobilized iron sulfide veins or coarse-grained iron sulfide disseminations (Latvalahti 1979).

The ore types can also be divided by economical elements composition. These ore types are Zn-Pb, Zn-Fe and Cu. These ore types can appear both separately and together. The Zn-Pb ores are located mainly in dolomitic limestones and diopside skarns. Main ore minerals in Zn-Pb ores are sphalerite, galena, pyrrhotite and pyrite. Accessory minerals, including chalcopyrite, magnetite and arsenopyrite, can be present. Some native metals and sulfosalts are often associated with galena, including gold, silver and arsenic. Zn-Fe ores are common in cordierite gneisses. Pyrrhotite, pyrite and sphalerite are predominant ore minerals in Zn-Fe ores. Accessory minerals are mainly chalcopyrite, galena, magnetite, ilmenite and marcasite. Cu ore lenses are occasionally present in cordierite gneisses, and the major ore minerals in those are chalcopyrite, pyrrhotite and pyrite. Galena, sphalerite, cubanite and native gold can occur as accessory minerals (Latvalahti 1979; Leväniemi & Hokka 2021).

4.5 Metsämonttu deposit deformation, metamorphism and alteration

The Metsämonttu deposit has been affected by post-depositional metamorphism and multiple deformation stages. This has resulted in the loss of primary structures of the ores. The peak metamorphism took place at a temperature of about 650 ± 30 °C and a pressure of about 3 kb, reaching the lower-pressure amphibolite facies. The ore deposit has been severely deformed, folded and some of the ores have been remobilized. The rocks were folded in two phases, F_1 and F_2. F_1 was likely caused by diapiric uplift of synorogenic intrusions, and F_2 occurred before the emplacement of post-orogenic granites. The peak metamorphism occurred between the two folding phases. These folding phases gave the ore bodies their current shape, but the younger post-metamorphic faulting and shearing has cut the ore bodies into multiple parts. The major Metsämonttu fault has cut the deposition in two parts (Latvalahti 1979).

There are alteration zones around the deposit. The alteration types include dolomitization, magnesium-iron metasomatism, sericization and silicification. Generally, the rocks around the ores are depleted in sodium and the amount of magnesium, iron, manganese and titanium have increased. The degree of alteration in the rocks varies greatly (Latvalahti 1979). The alteration in the deposit can be divided into 5 assemblages. The first is K-Si-S alteration which contains muscovite + quartz ± biotite ± phlogopite + pyrite. The second is Si-S

alteration which contains quartz + pyrite ± muscovite. The third is Mg-Fe-S alteration which contains cordierite + anthophyllite ± biotite ± phlogopite + pyrite ± pyrrhotite. The fourth is Ca-Mg-K alteration which contains tremolite + diopside ± biotite ± phlogopite ± chlorite skarn. The fifth is Mg-Ca alteration in dolomitic marbles, which mainly consist of calcite, chlorite, diopside, dolomite, olivine and tremolite (Hokka et al. 2024).

The alteration around the deposit can be divided into two zones, inner and outer alteration zone. The outer alteration zone is characterized by sericization. There is internal heterogeneity in the alteration of the zone which is caused by the heterogeneity of the primary rocks and variety in the degree of alteration. The outer alteration zone is about 3 km long and extends to both Metsämonttu and Aijala, and the width varies between 0.5 and 100 m. The inner zone is characterized by magnesium-iron metasomatism, silicification and alteration of impure limestones into dolomitic limestones and chloritic tremolite-diopside skarns. Acidic tuffs have altered into cordierite-anthophyllite rocks and cordierite-biotite gneisses. Silicification of acidic rocks has resulted in the formation of quartz rocks. Wall rocks of the deposits typically contain quartz rocks and tremolite-diopside skarns. Cordierite-anthophyllite rocks and cordierite-biotite gneisses occur in alteration pipe below the ores and are related to the mineralization. The pipe extends to a depth of over 600 m and is about 100 to 200 m long and 50 to 100 m wide. There is a sharp contact with the underlying phenocrystic tuff (Latvalahti 1979).

5 Material and methods

5.1 Materials

The materials are from the drill core collection from Aijala and Metsämonttu (MM) area. The drill cores were drilled in 1959–1961 by Outokumpu Oy in the Metsämonttu mine area. A portion of the drill cores were selected for the subproject of a Battery mineral potential survey project by GTK that begun in 2019. The project focused on researching the applicability of handheld analyzers to data collection of brownfield targets. The material of the project contains over 500 drill cores. Measurements were made in the years 2019-2020 by GTK. The drill cores have a diameter of 22 mm and are very thin compared to standard modern drill cores. The drill cores are mostly in good condition. The drill cores MM-190, MM-196, MM-198 and MM-241 were chosen for this study since they were previously researched by Siira (2021) and there is already existing pXRD analysis available for comparison. EUREF-FIN coordinates were used for the sample locations and maps in this study.

All selected drill cores have been drilled 150–300 m south of Metsämonttu mine main building (Figure 13). The drill cores consist mostly of mafic and intermediate volcanic rocks, schist, limestones and skarns. Ore mineralizations are typically in or near skarn units.

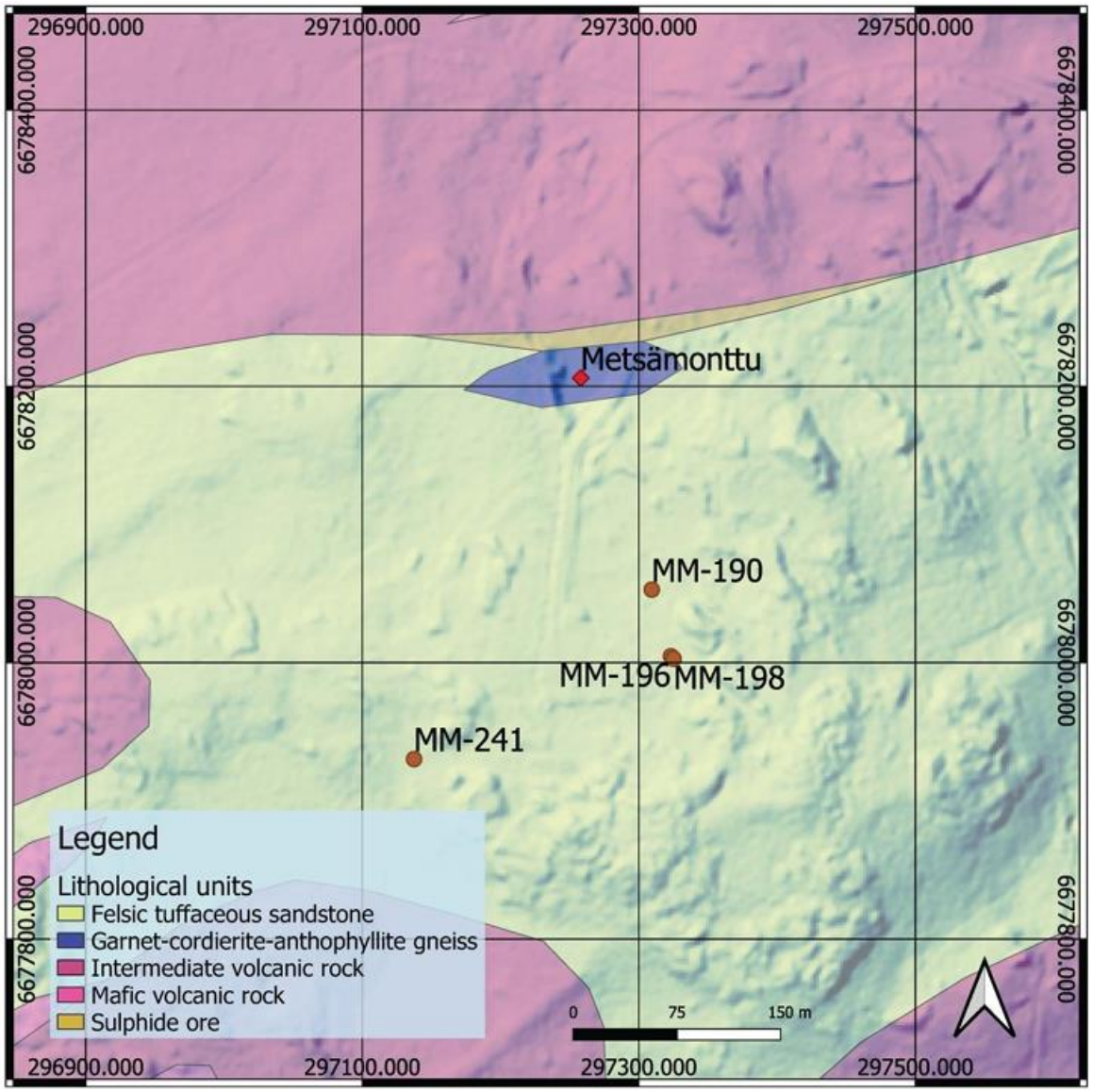

Figure 13. Map of the study area with drill core locations. (Siira [2021], Bedrock of Finland scale free, modified data © Geological Survey of Finland [2021]; CC BY 4.0, Hillshade 2 m, contains modified data from the National Land Survey of Finland Topographic Database 10/2021)

Lithologies of the selected drill cores (Figure 14) are based on original logging data by Outokumpu Oy (1959a–c, 1961) and new loggings made by GTK (Leväniemi, 2020). The archived drill core data was gathered by GTK in 2019. They digitized the data and during the process combined some of the lithological units that had been logged. It should be noticed that the lithologies here have been simplified, and some of the smaller lithologies have been merged into larger ones.

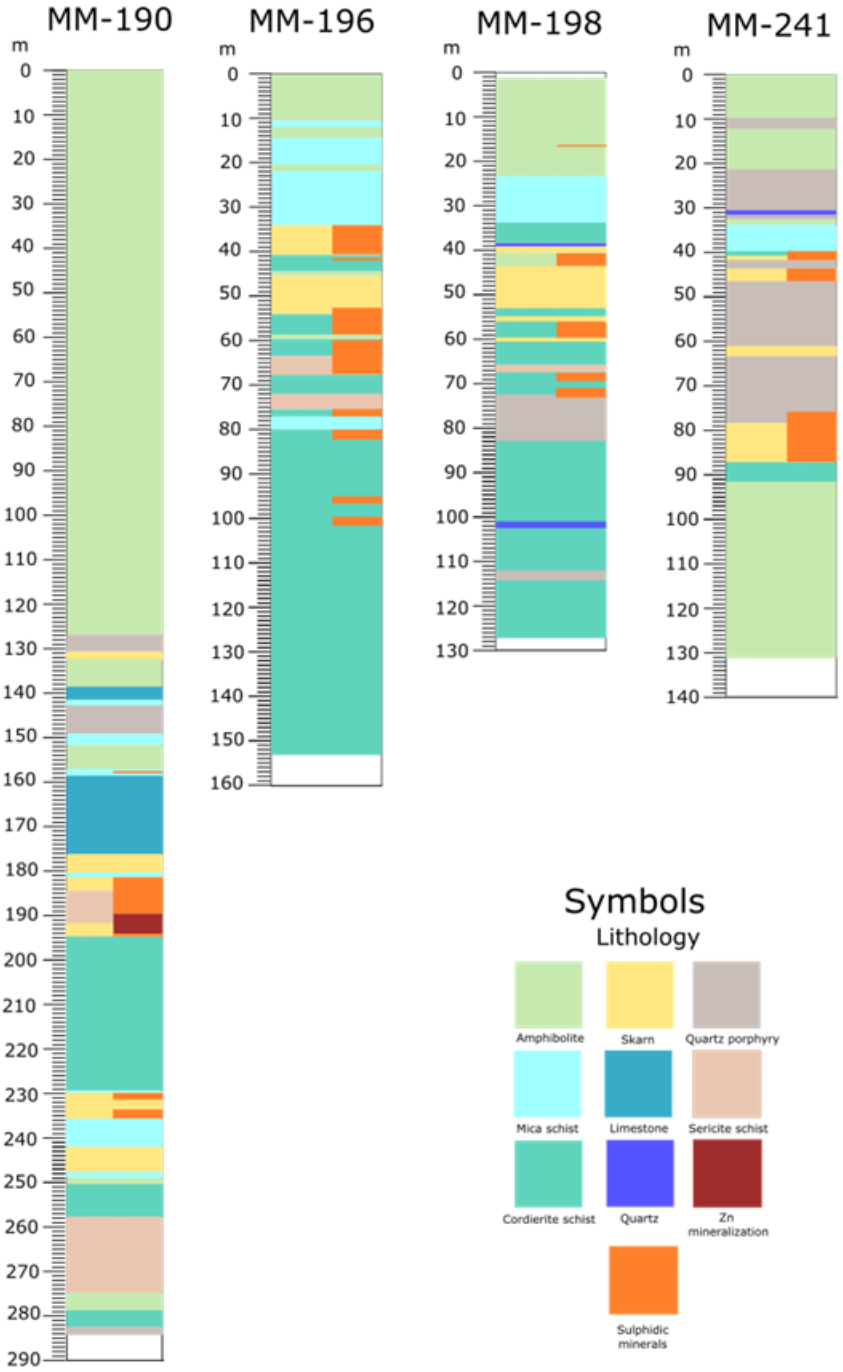

Figure 14. Lithologies of the selected drill cores (Siira 2021, drawing modified from the original drill core loggings by Outokumpu Oy [1959a–c, 1961] & new loggings by GTK [Leväniemi, 2020]).

5.1.1 Drill core MM190

The length of MM-190 is 284.4 m, and it was drilled from the +320 level (6678052.8544 N, 297309.3243 E, -255.62 Z EUREF-FIN). The azimuth of the drill core is 141.3225°. The dips of the core were 64.35° at 0 m, 56° at 95 m, 46.5° at 195 m and 30.5° at 284.4 m depth. Original logging of the core was done by geologist Arno Varma in 1959.

The drill core starts with a long amphibolite sequence, which is cut by a quartz porphyry and skarn units after the depth of 127.10 m. At this point the lithology changes to alternating amphibolite, skarn, quartz porphyry and mica schist sequences. At 176.20 m there is a sequence of altered limestone and skarn until 194.90 m with a 3.3 m long sericite schist sequence starting at 186.50 m. Some pyrite appears sparsely at the depth of 181.66–189.80 m. There is a Zn ore sequence at 189.80–194.03 m. After this there is a biotite-cordierite schist sequence at 194.90–229.20 m with some pyrite at 212.70–221.80 m and a tremolite rich skarn sequence at 229.20–235.72 m with some pyrite at the beginning and some galena near the end. At this point the lithology becomes more diverse in variety again, including units of mica schist, skarns, amphibolites, cordierite schist, quartz veins and sericite schist. The drill core ends with a 1.8 m long quartz porphyry sequence at the depth of 282.60 m.

5.1.2 Drill core MM196

The length of MM-196 is 153.6 m, and it was drilled from the +320 level (6678004.653 N, 297323.1769 E, -257.33 Z EUREF-FIN). The azimuth of the drill core is 162.0425°. The dips of the core were 49.33° at 0 m, 49° at 10 m, 49.2° at 25 m, 31° at 75 m and 14° at 153.6 m depth. Original logging of the core was done by geologist A. Stenberg in 1959.

The drill core begins with a sequence of varying amphibolite and mica schist units until the depth of 34.00 m. At this point the lithology changes to skarn until the depth of 40.60 m, and sulphidic ore minerals, mainly galena, pyrrhotite and pyrite start to occur dispersedly. At 40.60–44.30 m there is a sequence of brecciated cordierite schist with some galena and pyrite. There are a short sequence of amphibolite and a quartz vein at 44.30–45.30 m and then the rock changes to a skarn at 45.30–52.80 m with some pyrite and pyrrhotite. After this there is a sequence of alternating skarn and cordierite schist units until the depth of 58.75 m. There is some arsenopyrite at 52.8–53.20 m in cordierite schist and minor pyrrhotite at 53.20–54.00 m in skarn. At 54.0–54.30 m there is some arsenopyrite and at 56.90–58.75 m some pyrite, sphalerite, pyrrhotite and chalcopyrite in cordierite schist. Amphibolite vein without ore mineralization cuts the cordierite schist at the depth of 58.75–59.45 m. There is a sequence of alternating cordierite schist and sericite schist units beginning at the depth of 59.45 m with sulphide mineralizations at various depths. Sulphide ore mineralizations continues until the depth of 67.50 m. Sulphide ore minerals appear again at the depth of 75.25–77.82 m including pyrrhotite, sphalerite and chalcopyrite in cordierite schist. There is a mica schist sequence at 77.10–80.00 m. The rest of the drill core contains a sequence of cordierite schist until the

depth of 153.60 m. There are several sulphidic mineralization in this sequence until the depth of 101.45 m. The first one is at the depth of 80.10–82.20 m, containing chalcopyrite, pyrrhotite, sphalerite and galena. The next one is at the depth of 95.20–96.83 m, containing pyrite, sphalerite, and galena. The last one appears at the depth of 99.70–101.45 m, containing pyrite, galena and pyrrhotite.

5.1.3 Drill core MM198

The length of MM-198 is 127.4 m, and it was drilled from the +320 level (6678002.7762 N, 297325.1406 E, -254.56 Z EUREF-FIN). The azimuth of the drill core is 163.7992°. The dips of the core were -52.12° at 0 m, -45.5° at 30 m, -34.5° at 63 m and -23° at 127.4 m depth. Original logging of the core was done by geologist A. Stenberg in 1959.

The drill core begins with a sequence of amphibolite until the depth of 23.10 m. There is some arsenopyrite at the depth of 17.30 m. At 23.10–33.80 m there is a sequence of mica schist and at 33.80–38.30 m cordierite schist. There is a quartz vein at 38.30–39.10 m and then the rock changes to skarn at 39.10–40.70 m with some pyrite. There is an amphibolite sequence at 40.70–43.50 m with some pyrite and pyrrhotite grains. At 43.50 m the lithology changes to sequence of alternating skarn and cordierite schist units until the depth of 70.40 m. There is a short sericite-cordierite schist unit at 65.60–67.60 m. Some pyrite and pyrrhotite appears within cordierite schist at 55.40–59.45 m. There is a short quartz porphyry sequence at 70.40 m followed by amphibolite at 70.99 m. At 71.36 the lithology changes to sequence of alternating cordierite schist and quartz porphyry units until the end of the core at 127.40 m. A quartz vein appears at 101.35–102.55 m. Pyrite, pyrrhotite, sphalerite and chalcopyrite are present at 71.36–72.06 m in cordierite schist, and minor pyrite and galena at 72.06–72.90 m in quartz porphyry.

5.1.4 Drill core MM241

The length of MM-241 is 131.4 m, and it was drilled from the +510 level (6677930.3753 N, 297137.3862 E, -441.82 Z EUREF-FIN). The azimuth of the drill core is probably 163.0325°, but the writing in the drilling report is unclear. The dips of the core were 50.26° at 0 m, 38° at 50 m, 38° at 90 m and 36° at 131.4 m depth. Original logging of the core was done by geologist A. Stenberg in 1961.

The drill core begins with amphibolite sequence until the depth of 21.55 m, which is cut by a quartz porphyry at 9.70–12.17 m. At 21.55 m the drill core continues with sequences of quartz porphyry, amphibolite and mica schist without any sulphide mineralization until the depth of 39.90 m. At 39.90 m the lithology changes to cordierite schist with some pyrite and pyrrhotite until the depth of 40.75 m. At 40.75–87.08 m there is a sequence of alternating skarn and quartz porphyry. Some pyrite appears at 40.75–41.51 m and some galena at 44.76–46.40 m in skarn. Some sphalerite, galena and pyrite appear at 75.90–78.15 m in quartz porphyry. The skarn unit at 78.15 m–87.08 m contains galena, sphalerite and chalcopyrite at various depths. There is no sulphidic mineralizations after 87.08 m. The lithology changes to cordierite schist at 87.08 m and then to amphibolite at 91.50 m until the end of the core at 131.40 m.

5.2 Methods

5.2.1 Sample collecting and procedures

Selected drill cores were measured with pXRD and pXRF analyzers by GTK. Petrophysical and geochemical samples were taken from the drill cores as well. Only pXRD data was utilized in this study. Leväniemi et al. (2020) describes the measurements and sample preparation procedures in detail. The measurements were done in 2019–2020 by GTK.

5.2.2 Portable XRD measurements

The measurements were done with Olympus Terra-542 pXRD device. It weighs 14.5 kg, and a cobalt X-ray tube was used as the radiation generator. The device has 1024x256 pixel 2D charge-coupled device sensor with a Peltier cooler. The device works with both mains power and battery with the power supply of around 4 hours. The functional temperature range of the device is -10°–35°C. The XRD resolution was 0.25° 2θ FWHM and the angular resolution was 5-55° 2θ. The device does not contain moving parts, but the sample is rotated by vibrating sample holder. In laboratory XRD devices the sample remains stationary, but the parts of the device are moving during the measurement.

Sample interval for the pXRD was 10 m with a total of 268 samples. Some additional occasional measurements were done for mineral analysis as well. The 10 m sample interval was chosen as the sample preparation process was somewhat time consuming. pXRD samples were drilled from the drill core rock surface with diamond drill from around 1x2 cm area. The

sample was gathered on a piece of paper from which it was moved on a sieve. The sample powder was sieved to <150 µm particle size and the sieved powder was inserted into the measuring chamber. The optimal sample amount for the measurement was 15 mg, and it was estimated visually as the measurement chamber should be about half-filled. Some free space was required so that the material rotates properly during the measurement. The sampled powder was dry so that the particles would not stick together.

The measurement time was kept standard, samples containing sulphides were measured with 150 hits and other samples with 85 hits. Sulphide samples demanded longer measurement times due to fluorescence, especially if they contained galena (Figure 41). Measurements with 85 hits took about 25 minutes including sample preparation. This was enough to detect 3–5 mineral phases on average. The measurement chamber was cleaned with pressured air after each measurement and possibly with alcohol if the sample contained sulphides. Quality assurance was made using quartz standard. Quartz powder standard was measured atleast once per day or every 10^{th} measurement. The quartz sample measurements were compared to check the fidelity of peak locations and intensities and detect any possible sources of error. If needed, other mineral samples (Chemplex) were used for quality control in addition to quartz standard.

5.2.3 Portable XRD analysis

The pXRD data was analyzed using DIFFRAC.EVA version 6.0.7. Data from the samples was imported to the software for each drill hole. Clustering was made for each drill hole data set individually. Based on the resulting clusters, each sample was analyzed using the diffractometer and DIFFRAC.EVA's free crystallography open database. The software gave a list of suggested minerals. Based on the peak profile of the sample and the peak patterns of suggested minerals, the most likely present minerals were selected. After individual drill hole analyses, all of the data was imported in one data set, and clustering was made for all samples at once. For samples with multiple measurements, only the original one was selected for the clustering to avoid having two measurements of the same sample in the dendogram as in most cases the diffractogram for each measurement looked almost identical. The logging report from GTK was used to compare the analysis results with the logged rock types and minerals.

6 Results

6.1 The analysis software limitations

The software is not able to reliably distinguish plagioclase feldspar group minerals from each other (Appendix 13). Only one is selected for each sample to keep the diffractogram readable. As with plagioclase feldspars, the software is mostly not able to distinguish specific K-feldspars from each other (Appendix 12) and usually suggests multiple with similar peak patterns. The software is also not able to clearly distinguish most amphiboles like actinolite (act), tremolite (tr) or hornblende (hbl) from each other (Appendix 15). One exception is cummingtonite which usually seems to have enough different peak pattern.

In most cases the software is not able to clearly distinguish chlorite group minerals from each other and often suggests both chlorite (chl) and clinochlore (clc) (Appendix 16). In some cases, chamosite (chm) is detected with or without the other chlorite minerals. In addition, the software is not able to distinguish mica mineral biotite (bt) from phlogopite (phl) and usually suggests both at the same time (Apppendix 14). The same applies to muscovite (ms) and phengite (phg). The software is usually not able to clearly distinguish different pyroxenes and often suggests atleast both diopside (di) and augite (aug) (Appendix 17).

Some samples have messy or spiky backgrounds, likely because of sulphide minerals. These samples are challenging to analyze and sometimes only one or two minerals are clearly detectable. The software is also not able to match minerals to some of the peaks at the left side of the diffractograms, which likely represent clay minerals.

6.2 Drill core MM190

28 samples were available for the drill core MM190. The samples were taken in 10 m intervals. The samples were drilled south from Metsämonttu deposit. The samples were analyzed and clustered using the DIFRAC.EVA software.

6.2.1 Cluster 1

This cluster contains 3 samples (Figure 15 & Table 1). All the samples in this cluster contain amphibolite according to the logging report. Based on the analysis, each sample contains quartz and prehnite. Chlorite minerals are also detected in each sample. The diffractogram of

the sample MM190_35 can be seen on Figure 16 and it represents the typical peak profile in this cluster.

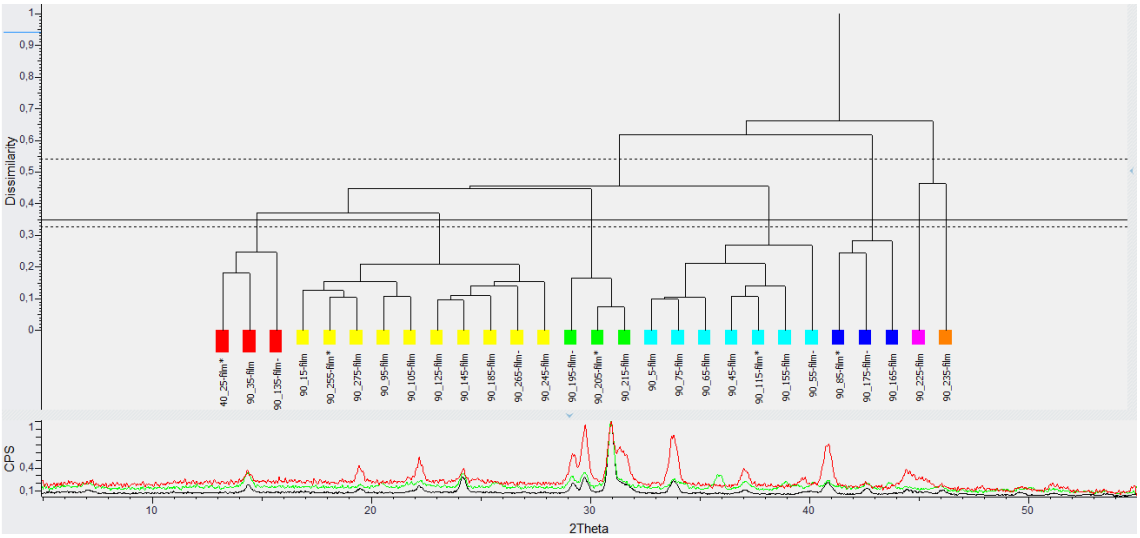

Figure 15. Dendogram of the drill core MM190 with cluster 1 (red) highlighted. Combined diffractograms of the cluster 1 are at the bottom of the figure. The sample MM190_25 has been mistakenly named MM140_25 in the original GTK files.

Table 1. Details of the cluster 1 of MM190. “GTK rock type” refers to the rock type stated by the GTK logging report at the certain depth interval. “GTK minerals” refers to any specific minerals noted by the GTK logging report in the depth interval. “Detected minerals” refers to minerals that have been detected with high confidence based on the sample peak profile and list of suggested minerals given by the DIFFRAC.EVA software. “Possibly detected minerals” refers to minerals that could possibly be present based on the peak profile, the software mineral suggestions and the stated rock type by GTK, but the peaks for the mineral are weaker or not as clearly matching, or the mineral has shared peaks with another mineral that is more certainly present.

Sample	Depth interval (m)	GTK rock type	GTK minerals	Detected minerals	Possibly detected minerals
MM190_25	20.80–26.30	Amphibolite		Quartz, Prehnite, Chlorites (clc)	
MM190_35	26.30–49.80	Amphibolite		Quartz, Epidotes, Prehnite, Chlorites (chm)	Babingtonite
MM190_135	132.50–138.80	Amphibolite		Quartz, Prehnite, Chlorites (clc / chl)	

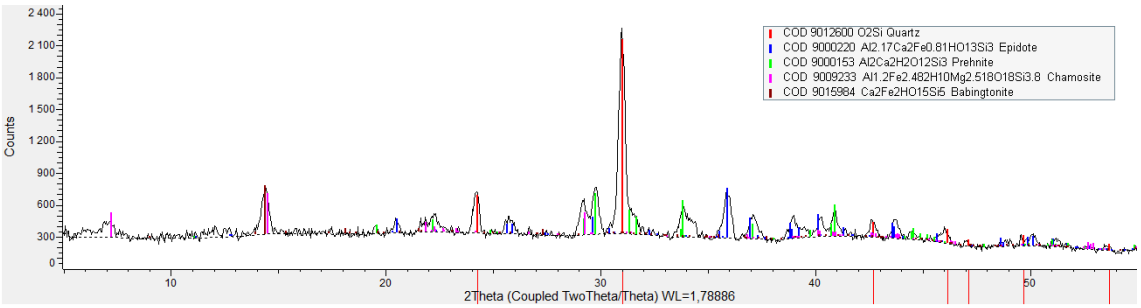

Figure 16. The diffractogram of the sample MM190_35.

6.2.2 Cluster 2

This cluster contains 10 samples (Figure 17 & Table 2). Majority of the rock types stated by the logging report are amphibolite or other rock types where quartz and feldspars are major minerals. Couple of the samples contain schist or skarn. Based on the analysis, all of the samples contain quartz and most of them clearly contain plagioclase feldspars. Other minerals vary much in each sample, but micas, amphiboles, chlorite minerals and pyroxenes are present in many of the samples. There are indications of the presence of sulphides in some samples even though they are not mentioned in the logging report. In couple of the samples, it was challenging to match any logical minerals to some of the smaller peaks. On MM190_185 quartz dominates the peak profile, and other peaks are very low. The sample could possibly be from a quartz vein for example, but the logging report is not detailed enough to confirm that. On MM190_185 the only suggested plagioclase mineral was anorthite. Chlorite was not detected in MM190_245, cordierite was not detected in MM190_255 and MM190_265 and cummingtonite was not detected in MM190_105 although they are mentioned in the logging report. Sulphides were not detected in MM190_185. Diffractograms of selected samples in the cluster can be seen in Figures 18–22.

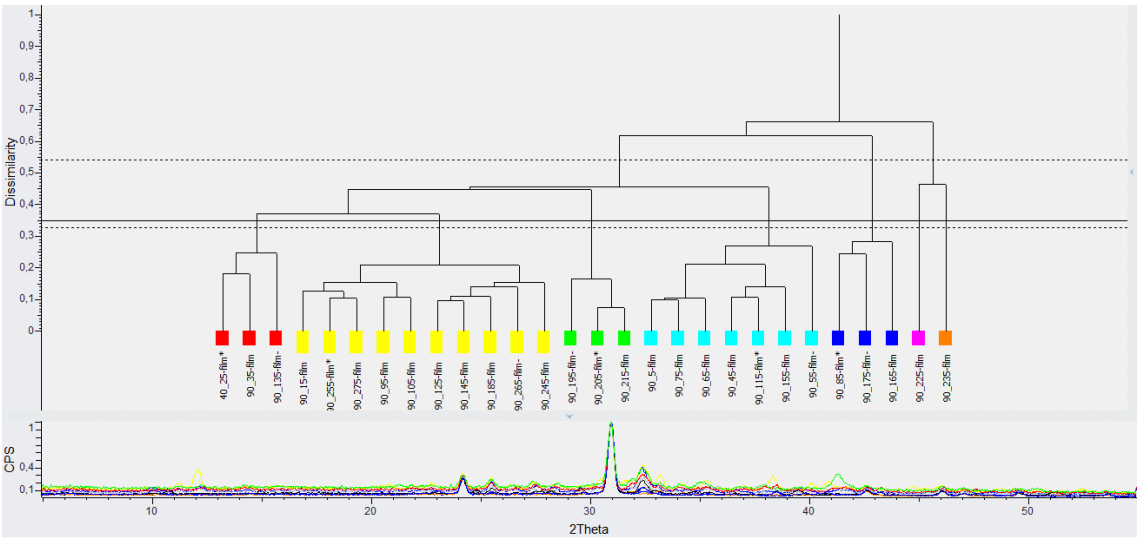

Figure 17. Dendogram of the drill core MM190 with the cluster 2 (yellow) highlighted. Combined diffractograms of the cluster 2 are at the bottom of the figure.

Table 2. Details of the cluster 2.

Sample	Depth interval (m)	GTK rock type	GTK minerals	Detected minerals	Possibly detected minerals
MM190_15	14.30–20.80	Amphibolite		Quartz, Plagioclases, Micas (bt / phl), Amphiboles (act / tr / hbl)	Cordierite
MM190_255	254.90–257.80	Cordierite gneiss		Quartz, Plagioclases, Pyrite	Amphiboles (cummingtonite), Ilmenite
MM190_275	274.40–278.60	Amphibolite	Cummingtonite	Quartz, Plagioclases, Magnetite	Amphiboles (cummingtonite), Ilmenite
MM190_95	49.80–101.80	Amphibolite		Quartz, Amphiboles (act / tr / hbl), Plagioclases	
MM190_105	101.80–111.50	Amphibolite	Cummingtonite	Quartz, Amphiboles (act / tr / hbl), Plagioclases	Pyroxenes, Cordierite
MM190_125	111.50–127.10	Amphibolite		Quartz, Plagioclases	Anatase, Laumontite
MM190_145	142.60–148.90	Quartz feldspar schist		Quartz, Plagioclases	Micas (bt / phl)
MM190_185	184.92–186.50	Skarn	Quartz, Feldspars, Sulphides	Quartz, Plagioclases	Calcite
MM190_265	257.80–274.40	Sericite schist	Cordierite	Quartz, Micas (bt / phl + ms / phg), Pyrite	Plagioclases
MM190_245	241.90–247.60	Skarn chlorite schist		Quartz, Plagioclases, Pyrite, Pyrrhotite	Micas (ms)

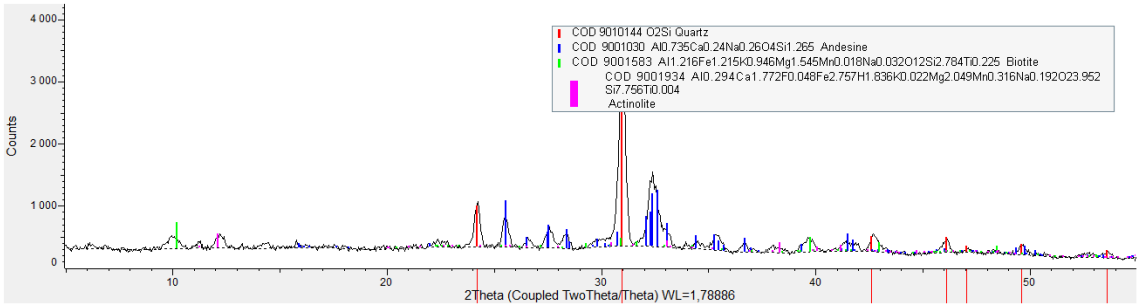

Figure 18. Diffractogram of the sample MM190_15. This diffractogram represents a basic amphibolite rock in the cluster.

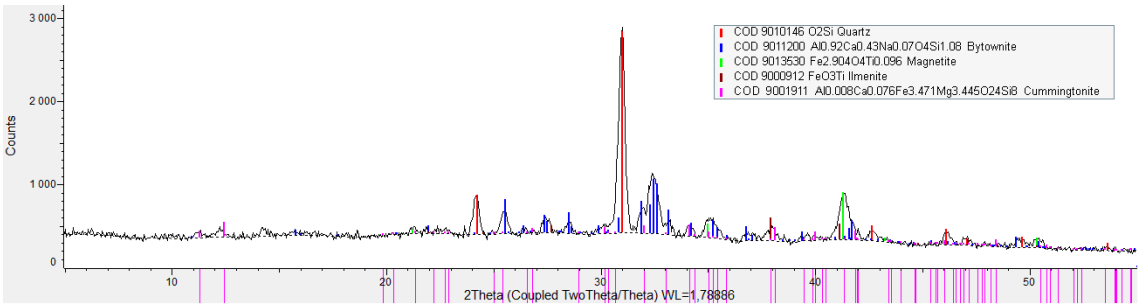

Figure 19. Diffractogram of the sample MM190_275. This diffractogram represents a potentially magnetite-bearing rock.

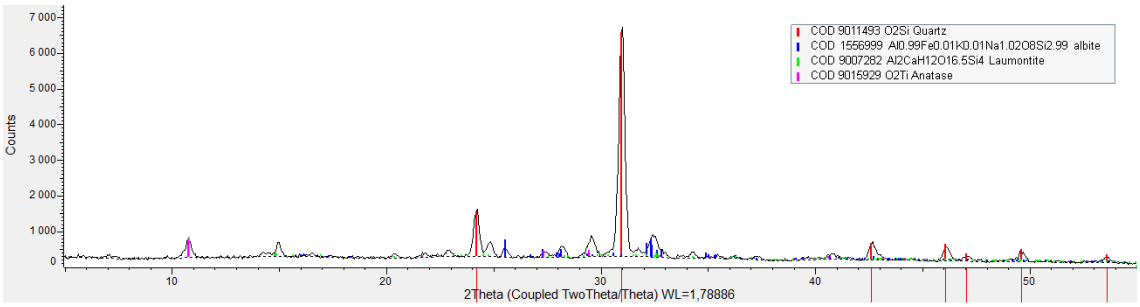

Figure 20. Diffractogram of the sample MM190_125. This sample only certainly contains quarts and plagioclase minerals.

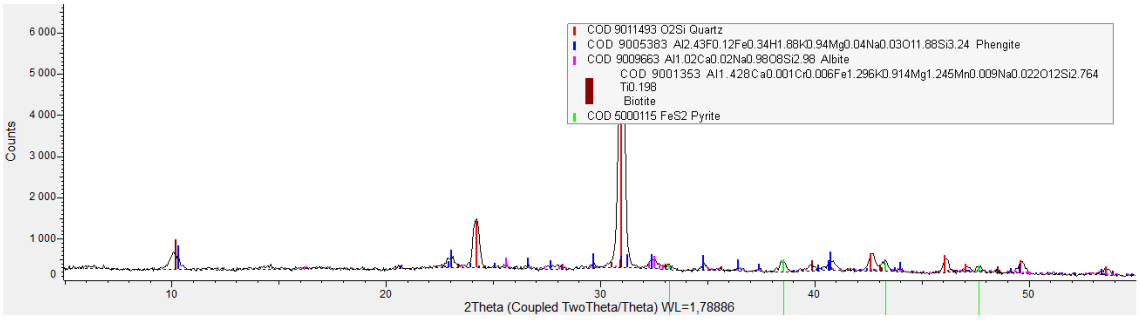

Figure 21. Diffractogram of the sample MM190_265. This diffractogram represents pyrite bearing rock.

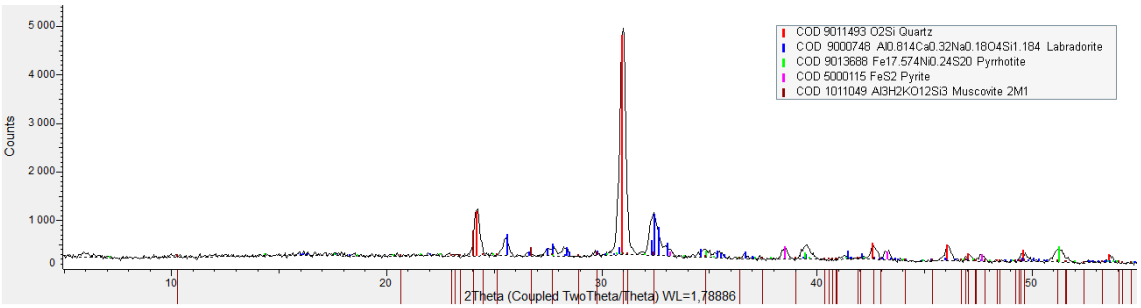

Figure 22. Diffractogram of the sample MM190_245. This diffractogram represents pyrite and pyrrhotite bearing rock.

6.2.3 Cluster 3

This cluster contains 3 samples (Figure 23 & Table 3). All of the samples in this cluster contain biotite cordierite anthophyllite quartz schist according to the logging report and the samples are from the same part of the drill core. Based on the analysis, all of the samples contain cordierite, anthophyllite, micas and likely quartz. Occasional sulphide minerals are possibly present. On MM190_205 the clinochlore peak profile bars act weirdly. If the mineral is not activated on the list (Figure 26), the bars fit the peak profile very well, but if the mineral is activated on the list (Figure 25), the bars grow much higher. This “clinochlore anomaly” happens on some other samples as well. On MM190_195 (Appendix 2) quartz fits to the peak profile, but the peaks are shared with other minerals present. No anthophyllite was detected on MM190_205 although it is mentioned in the logging report. The software seemingly detects pyrrhotite on MM190_215, but no pyrite or anthophyllite. Diffractograms of the samples can be seen in Figures 24–26.

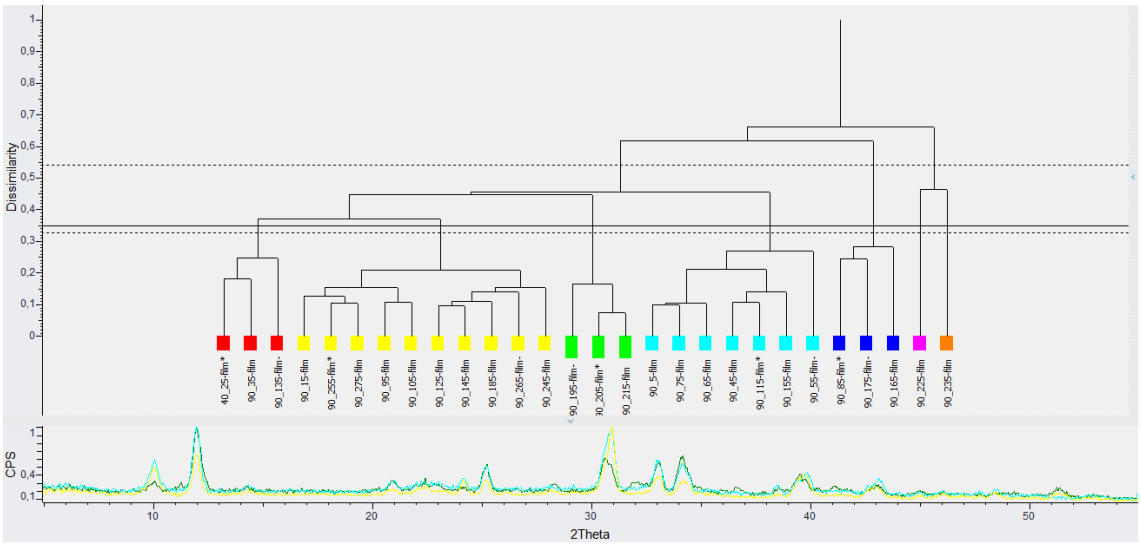

Figure 23. Dendogram of the drill core MM190 with the cluster 3 (green) highlighted. Combined diffractograms of the cluster 3 are at the bottom of the figure.

Table 3. Details of cluster 3

Sample	Depth interval (m)	GTK rock type	GTK minerals	Detected minerals	Possibly detected minerals
MM190_195	194.90–212.70	Cordierite schist	Biotite, Quartz, Anthophyllite	Cordierite, Anthophyllite, Micas (bt / phl), Pyrrhotite	Quartz
MM190_205	194.90–212.70	Cordierite schist	Biotite, Quartz, Anthophyllite	Cordierite, Quartz, Micas (bt / phl), Chlorites (clc)	
MM190_215	212.70–221.80	Cordierite schist	Biotite, Cordierite, Anthophyllite, Pyrite	Cordierite, Quartz, Micas (bt / phl)	Pyrrhotite

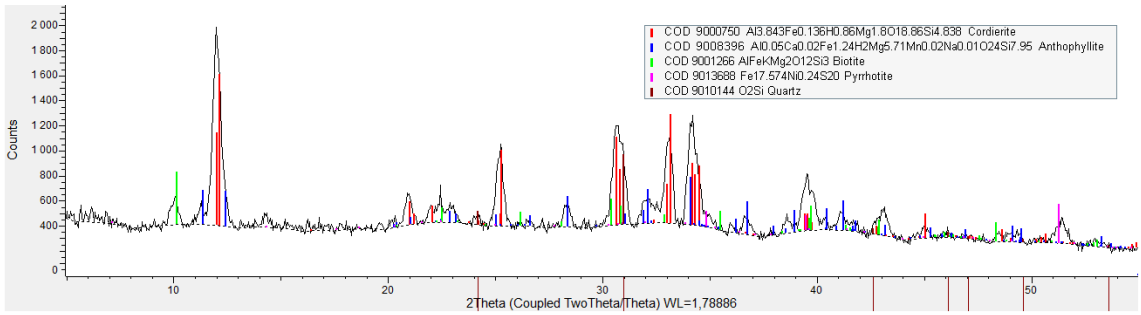

Figure 24. Diffractogram of the sample MM190_195. This diffractogram represents sample with both cordierite and anthophyllite in the cluster.

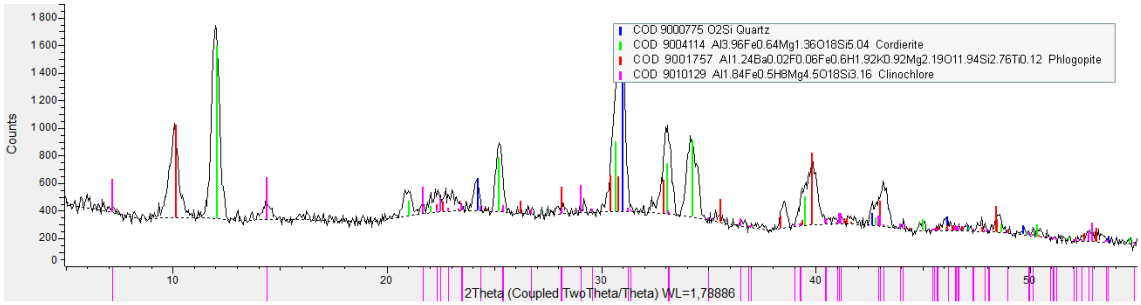

Figure 25. Diffractogram of the sample MM190_205 with clinochlore activated.

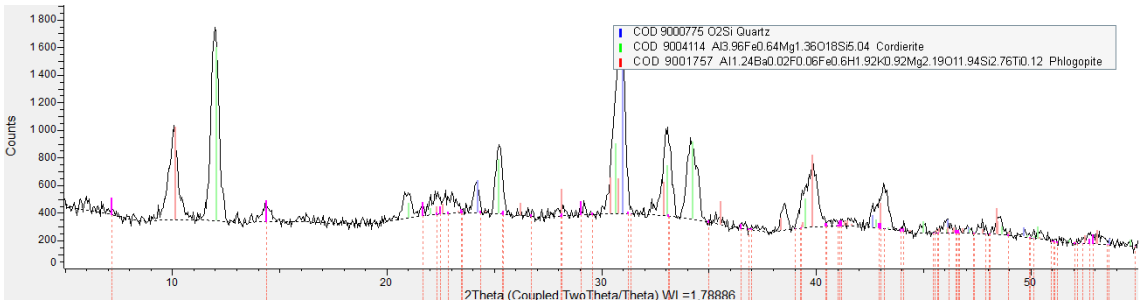

Figure 26. Diffractogram of the sample MM190_205 with clicnochlore not activated.

6.2.4 Cluster 4

This cluster contains 7 samples (Figure 27 & Table 4). All of the samples in this cluster contain amphibolite according to the logging report. Based on the analysis, all of the samples contain amphibole and plagioclase minerals, while the presence of quartz is not fully certain in every sample. Cordierite fits into the peak profile of couple samples, but the peaks share locations with other minerals present, so it is not certain if the samples also contain cordierite or not. MM190_55 is the only sample that clearly also contains chlorite minerals, but according to the dendogram, it is also the most different compared to the other samples in the cluster. Garnet was not detected on MM190_5 although it is mentioned in the logging report. Diffractograms of the selected samples can be seen in Figures 28–29.

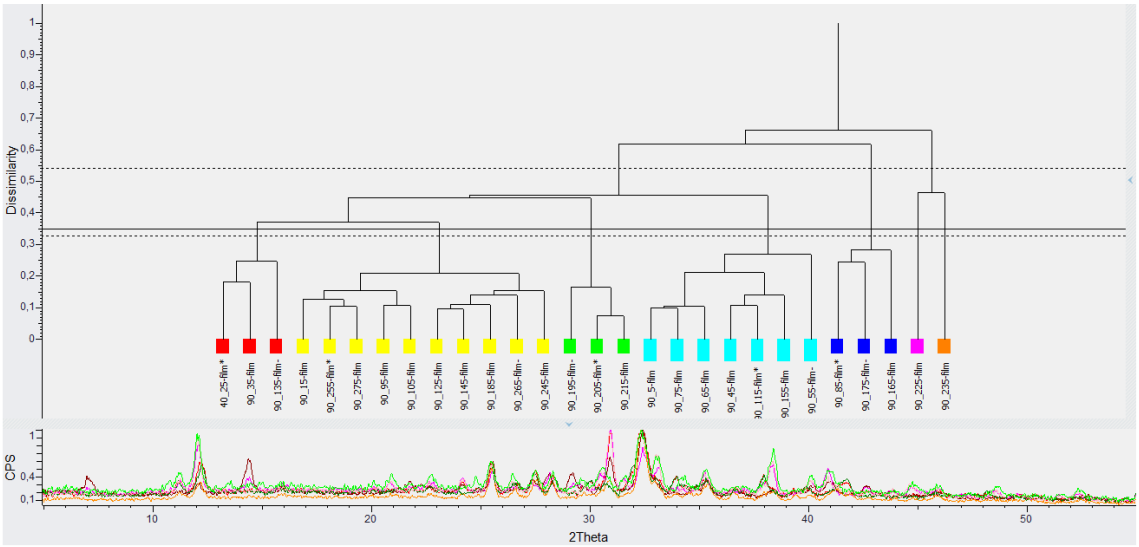

Figure 27. Dendogram of the drill core MM190 with cluster 4 (cyan) highlighted. Combined diffractograms of cluster 4 are at the bottom of the figure.

Table 4. Details of the cluster 4.

Sample	Depth interval (m)	GTK rock type	GTK minerals	Detected minerals	Possibly detected minerals
MM190_5	1.80–10.00	Amphibolite	Garnet	Plagioclases, Quartz, Amphiboles (cummingtonite)	Cordierite
MM190_75	49.80–101.80	Amphibolite		Plagioclases, Amphiboles (cummingtonite + act / tr / hbl)	Cordierite
MM190_65	49.80–101.80	Amphibolite		Plagioclases, Amphiboles (cummingtonite + act / tr / hbl)	Quartz
MM190_45	26.30–49.80	Amphibolite		Quartz, Amphiboles (act / tr / hbl), Plagioclases	Chlorites (clc)
MM190_115	111.50–127.10	Amphibolite with some skarn		Amphiboles (act / tr / hbl), Plagioclases, Quartz	
MM190_155	151.80–157.30	Amphibolite		Amphiboles (act / tr / hbl), Plagioclases	Cordierite
MM190_55	49.80–101.80	Amphibolite		Amphiboles (act / tr / hbl), Plagioclases, Quartz, Chlorites (clc / chl)	

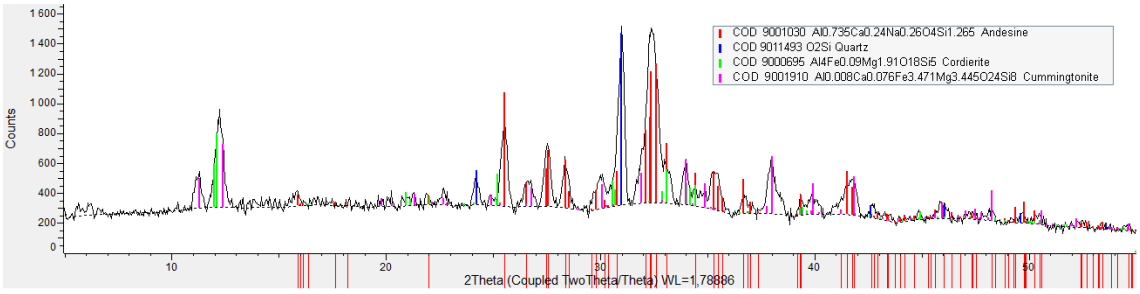

Figure 28. Diffractogram of the sample MM190_5. This diffractogram represents an average, possibly cordierite bearing sample in the cluster with clear quartz peak.

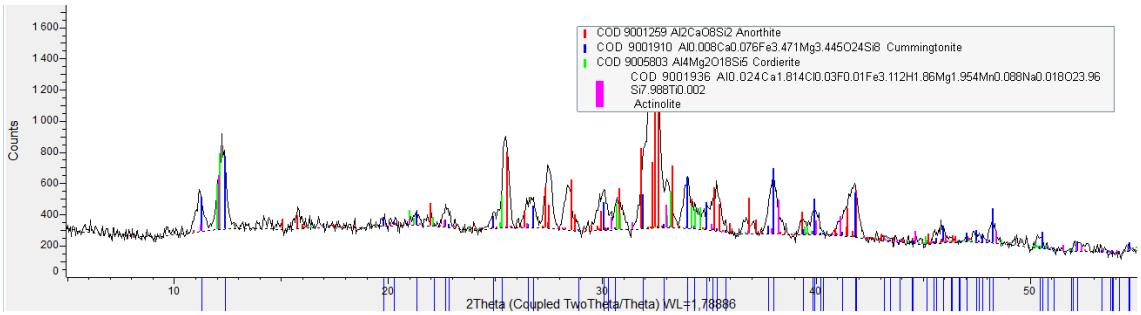

Figure 29. Diffractogram of the sample MM190_75. This diffractogram represents an average, possibly cordierite bearing sample in the cluster without quartz.

6.2.5 Cluster 5

This cluster contains 3 samples (Figure 30 & Table 5). All of the samples in this cluster contain limestone according to the logging report, with the exception of MM190_85, which contains amphibolite with narrow calcite zones. Based on the analysis, all of the samples contain calcite, but other minerals vary between samples. MM190_175 and MM190_165 both contain amphibole minerals and other minerals typical in limestones. Only MM190_165 contains dolomite. MM190_85 contains pyroxene and epidote minerals. In MM190_175 only chalcopyrite fitted one smaller peak, but the main peak of chalcopyrite was shared with calcite. It was somewhat challenging to match all peaks to logical minerals on MM190_175. Diffractograms of the samples can be seen in Figures 31–33.

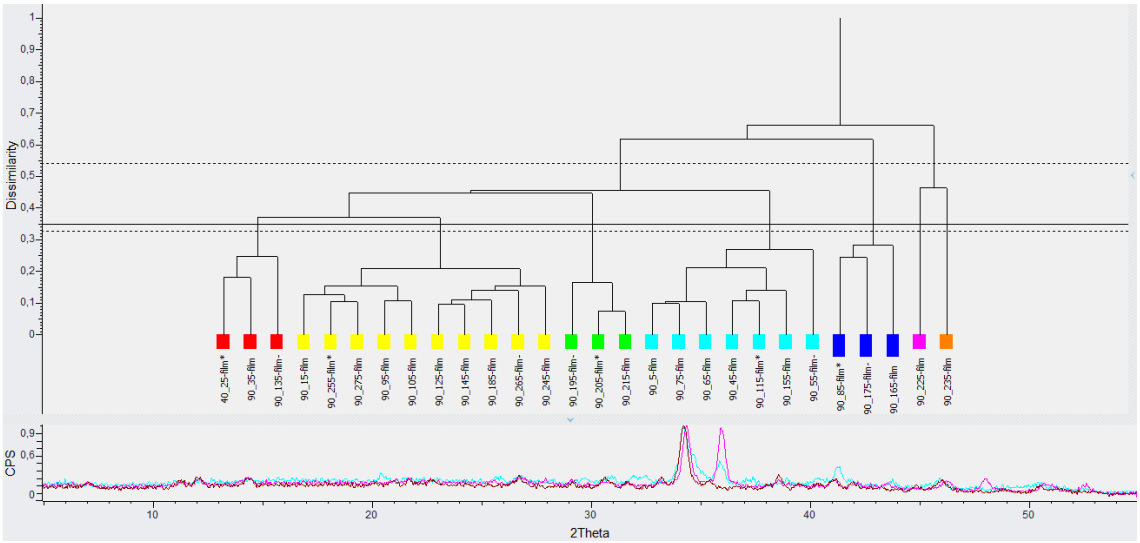

Figure 30. Dendogram of the drill core MM190 with cluster 5 (blue) highlighted. Combined diffractograms of the samples are at the bottom of the figure.

Table 5. Details of cluster 5 samples.

Sample	Depth interval (m)	GTK rock type	GTK minerals	Detected minerals	Possibly detected minerals
MM190_85	49.80–101.80	Amphibolite	Occasional narrow Calcite zones	Pyroxenes (di / aug), Epidote, Calcite	Plagioclases
MM190_175	158.40–176.20	Limestone		Amphiboles (act / tr / hbl), Calcite	Cronstedtite, Chalcopyrite
MM190_165	158.40–176.20	Limestone		Calcite, Dolomite, Amphiboles (act / tr / hbl / pargasite), Chlorites (clc / chm / penninite)	Pyrrhotite

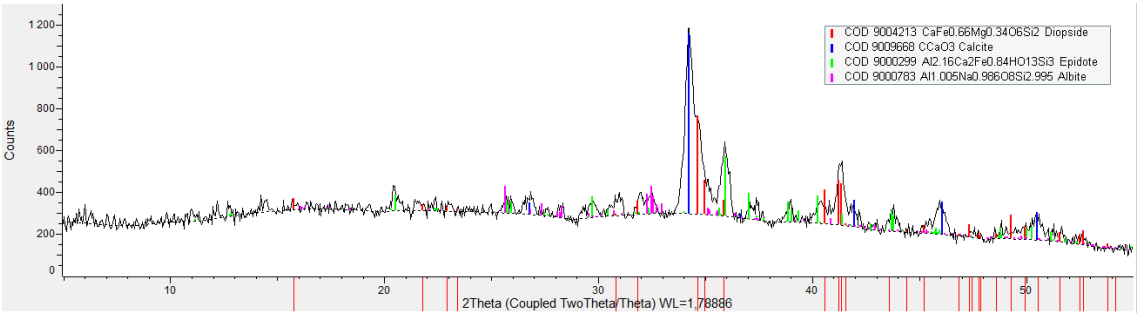

Figure 31. Diffractogram of the sample MM190_85. Calcite is clearly detected in this sample.

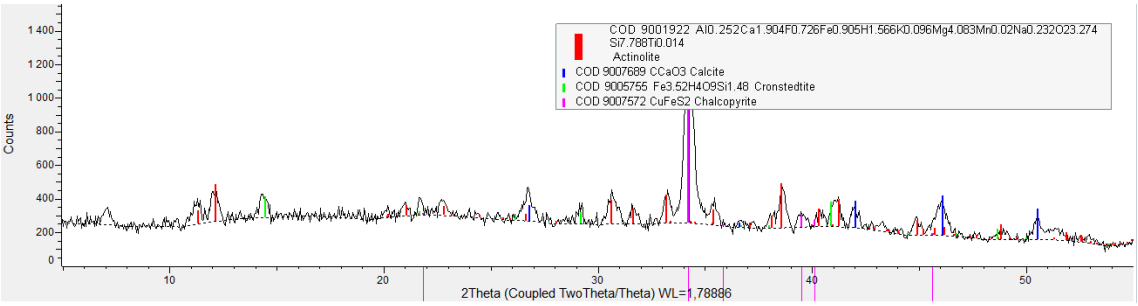

Figure 32. Diffractogram of the sample MM190_175. Only calcite and amphibole minerals are clearly detected.

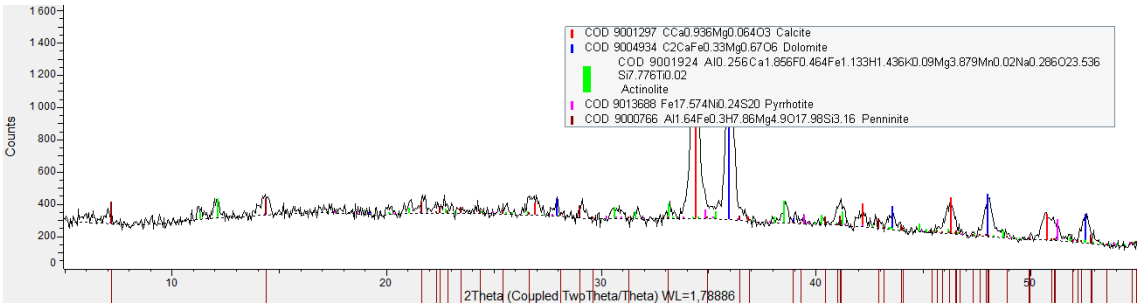

Figure 33. Diffractogram of the sample MM190_165. This sample contains both calcite and dolomite.

6.2.6 Singular samples without cluster

The sample MM190_225 has two different measurements (Table 6). The first one had measurement time of 850 seconds, and the "b" measurement was measured for 1500 seconds. The diffractograms are very messy and challenging to analyze (Figure 34). It was challenging to match many of the peaks with any logical minerals possibly present in biotite cordierite schist. No major differences in peak profiles or mineral suggestions by the software between the two measurements. The sample likely contains sulphides and altered minerals. Many manganese related minerals were suggested, which matches the peaks very well, but do not match the sample rock type. These include hausmannite, gaudefroyite and bixbyite. Also, it suggests various chromite rich minerals, which do not match the rock type. The sample could contain some clay minerals as there are multiple peaks near the left side of the diffractogram, or minerals formed by alteration or weathering as the software suggested such minerals, many of which did not seem logical to be present in this rock type. Picture of the drill core can be seen in Appendix 3.

Table 6. Details of the samples MM190_225 and MM190_225b.

Sample	Depth interval (m)	GTK rock type	GTK minerals	Detected minerals	Possibly detected minerals
MM190_225 + MM190_225b	221.80–229.20	Biotite cordierite schist	Chlorite	Pyrite, Pyrrhotite	Analcime, Spinel, Xenotime

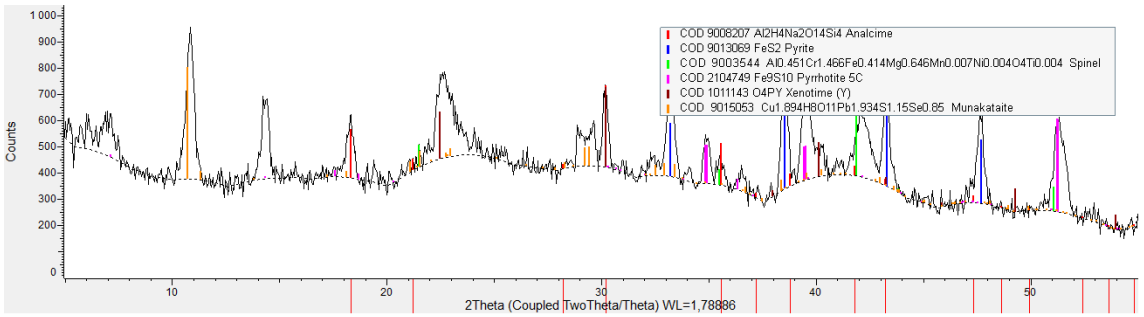

Figure 34. Diffractogram of the sample MM190_225. The background of the diffractogram is somewhat messy and high and it was not possible to match suitable minerals to some of the peaks.

The sample MM190_235 contains tremolite skarn and possibly galena according to the logging report (Table 7). Based on the analysis, this sample contains minerals typical for skarn. For amphibole minerals the software suggests atleast actinolite, hornblende and pargasite in addition to tremolite, and tremolite was in fact quite low on the list. The software was able to detect pyrrhotite but not galena (Figure 35).

Table 7. Details of the sample MM190_235.

Sample	Depth interval (m)	GTK rock type	GTK minerals	Detected minerals	Possibly detected minerals
MM190_235	233.90–235.72	Tremolite skarn	Galena	Amphiboles (act / tr / hbl), Chlorites (clc / chl), Pyrrhotite	

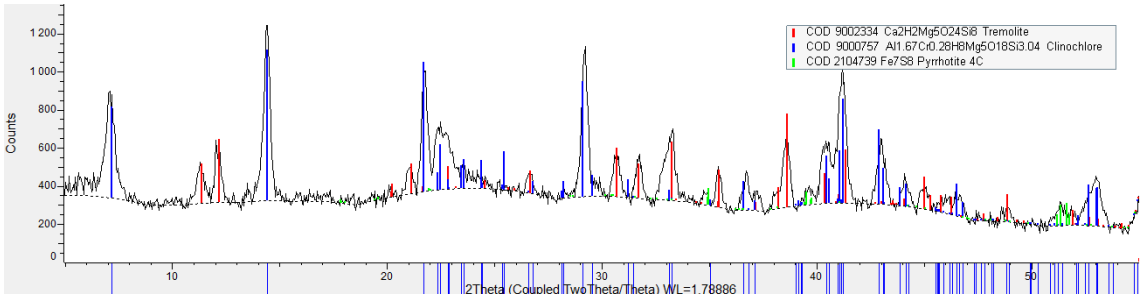

Figure 35. Diffractogram of the sample MM190_235.

6.3 Drill Core MM196

21 samples were available for the drill core MM196. Most of the samples were taken in about 10 m intervals. In addition, some samples were taken from specific depths of the drill core. The samples were drilled south from Metsämonttu deposit and south of the drill core MM190. The samples were analyzed and clustered using the DIFRAC.EVA software.

6.3.1 Cluster 1

This cluster contains only 2 samples (Figure 36 & Table 8). Both of the samples in this cluster contain amphibolite according to the logging report. Based on the analysis, both of the samples contain plagioclase minerals and pyroxenes, likely diopside. Both of the samples possibly contain micas as well. MM196_003 clearly contains amphibole minerals while MM196_013 does not have clear signal for amphibole minerals and there are some other differences in the possible mineral composition too. MM196_013 (Figure 38) also has much more spiky background than MM196_003 (Figure 37), making it challenging to match all peaks with suitable minerals. No suitable sulphides match the peak profile on MM196_013 to explain the messy background. MM196_003 has two measurements, but 003b has lower quality peak profile even though the “b” measurement had longer measurement time. MM196_003 has the “clinochlore anomaly” but it doesn’t happen if activating chlorite instead. On MM196_013 clay minerals are also possibly present as there are peaks near the left side of the diffractogram.

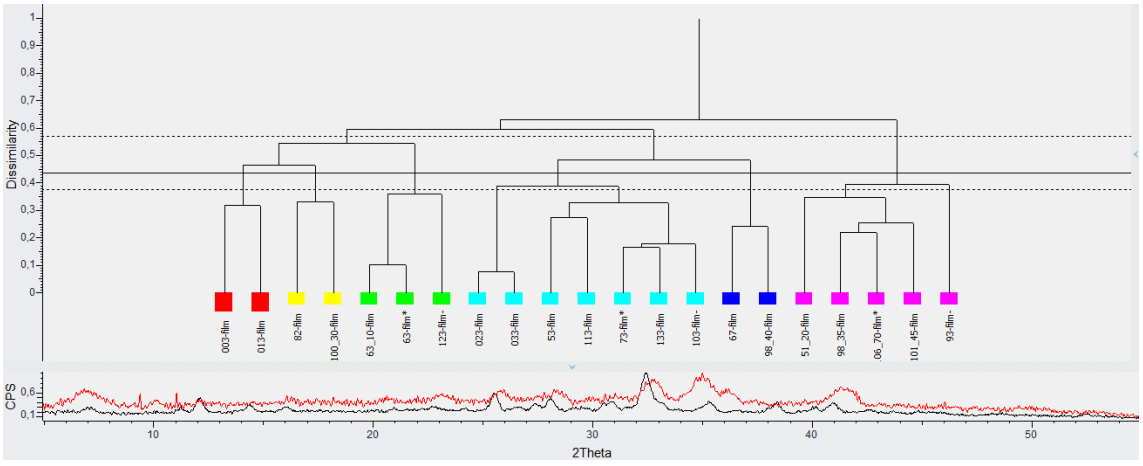

Figure 36. Dendogram of the drill core MM196 with cluster 1 (red) highlighted. Combined diffractograms of cluster 1 are at the bottom of the figure.

Table 8. Details of the cluster 1 samples.

Sample	Depth interval (m)	GTK rock type	GTK minerals	Detected minerals	Possibly detected minerals
MM196_003 + MM196_003b	0.80–10.60	Diopside amphibolite		Plagioclases, Amphiboles (act / tr / hbl), Chlorites (clc / chl)	Quartz, Pyroxenes (di)
MM196_013	12.00–14.20	Amphibolite		Plagioclases, Pyroxenes (di), Micas (phl + phg)	Calcite

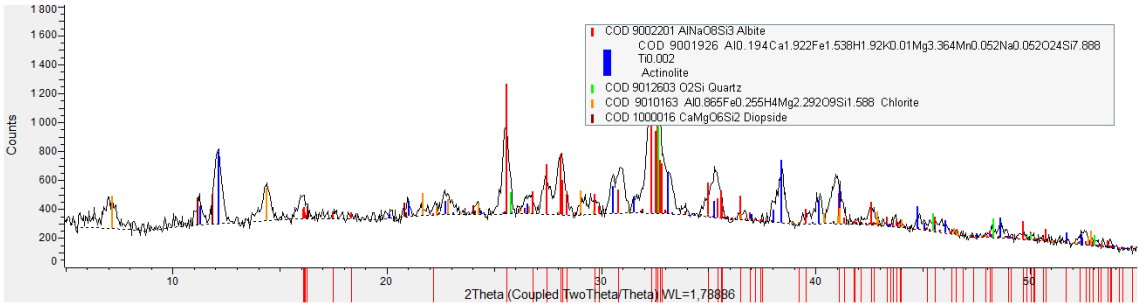

Figure 37. Diffractogram of the sample MM196_003. Quartz fits into the peak profile but is not needed to fill the peaks.

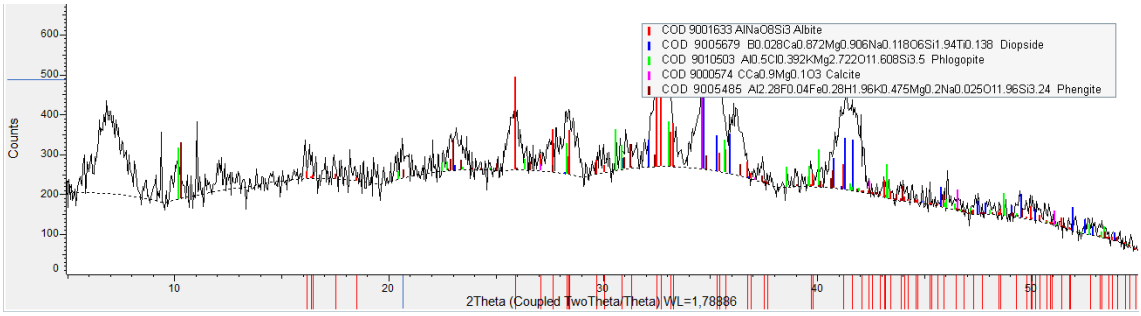

Figure 38. Diffractogram of the sample MM196_013. The background is very spiky, and the real peaks do not stand out well from the background.

6.3.2 Cluster 2

This cluster contains only 2 samples (Figure 39 & Table 9). Both of the samples in this cluster contain cordierite schist/gneiss according to the logging report. Based on the analysis, both of the samples contain sulphide minerals and possibly pyroxenes. Both of the samples and especially MM196_100_30 have somewhat high and spiky background (Figures 40 & 41), so it was challenging to detect many logical minerals. Main minerals that should be present in

cordierite schist were not detected, including cordierite. MM196_82 could contain some less common sulphides or minerals formed by hydrothermal alteration. On MM196_100_30 (Appendix 6) only galena is clearly detected.

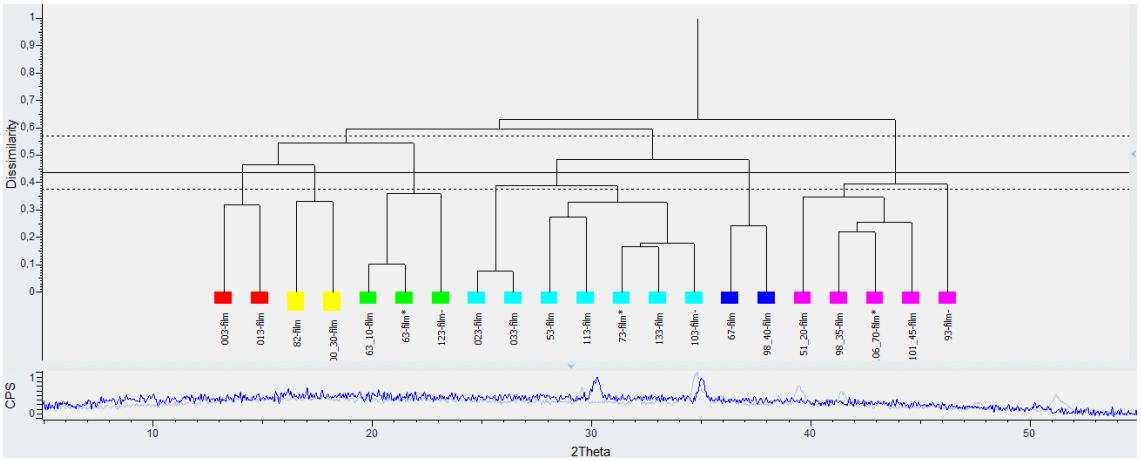

Figure 39. Dendogram of drill core MM196 with cluster 2 (yellow) highlighted. Combined diffractograms of the cluster 2 are at the bottom of the figure.

Table 9. Details of the cluster 2 samples.

Sample	Depth interval (m)	GTK rock type	GTK minerals	Detected minerals	Possibly detected minerals
MM196_82	80.00–153.60	Cordierite schist / gneiss	Sulphides	Pyroxenes (di), Pyrite, Pyrrhotite	Pentlandite, Grossular, Anhydrite, Anatase
MM196_100_30	80.00–153.60	Cordierite schist / gneiss	Sulphides	Galena	Pentlandite, Micas (bt / phl), Pyroxenes

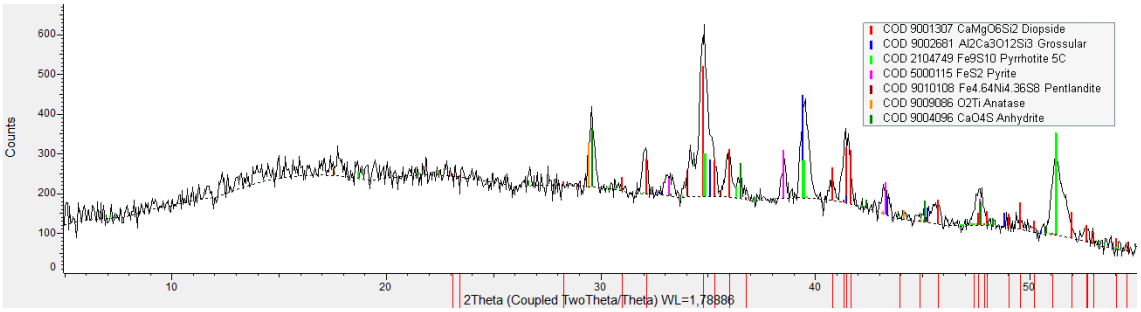

Figure 40. Diffractogram of the sample MM196_82.

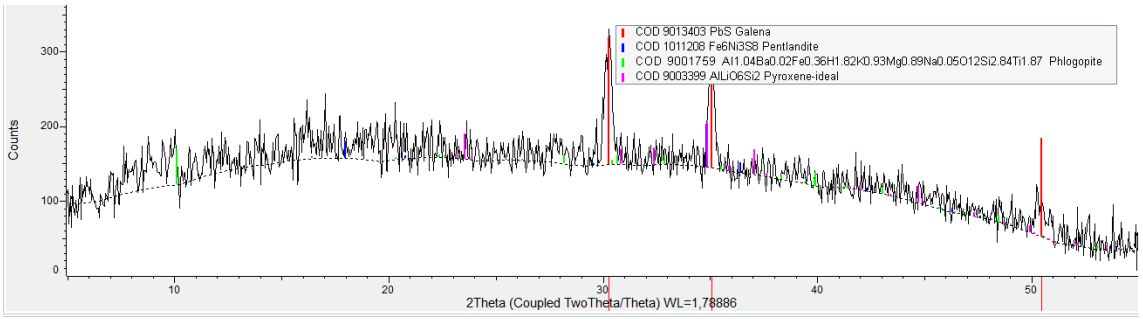

Figure 41. Diffractogram of the sample MM196_100_30. The background is very spiky.

6.3.3 Cluster 3

This cluster contains 3 samples (Figure 42 & Table 10). All of the samples in this cluster contain cordierite schist/gneiss with some sulphide minerals according to the logging report. Based on the analysis, all of the samples contain amphibole minerals and pyrite. MM196_63_10 (Figure 43) and MM196_63 have almost identical diffractograms and also likely contain quartz. Only MM196_63_10 contains feldspars according to the analysis. MM196_123 (Figure 44) has somewhat different mineral composition and contains chlorite, talc and possibly gypsum. Cordierite was not detected on any of the samples.

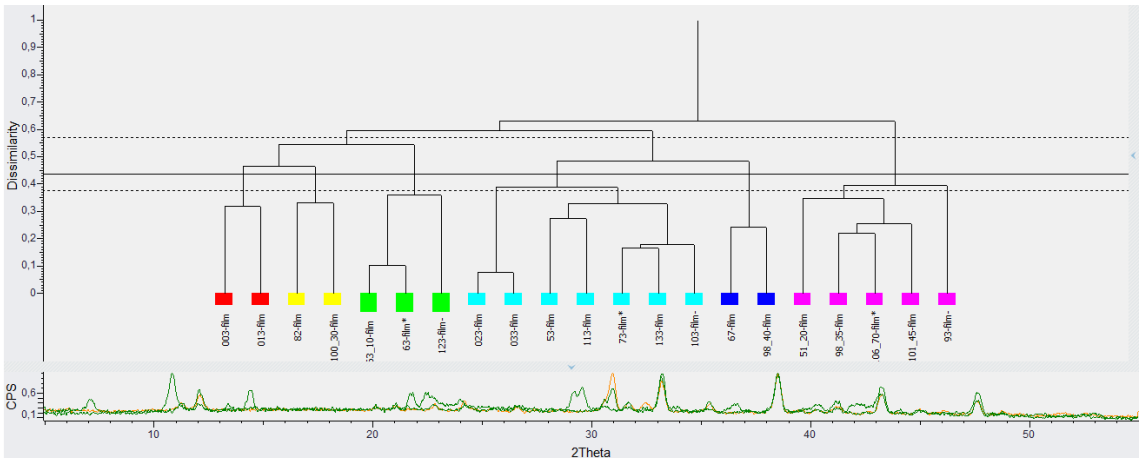

Figure 42. Dendogram of the drill core MM196 with cluster 3 (green) highlighted. Combined diffractograms of cluster 3 are at the bottom of the figure.

Table 10. Details of the cluster 3 samples.

Sample	Depth interval (m)	GTK rock type	GTK minerals	Detected minerals	Possibly detected minerals
MM196_63_10 + MM196_63	59.45–63.85	Cordierite schist / gneiss	Sulphides	Amphiboles (act / tr / hbl), Pyrite, Plagioclases (Bytowtite), Quartz	
MM196_123	80.00–153.60	Cordierite chist / gneiss	Sulphides	Chlorites (chl / clc), Amphiboles (act / tr / hbl), Pyrite, Talc	Gypsum

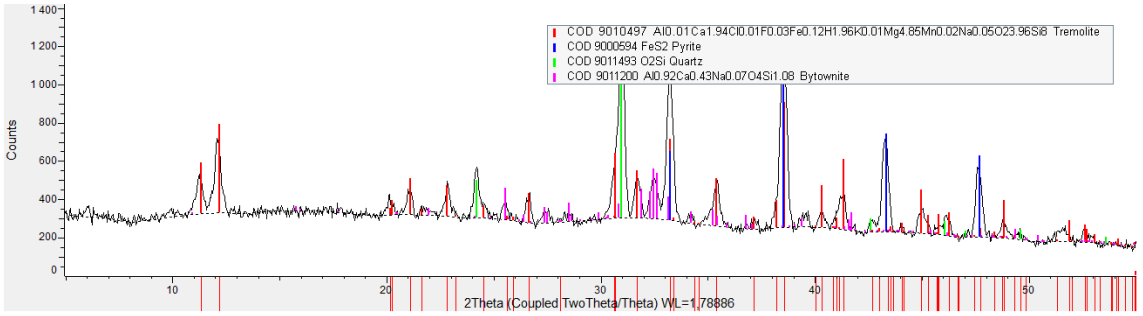

Figure 43. Diffractogram of the sample MM196_63_10. The software mainly suggested Bytowtite as the plagioclase mineral.

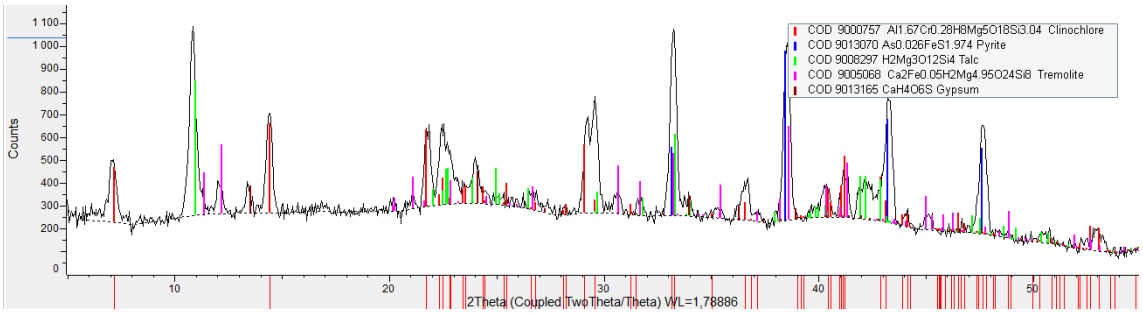

Figure 44. Diffractogram of the sample MM196_123. Couple of the peaks match gypsum relatively well.

6.3.4 Cluster 4

This cluster contains 7 samples and is the largest cluster in this drill core (Figure 45 & Table 11). All of the samples in this cluster contain various schist rocks, mostly cordierite or mica schist according to the logging report. Based on the analysis, all of the samples contain quartz

and most of the samples contain micas and plagioclase minerals. Chlorite minerals are also present in few samples. Cordierite was not detected in most of the samples that are stated to contain cordierite by the logging report. Appendix 1 shows picture of the drill core of the sample MM196_133. Only MM196_113 contains cordierite based on the analysis. Only MM196_53 possibly contains sulphides. In couple of the samples, quartz has dominating peaks and it is not possible to detect many other minerals. Cordierite was not detected from almost any sample stated as cordierite schist. On MM196_73 the peaks for micas are somewhat weak, but micas can be assumed to be present according to the logging report (Appendix 5). MM196_103 (Appendix 11) has two measurements, and "b" had longer measurement time. Original measurement only shows quartz, but 103b has relatively clear peaks for galena and micas, and possible peaks for pyrrhotite and stannite. Diffractograms of selected samples can be seen in Figures 46–50.

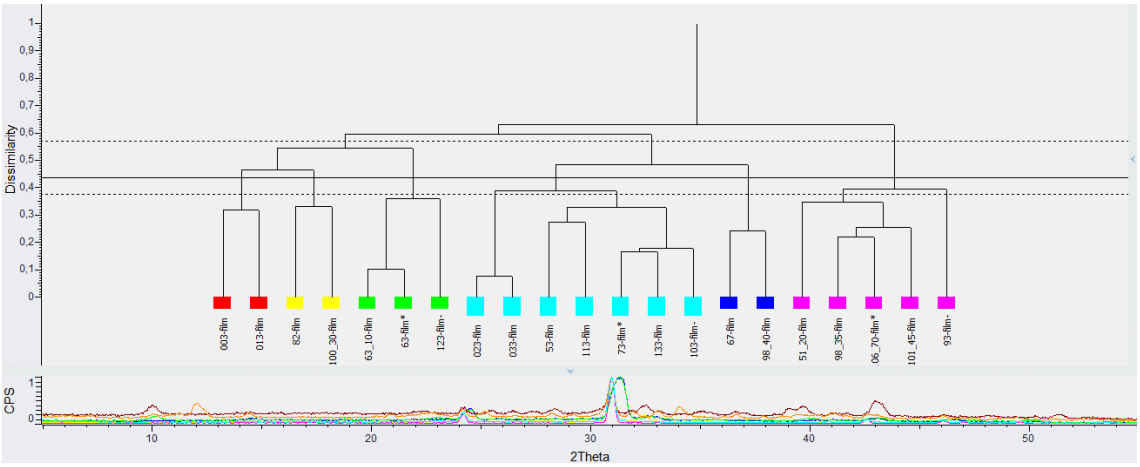

Figure 45. Dendogram of the drill core MM196 with cluster 4 (cyan) highlighted. Combined diffractograms of cluster 4 are at the bottom of the figure.

Table 11. Details of cluster 4 samples.

Sample	Depth interval (m)	GTK rock type	GTK minerals	Detected minerals	Possibly detected minerals
MM196_023	22.80–28.10	Mica schist		Quartz, Plagioclases	Chlorites (clc)
MM196_033	28.10–34.00	Mica schist / gneiss		Quartz, Plagioclases, Micas (bt / phl)	
MM196_53	52.80–53.20	Cordierite schist / gneiss	Arsenopyrite	Quartz, Micas (bt / phl), Plagioclases	Arsenopyrite, Pyrrhotite
MM196_113	80.00–153.60	Cordierite schist / gneiss		Quartz, Cordierite, Anthophyllite, Chlorites, Micas (bt / phl)	
MM196_73	72.00–75.25	Sericite schist / quartzite		Quartz, Plagioclases, Micas (ms / phg)	
MM196_133	80.00–153.60	Cordierite schist / gneiss		Quartz	Micas (phg)
MM196_103 + MM196_103b	80.00–153.60	Cordierite schist / gneiss		Quartz, Galena, Micas (phg / ms)	Pyrrhotite, Stannite

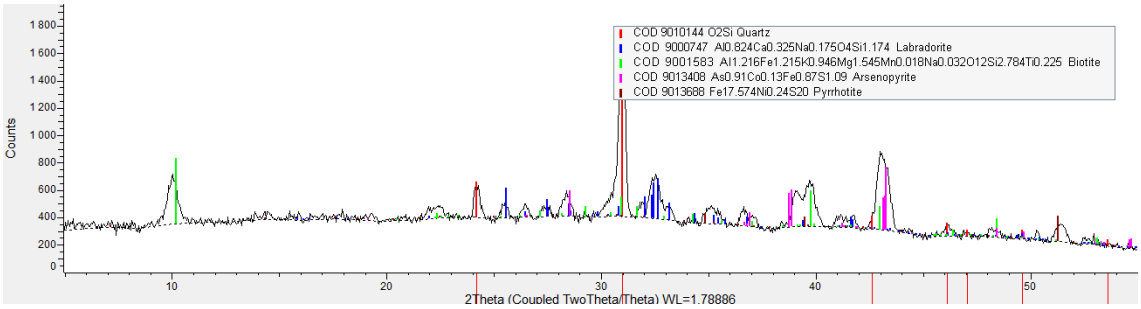

Figure 46. Diffractogram of the sample MM196_53. Arsenopyrite and pyrrhotite are likely present in the sample, although arsenopyrite peaks share locations with other minerals.

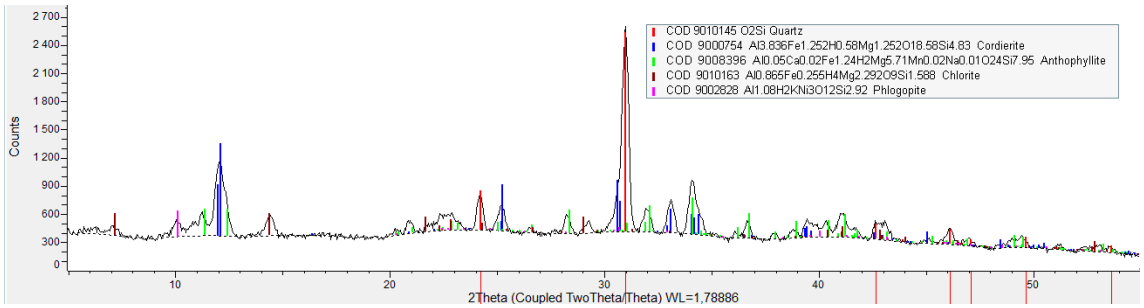

Figure 47. Diffractogram of the sample MM196_113. The diffractogram represents sample with cordierite and anthophyllite present.

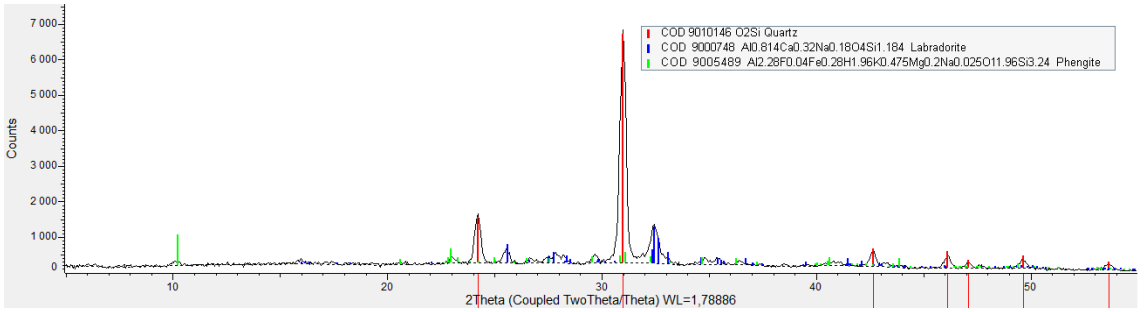

Figure 48. Diffractogram of the sample MM196_73. The mica peak on the left is quite low.

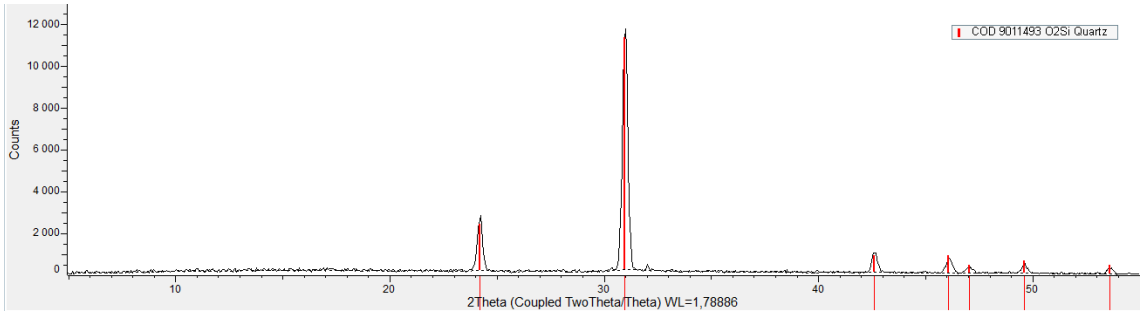

Figure 49. Diffractogram of the sample MM196_103. Only quartz is clearly present in this sample.

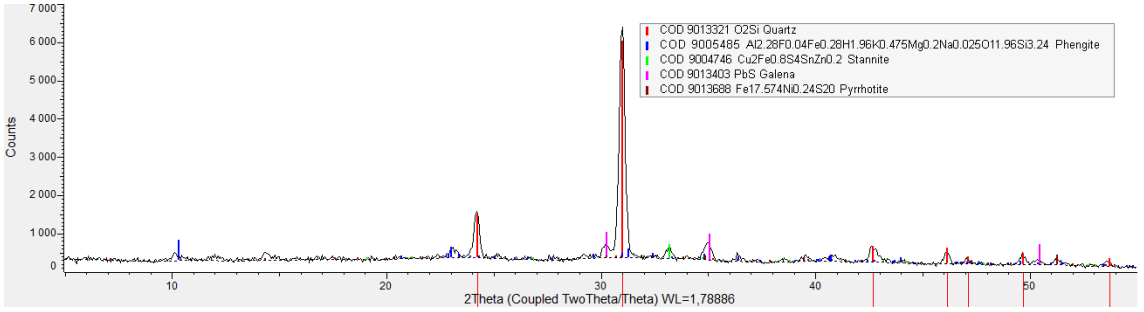

Figure 50. Diffractogram of the sample MM196_103b. This sample possibly contains galena and pyrrhotite.

6.3.5 Cluster 5

This cluster contains only 2 samples (Figure 51 & Table 12). Both of the samples in this cluster contain different schist rocks according to the logging report. Based on the analysis, the only minerals present in both of the samples are quartz and pyrite. On MM196_98_40 (Figure 53) quartz has the dominating peaks and only galena peaks are clearly visible in addition. MM196_67 (Figure 52) instead has relatively clear signal for micas and pyrrhotite. On MM196_67 the background is somewhat spiky. Micas are likely present, but the peaks are weak compared to quartz. Cordierite was not detected on MM196_98_40 although it should be present based on the logging report.

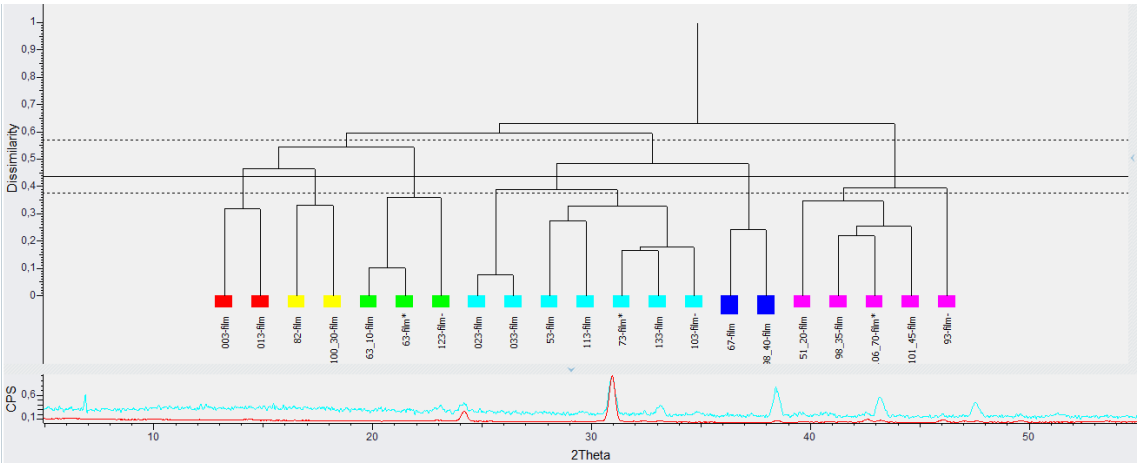

Figure 51. Dendogram of the drill core MM196 with cluster 5 (blue) highlighted. Combined diffractograms are at the bottom of the figure.

Table 12. Details of the cluster 5 samples.

Sample	Depth interval (m)	GTK rock type	GTK minerals	Detected minerals	Possibly detected minerals
MM196_67	63.85–67.60	Sericite schist	Sulphides	Quartz, Pyrite, Micas (phg / ms), Pyrrhotite	
MM196_98_40	80.00–153.60	Cordierite schist / gneiss	Sulphides	Quartz, Pyrite	Micas (ms / phg)

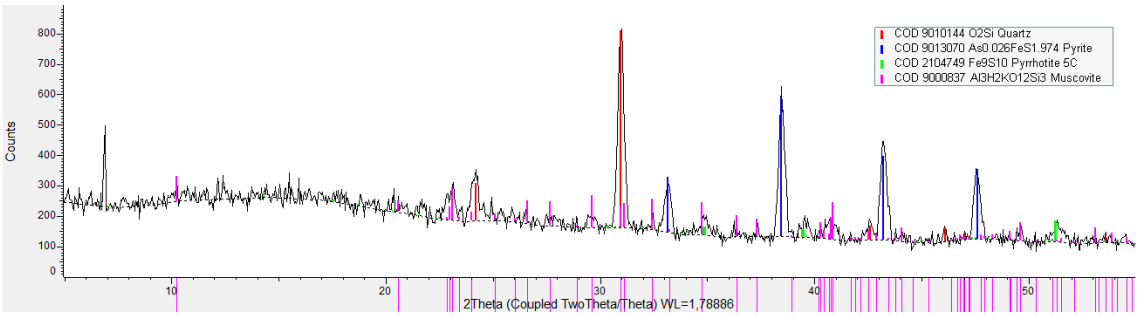

Figure 52. Diffractogram of the sample MM196_67. Pyrite has very strong peaks.

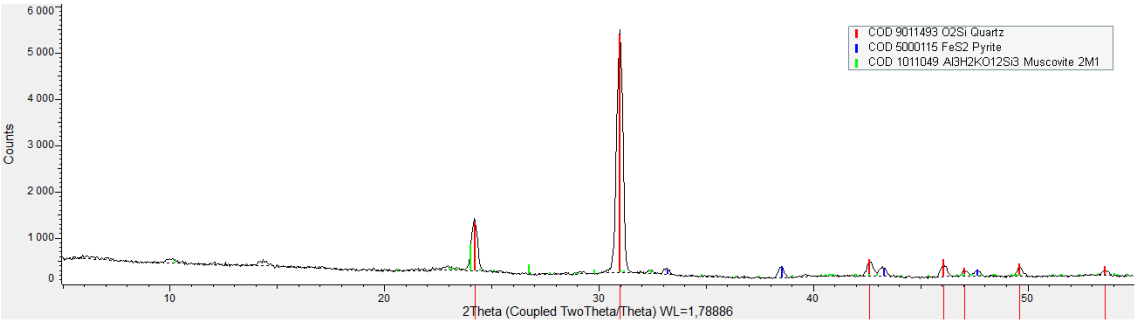

Figure 53. Diffractogram of the sample MM196_98_40. Quartz is dominating the peak profile.

6.3.6 Cluster 6

This cluster contains 5 samples (Figure 54 & Table 13). All of the samples in this cluster contain cordierite schist, except MM196_51_20 that contains skarn (Appendix 4) according to the logging report. Based on the analysis, only chlorite is present in all of the samples. The background is more or less messy and spiky in all of the samples, so it is challenging to match suitable minerals to the peak profiles. Only MM196_51_20 shows potential presence of cordierite, while the samples stated as cordierite schist/gneiss do not show any signals for cordierite. Sulphides are not detected on MM196_98_35 and MM196_101_45 although the logging report mentions they possibly contain sulphides. Diffractograms of selected samples can be seen in Figures 55–59.

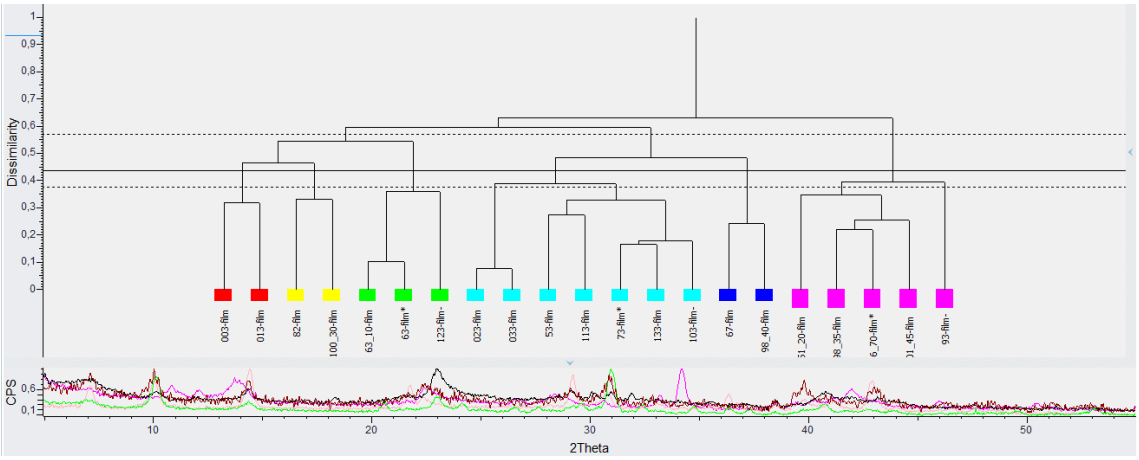

Figure 54. Dendogram of the drill core MM196 with cluster 6 (pink) highlighted. Combined diffractograms of cluster 6 are at the bottom of the figure.

Table 13. Details of the cluster 6 samples.

Sample	Depth interval (m)	GTK rock type	GTK minerals	Detected minerals	Possibly detected minerals
MM196_51_20	45.30–52.80	Skarn	Sulphides	Calcite, Amphiboles (act / tr / hbl), Chlorites (clc)	Cordierite, Magnetite, Chalcopyrite, Lizardite, Greenalite
MM196_98_35	80.00–153.60	Cordierite schist / gneiss	Sulphides	Chlorites (clc / chl)	Siderophyllite, Analcime, Quartz
MM196_106_70	80.00–153.60	Cordierite schist / gneiss		Quartz, Micas (bt / phl), Chlorites, Pyrite	Cronstedtite, Zircon
MM196_101_45	80.00–153.60	Cordierite schist / gneiss	Sulphides	Quartz, Micas (bt / phl + ms / phg), Chlorites (clc / chl)	
MM196_93	80.00–153.60	Cordierite schist / gneiss		Chlorites (clc / chl), Micas (bt / phl / annite)	Spinel / Gahnite

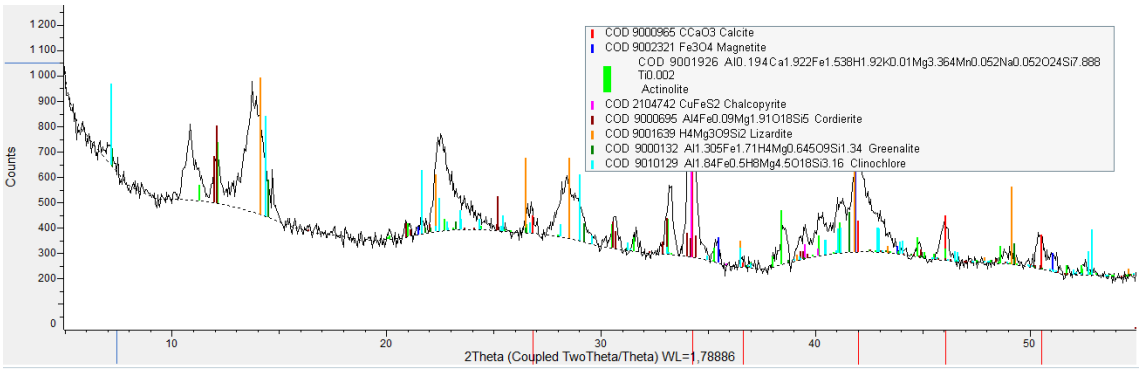

Figure 55. Diffractogram of the sample MM196_51_20. The peak profile is weirdly high on the left side of the diffractogram.

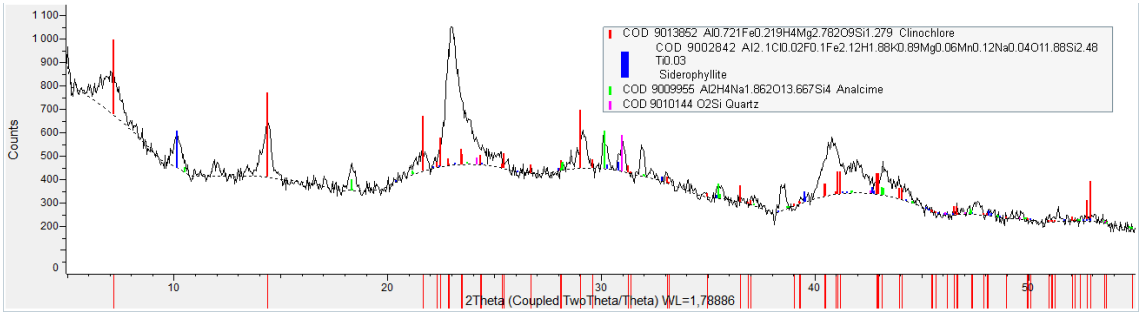

Figure 56. Diffractogram of the sample MM196_98_35. It was very challenging to match logical minerals to most of the peaks. The peak profile is somewhat messy.

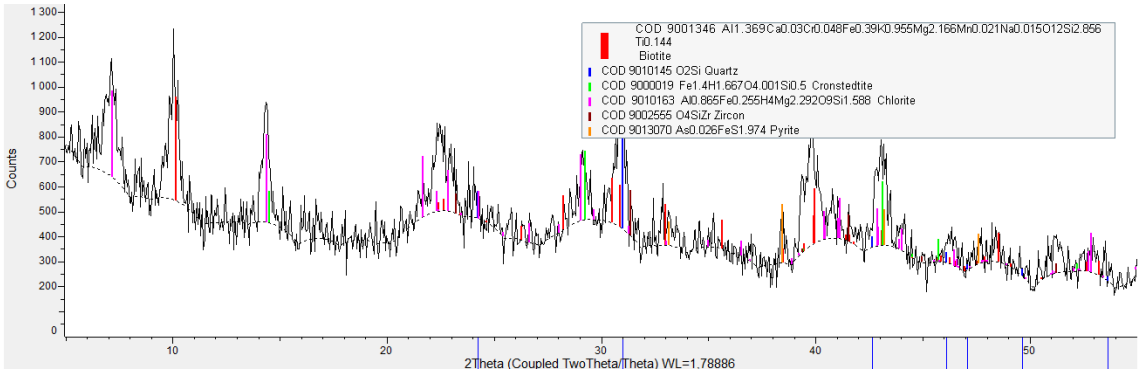

Figure 57. Diffractogram of the sample MM196_106_70. The background is very spiky, making it challenging to reliably match minerals to the peaks.

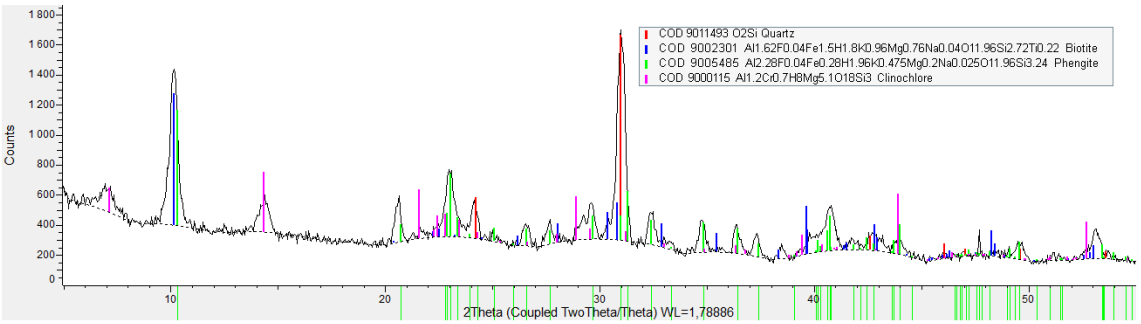

Figure 58. Diffractogram of the sample MM196_101_45. Biotite/phlogopite and phengite/muscovite share the high peak on the left side of the diffractogram, but other peaks are not shared.

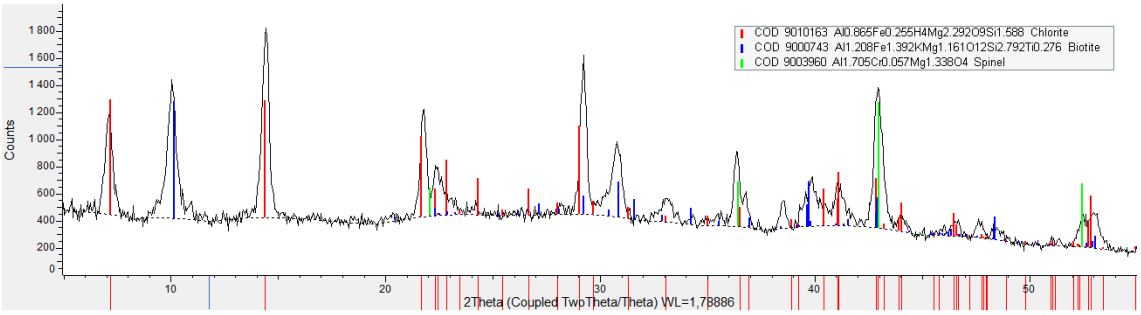

Figure 59. Diffractogram of the sample MM196_93. Spinel could be present, but shares peaks with other minerals.

6.4 Drill core MM198

12 samples were available for the drill core MM198. The samples were taken in about 10 m intervals. The samples were drilled south from Metsämonttu deposit and next to drill core MM196. The samples were analyzed and clustered using the DIFRAC.EVA software.

6.4.1 Cluster 1

This cluster contains only 2 samples (Figure 60 & Table 14). Both of the samples in this cluster contain diopside amphibolite according to the logging report. Based on the analysis, both of the samples contain plagioclase minerals, but other minerals are different. No pyroxenes detected on MM198_4 (Figure 61) despite being diopside amphibolite according to the logging report. M198_14 (Figure 62) likely contains clays, and the software is able to match vermiculite to the peak on the left side of the diffractogram. Picture of the sample MM198_14 drill core can be seen in Appendix 7. Chalcopyrite or pentlandite were in the suggested minerals list for this sample, but the peaks were not fitting very well and were shared with other minerals that are more reliably present in the sample.

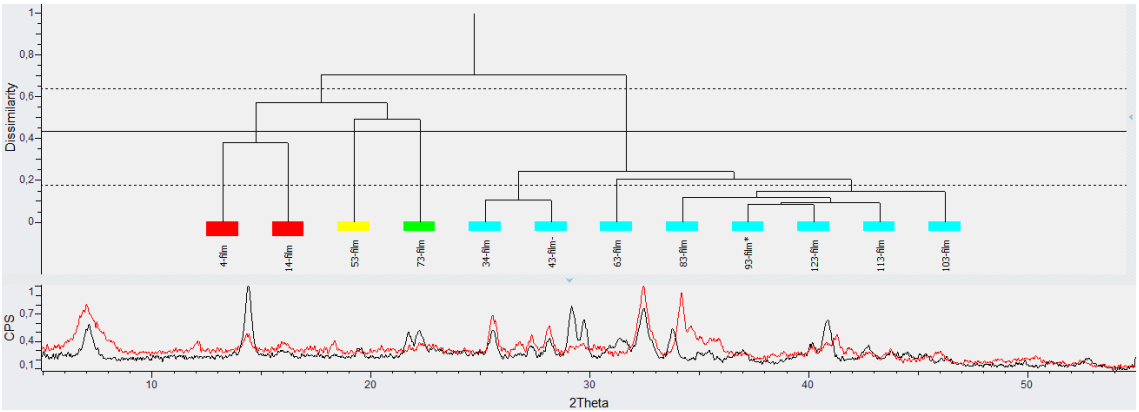

Figure 60. Dendogram of the drill core MM198 with cluster 1 (red) highlighted. Combined diffractograms are at the bottom of the figure.

Table 14. Details of cluster 1 samples.

Sample	Depth interval (m)	GTK rock type	GTK minerals	Detected minerals	Possibly detected minerals
MM198_4	1.20–21.10	Diopside amphibolite		Plagioclases, Chlorites (clc / chl / chm), Prehnite	Garnet, Quartz
M198_14	1.20–21.10	Diopside amphibolite		Plagioclases, Calcite, Pyroxenes (di), Epidote	Cordierite, Vermiculite

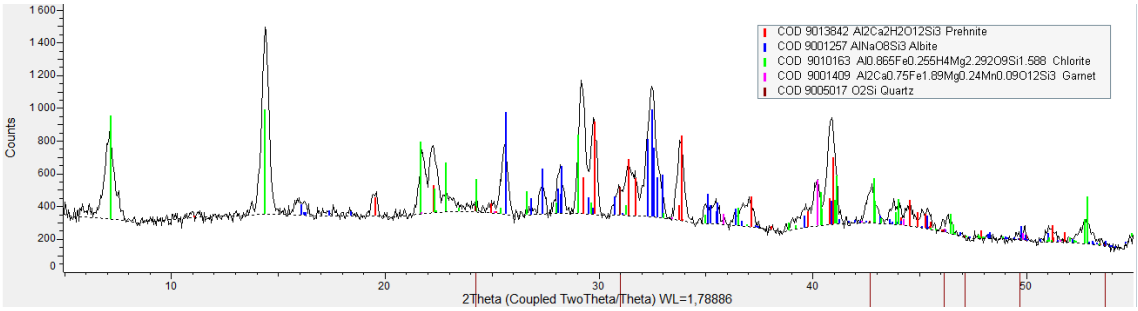

Figure 61. Diffractogram of the sample MM198_4. The sample has very high peak for chlorite group minerals.

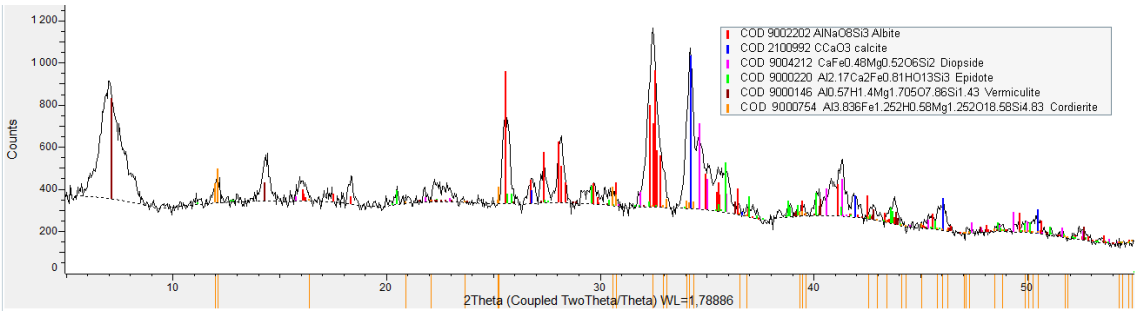

Figure 62. Diffractogram of the sample M198_14. It was possible to match vermiculite to the high peak on the left side of the diffractogram.

6.4.2 Cluster 2

This cluster contains 8 samples (Figure 63 & Table 15). All of the samples in this cluster contain schist or gneiss rocks according to the logging report. Most of the samples are stated as cordierite schist or gneiss. Based on the analysis, all of the samples contain quartz and most of the samples contain micas. Few samples also contain chlorites. Cordierite or feldspars were not detected on almost any of the samples. The software was not able to detect anything logical on MM_198_34 (Appendix 8), even though the peak pattern seemingly contains peaks of quartz, micas and possibly plagioclase minerals. The diffractogram also looks similar to the sample MM198_43 (Appendix 9). Amphiboles are not detected on MM198_43 although the sample contains hornblende gneiss according to the logging report. Diffractograms of selected samples can be seen in Figures 64–66.

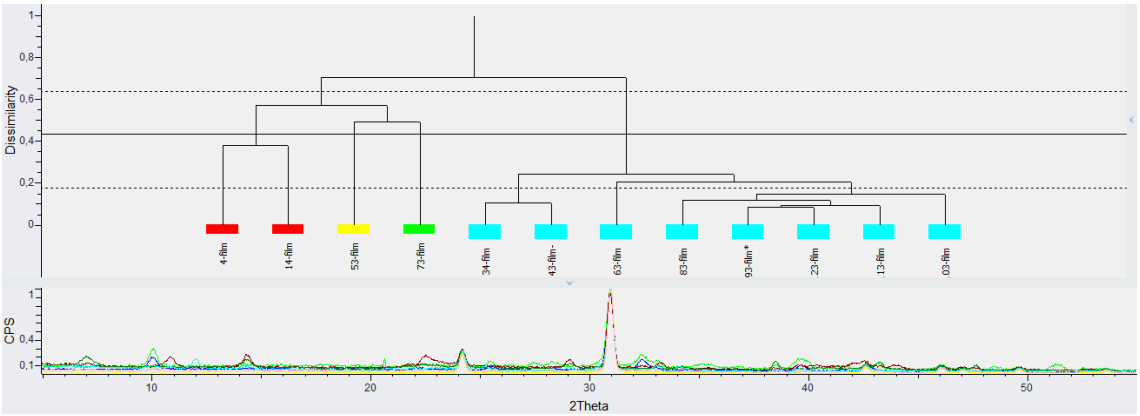

Figure 63. Dendogram of the drill core MM198 with cluster 2 (cyan) highlighted. Combined diffractograms are at the bottom of the figure.

Table 15. Details of the cluster 2 samples.

Sample	Depth interval (m)	GTK rock type	GTK minerals	Detected minerals	Possibly detected minerals
MM_198_34	33.80–35.10	Mica cordierite schist	Garnet	Quartz? Plagioclases? Micas?	
MM198_43	40.70–43.50	Hornblende gneiss	Pyrrhotite	Quartz, Micas (bt / phl), Plagioclases, Pyrrhotite	
MM198_63	60.00–65.60	Cordierite schist / gneiss		Quartz, Chlorites, Talc	
MM198_83	82.30–83.50	Cordierite schist		Quartz, Pyrite, Chlorites (chm)	Vermiculite
MM198_93	83.50–101.35	Cordierite schist / gneiss		Quartz, Cordierite, Micas (bt / phl)	
MM198_123	118.90–127.40	Cordierite schist / gneiss		Quartz, Micas (bt / phl)	Pyrrhotite
MM198_113	112.05–114.60	Quartz feldspar schist		Quartz, Pyrite, Micas (bt / phl)	
MM198_103	102.55–112.05	Cordierite gneiss		Quartz	

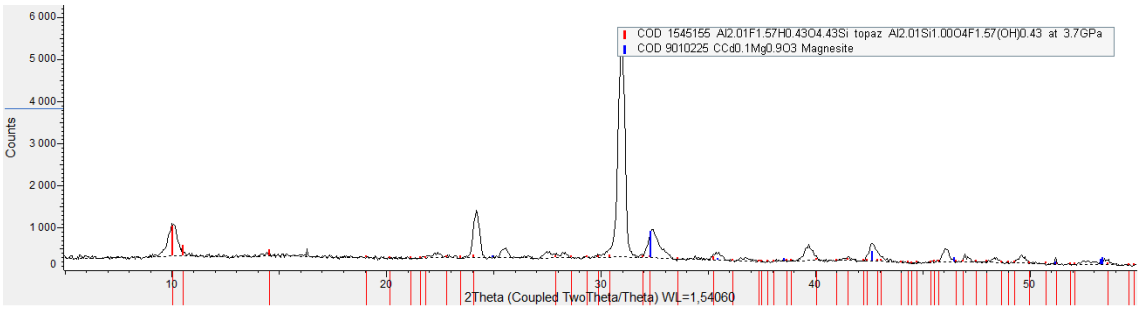

Figure 64. Diffractogram of the sample MM_198_34. For unknown reason the software was unable to match quartz and plagioclase feldspar minerals to the peak profile even though they are clearly present. Micas are likely present as well.

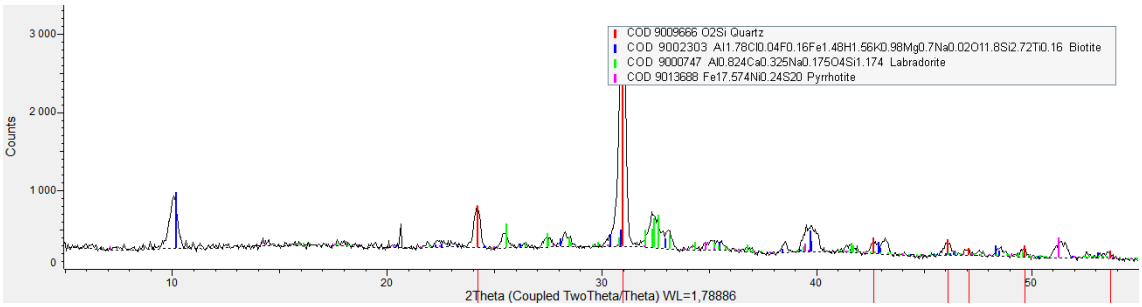

Figure 65. Diffractogram of the sample MM198_43. This represents a typical diffractogram in this cluster with dominating quartz peak and only few other minerals detected.

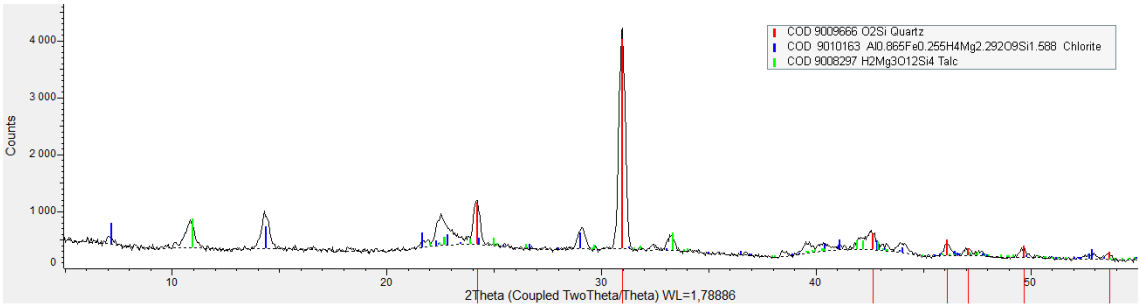

Figure 66. Diffractogram of the sample MM198_63. One of the few samples with talc detected.

6.4.3 Singular samples without cluster

The sample MM198_53 contains skarn according to the logging report (Table 16). The software suggested large amount of minerals that somewhat fit the peak profile and match the rock type or formation environment but are not necessary to fill all the peaks (Figure 67).

Table 16. Details of the sample MM198_53

Sample	Depth interval (m)	GTK rock type	GTK minerals	Detected minerals	Possibly detected minerals
MM198_53	43.50–53.10	Skarn		Calcite, Pyroxene (di), Chlorites (chl / clc), Dolomite	Colusite, Magnetite, Chalcopyrite, Perovskite

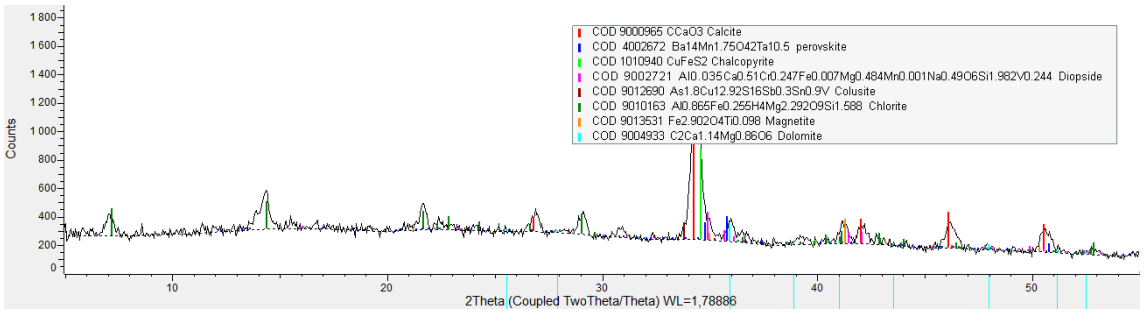

Figure 67. Diffractogram of the sample MM198_53.

The sample MM198_73 has two measurements (Table 17) and the "b" one had slightly shorter measurement time. The background of the diffractogram is very spiky, especially on MM198_73 (Figure 68). On MM198_73 only pyrite is reliably detected and possibly calcite. Pyrrhotite and chalcopyrite were detected on MM198_73b (Figure 69) in addition to pyrite, but calcite was not detected. Picture of the sample drill core can be seen in Appendix 10.

Table 17. Details of the samples MM198_73 and MM198_73b

Sample	Depth interval (m)	GTK rock type	GTK minerals	Detected minerals	Possibly detected minerals
MM198_73	42.90–82.30	Quartz feldspar schist and some skarn		Pyrite	Calcite
MM198_73b	42.90–82.30	Quartz feldspar schist and some skarn		Pyrite, Pyrrhotite, Chalcopyrite	

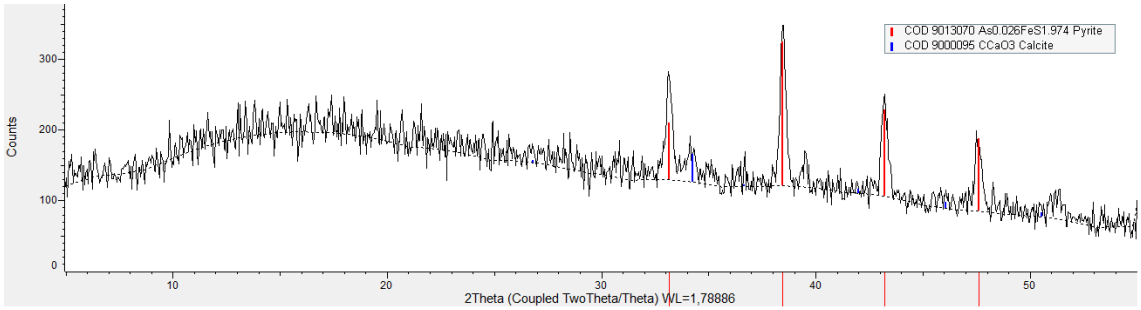

Figure 68. Diffractogram of the sample MM198_73. The diffractogram is somewhat spiky.

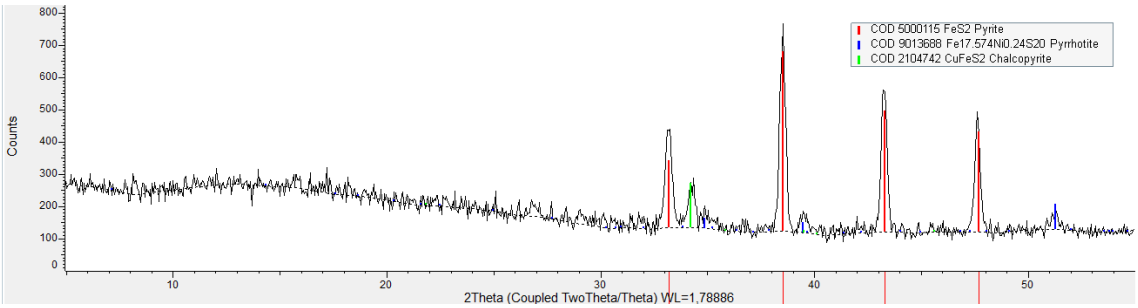

Figure 69. Diffractogram of the sample MM198_73b. This is the only “b” sample where the measurement “b” has clearly better diffractogram than the original measurement.

6.5 Drill core MM241

12 samples were available for the drill core MM196. The samples were taken in 10 m intervals, but no sample data was provided for the study from the depth of 115 m. The samples were drilled south from Metsämonttu deposit and south-west of the other drill cores in this study. The samples were analyzed and clustered using the DIFRAC.EVA software.

6.5.1 Cluster 1

This cluster contains 8 samples (Figure 70 & Table 18). All of the samples in this cluster contain amphibolite or schist rocks according to the logging report. Schist rock samples include mica and quartz feldspar schists. Based on the analysis, all of the samples contain quartz and plagioclase minerals. Multiple samples seem to contain K-feldspars in addition to plagioclases. All of the plagioclase samples contain epidote. Micas and amphibole minerals are present in some samples, but the peaks are mostly not very high. Sulphides are absent from most of the samples. Pyroxenes are not detected on MM241_5 and grossular is not detected on MM241_95 and MM241_125 even though the GTK logging report states the samples contain them. Diffractograms of selected samples can be seen in Figures 71–74.

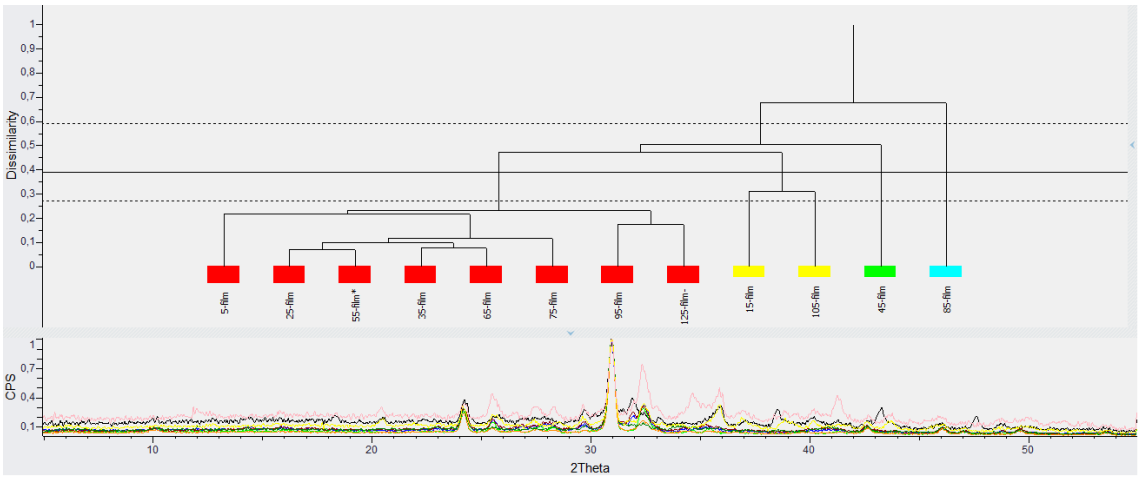

Figure 70. Dendogram of the drill core MM241 with cluster 1 (red) highlighted. Combined diffractograms are at the bottom of the figure.

Table 18. Details of the cluster 1 samples.

Sample	Depth interval (m)	GTK rock type	GTK minerals	Detected minerals	Possibly detected minerals
MM241_5	2.00–9.70	Diopside amphibolite		Quartz, Epidotes, Plagioclases, K-feldspars, Pyrite	Analcime, Micas (bt / phl)
MM241_25	21.55–30.45	Quartz feldspar schist		Quartz, Plagioclases, K-feldspars	
MM241_55	46.50–61.00	Quartz feldspar schist		Quartz, Plagioclases, K-feldspars	Micas (bt / phl)
MM241_35	33.70–39.90	Mica schist / gneiss		Quartz, Plagioclases	Micas (bt / phl)
MM241_65	63.20–75.90	Quartz feldspar schist		Quartz, Plagioclases	
MM241_75	63.20–75.90	Quartz feldspar schist		Quartz, Plagioclases, K-feldspars (orthoclase)	Amphiboles (act / tr / hbl), Micas (bt / phl)
MM241_95	91.50–118.00	Amphibolite	Epidote, Grossular	Quartz, Plagioclases (anorthite), Epidotes	
MM241_125	118.00–131.40	Amphibolite	Grossular	Quartz, Pyroxenes (di), Plagioclases, Epidotes, Amphiboles (act / tr / hbl)	

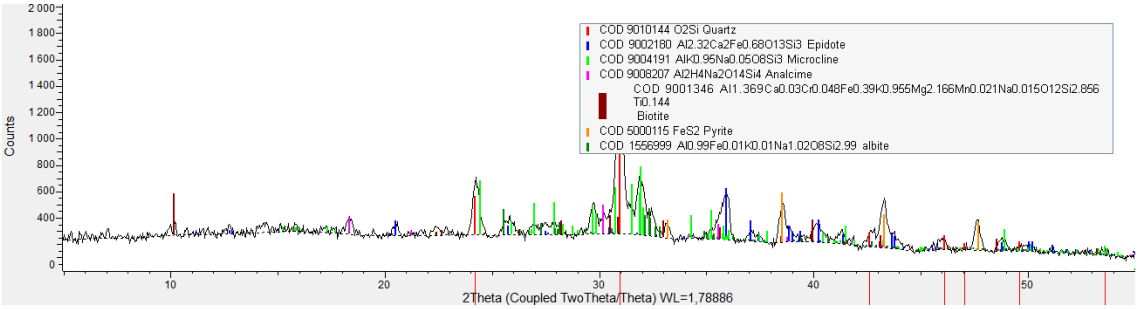

Figure 71. Diffractogram of the sample MM241_5. This sample contains the largest number of detected minerals in the cluster, including pyrite.

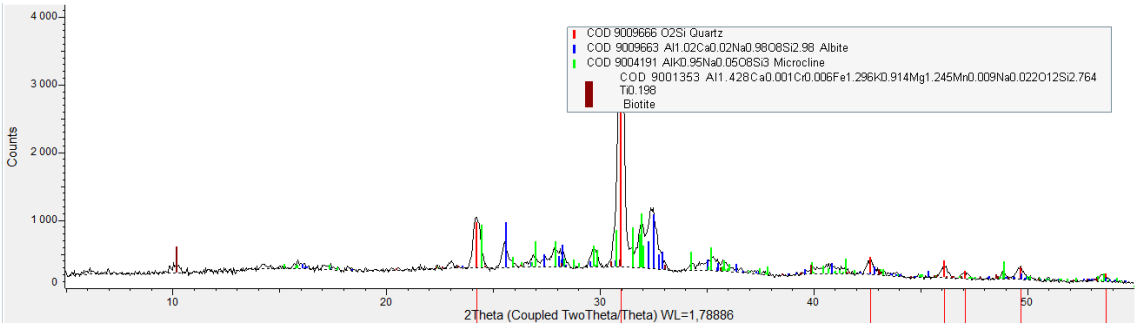

Figure 72. Diffractogram of the sample MM241_55. This sample possibly contains both plagioclase feldspars and K-feldspars.

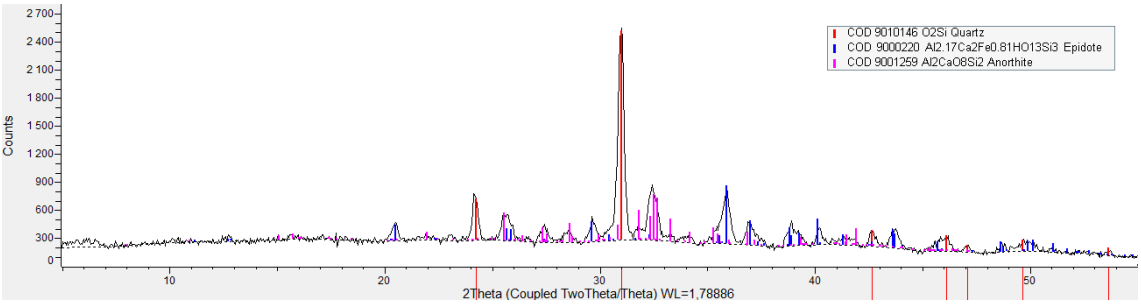

Figure 73. Diffractogram of the sample MM241_95. The software mainly suggested anorthite as the plagioclase feldspar.

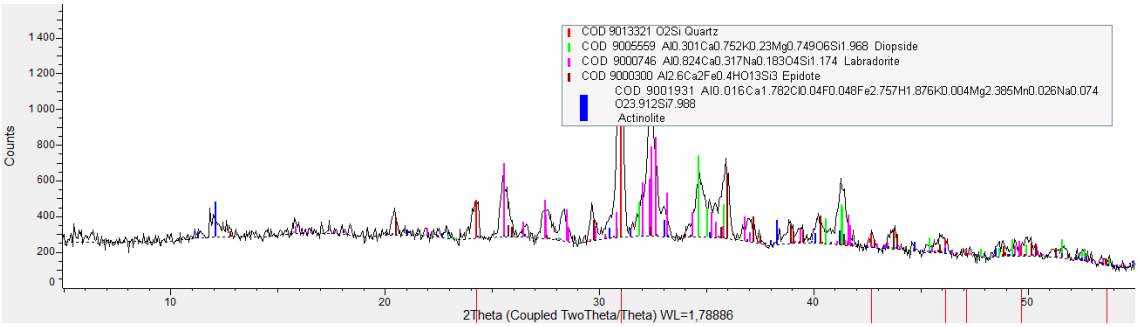

Figure 74. Diffractogram of the sample MM241_125. Another sample with large number of minerals detected.

6.5.2 Cluster 2

This cluster contains only 2 samples (Figure 75 & Table 19). Both of the samples in this cluster contain amphibolite according to the logging report. Based on the analysis, both of the samples contain plagioclase feldspars and amphibole minerals. Quartz is also possibly present in both. Rest of the minerals are different in both samples. It was also somewhat challenging to find suitable matching minerals for some peaks on MM241_15 (Figure 76) as it has spiky

background. No epidote or grossular detected on MM241_105 (Figure 77) although they are stated to be present by the logging report.

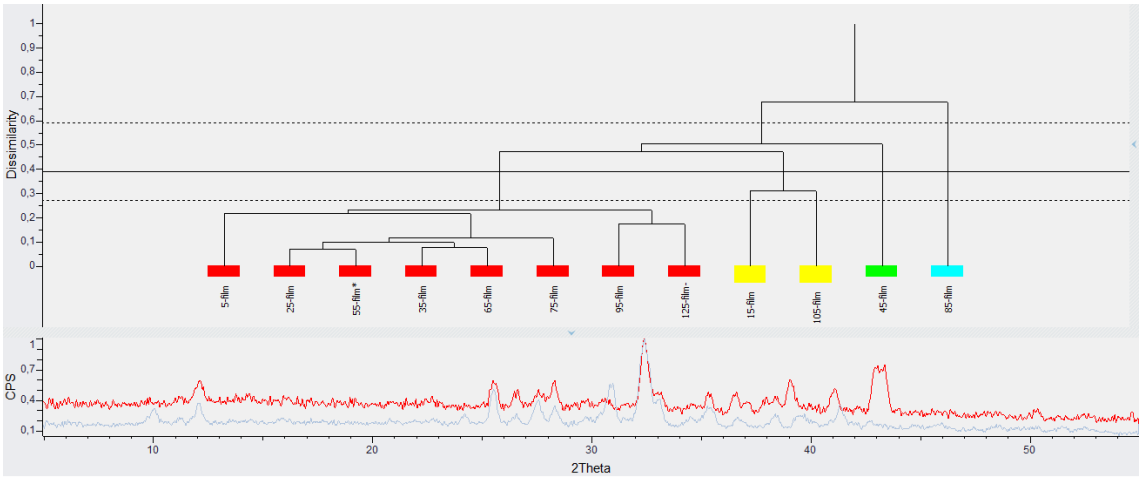

Figure 75. Dendogram of the drill core MM241 with cluster 2 (yellow) highlighted. Combined diffractograms are at the bottom of the figure.

Table 19. Details of the cluster 2 samples.

Sample	Depth interval (m)	GTK rock type	GTK minerals	Detected minerals	Possibly detected minerals
MM241_15	12.17–21.55	Amphibolite		Plagioclases, Amphiboles (act / tr / hbl)	Quartz, Cordierite, Gahnite, Arsenopyrite
MM241_105	91.50–118.00	Amphibolite	Epidote, Grossular	Plagioclases, Quartz, Amphiboles (act / tr / hbl), Micas (bt / phl)	

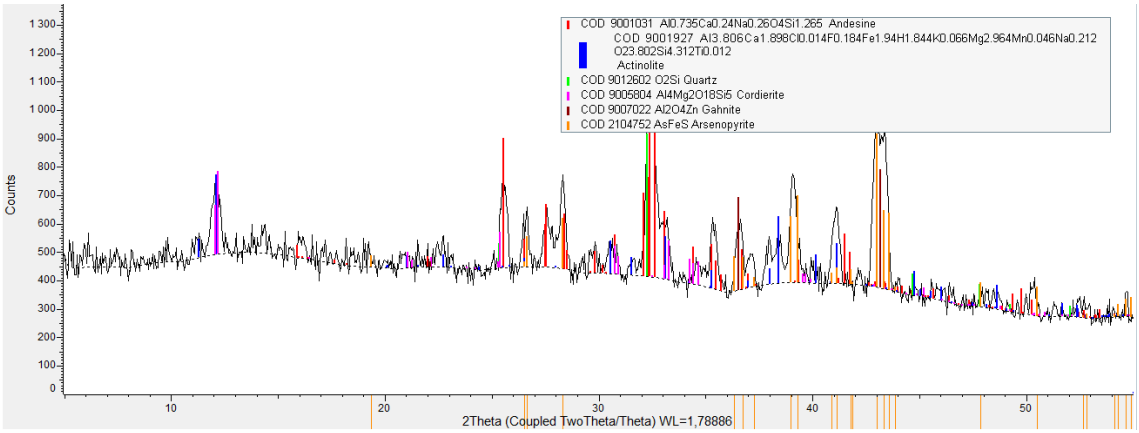

Figure 76. Diffractogram of the sample MM241_15. The background is quite spiky, making the real peaks not stand out well from the background.

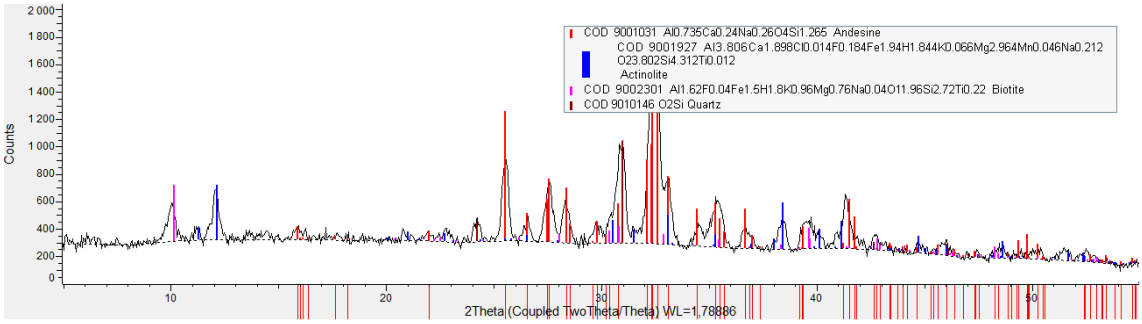

Figure 77. Diffractogram of the sample MM241_105.

6.5.3 Singular samples without cluster

The sample MM241_45 contains skarn according to the logging report (Table 20). It is challenging to match some peaks with suitable minerals. Only pyroxene and quartz are certainly detected. Dolomite matches the peak profile but shares peak with diopside (Figure 78).

Table 20. Details of the sample MM241_45.

Sample	Depth interval (m)	GTK rock type	GTK minerals	Detected minerals	Possibly detected minerals
MM241_45	44.63–46.50	Skarn	Tremolite, possibly PbS	Pyroxenes (di), Quartz	Dolomite, Clinozoisite, Scapolite

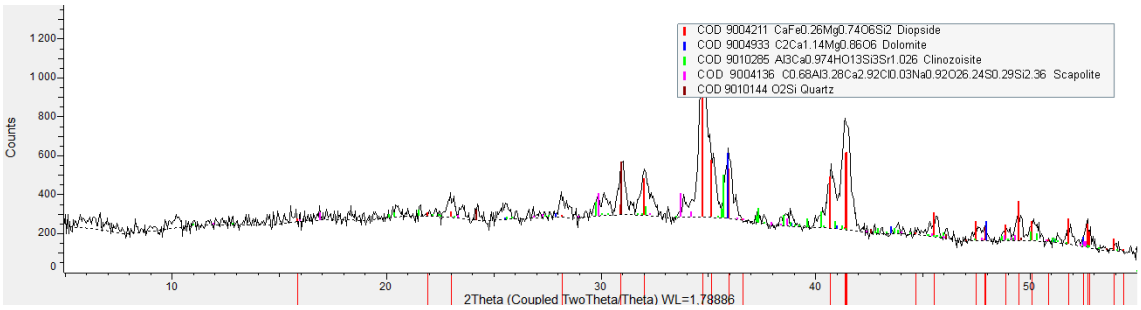

Figure 78. Diffractogram of the sample MM241_45.

The sample MM241_85 contains tremolite skarn according to the logging report (Table 21). This sample diffractogram has large number of peaks, but it was relatively easy to match all of the peaks to just few minerals (Figure 79). No sulphides were detected although the logging report states they might be present.

Table 21. Details of the sample MM241_85.

Sample	Depth interval (m)	GTK rock type	GTK minerals	Detected minerals	Possibly detected minerals
MM241_85	78.15–87.08	Tremolite skarn	Some sulphides	Amphiboles (tr), Calcite, Chlorite	

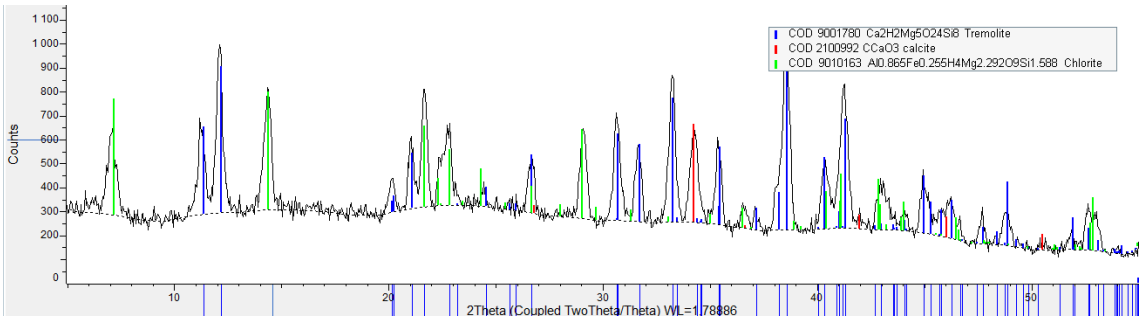

Figure 79. Diffractogram of the sample MM241_85. The diffractogram contains large number of peaks, but only 3 minerals were required to fit all of them.

6.6 Clustering of all samples

Clustering was made for all of the samples together (Figure 80). Combined diffractograms of every sample in each cluster can be seen in Figures 81a– 81l.

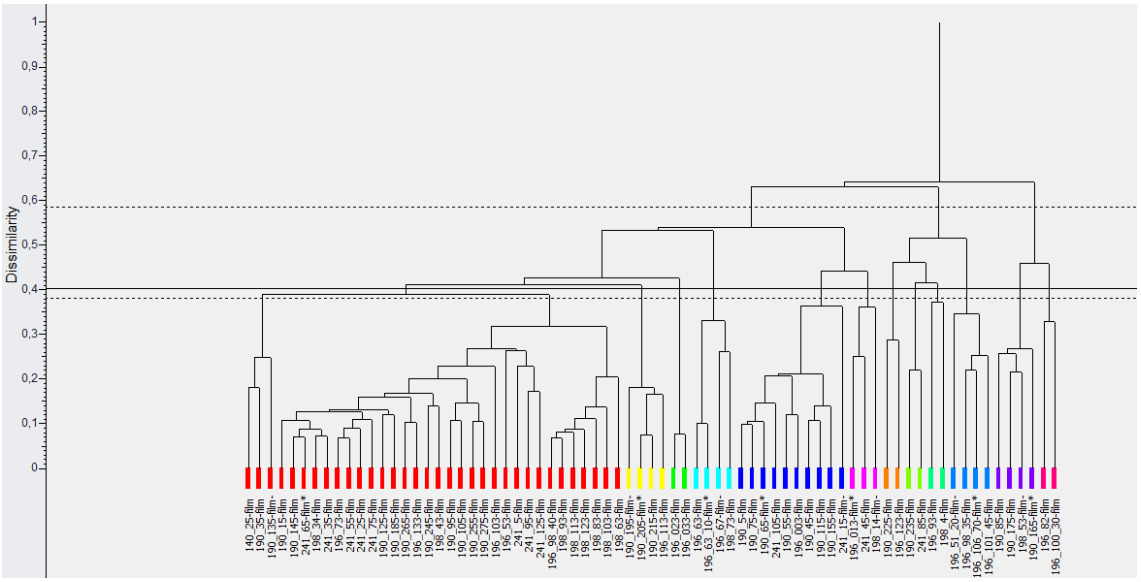

Figure 80. Dendogram view of the clustering of all of the samples. Clusters in order from left to right: red, yellow, green, cyan, blue, pink, orange, light green, green cyan, light blue, violet, deep pink.

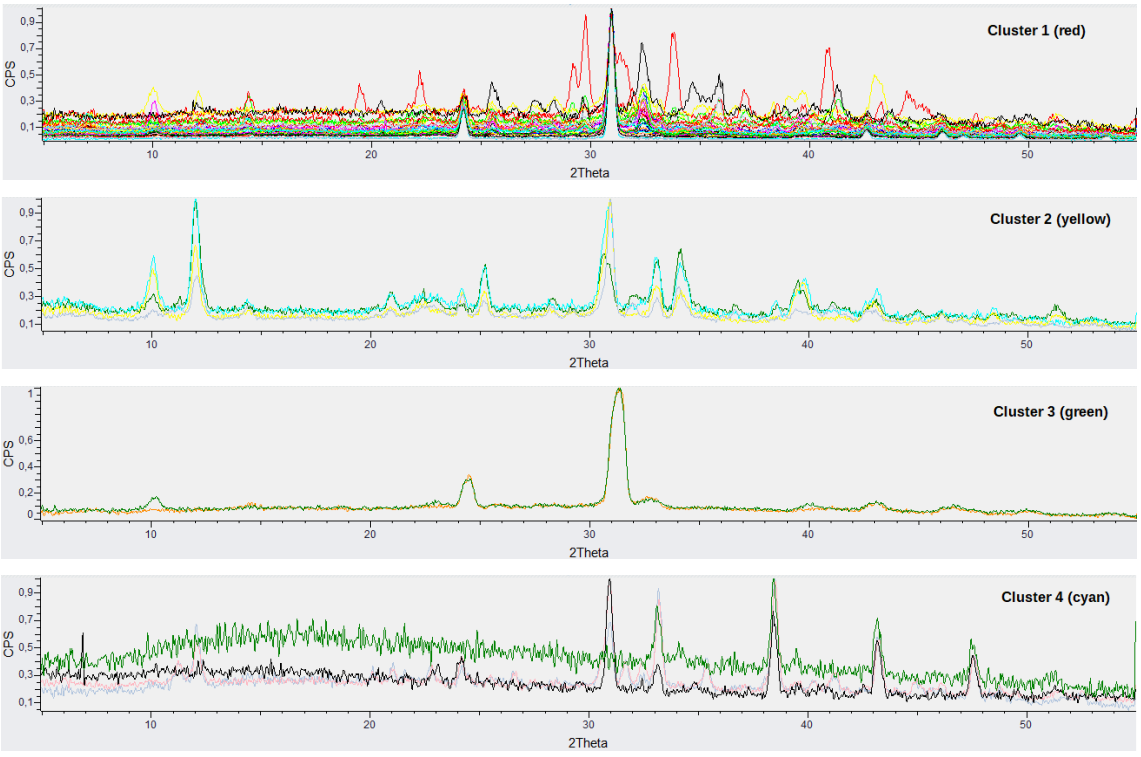

Figures 81a (Cluster 1, uppermost) – 81d (Cluster 4, lowermost). Combined diffractograms of each sample in every cluster.

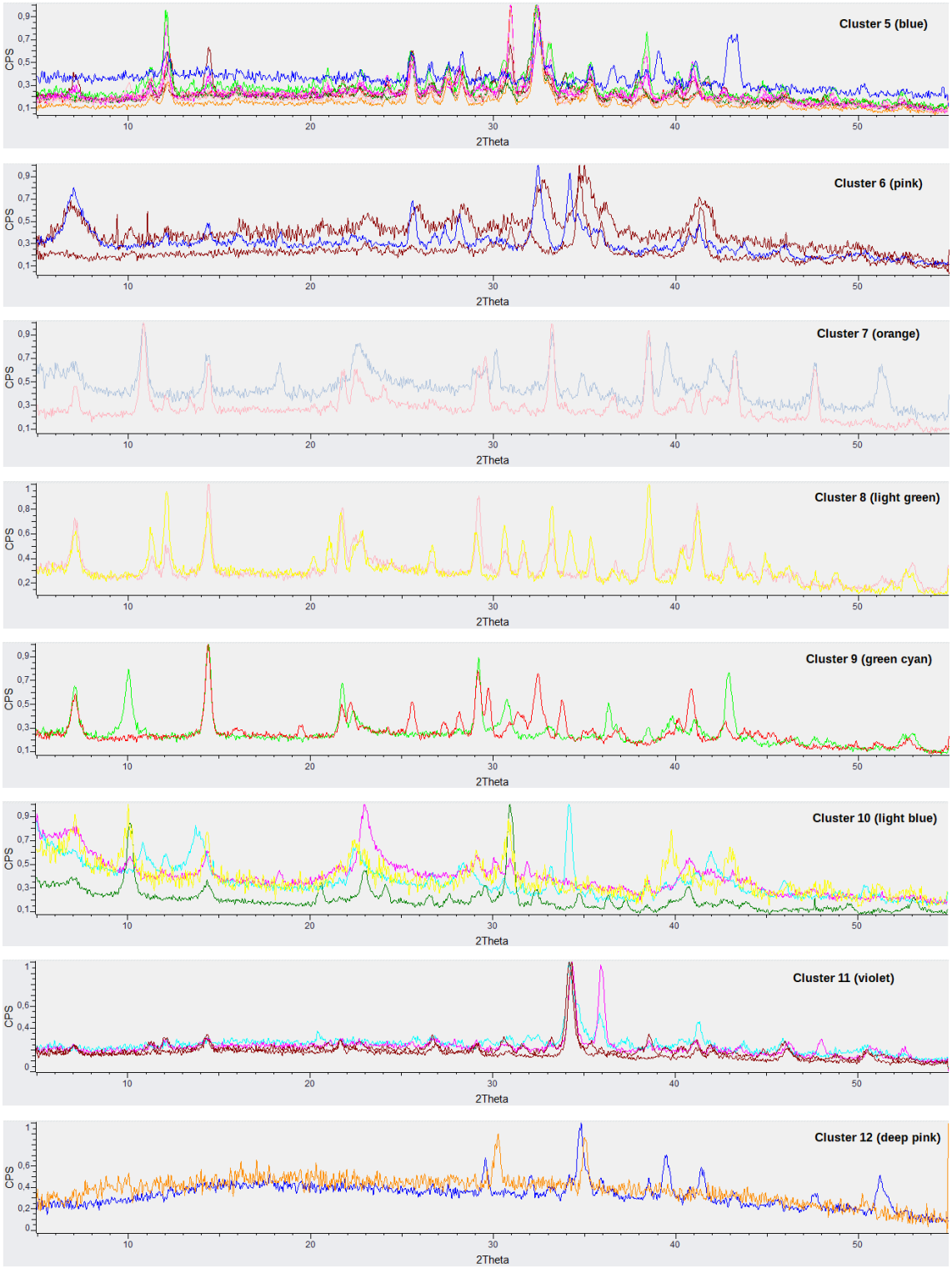

Figures 81e (Cluster 5, uppermost) – 81l (Cluster 12, lowermost). Combined diffractograms of each sample in every cluster.

7 Discussion

7.1 Overview of the study

This study was made to find out if pXRD mineralogical analysis and clustering methods could be useful for mineral exploration. Analysis results and clusters were compared with available logging report to see if the results match the observations from the report. Some previous studies about the pXRD's ability to detect minerals were compared with the observations from this study. The interpretations were made based on how well the clusters separated sulphide and indicator mineral bearing samples from barren basic rock samples.

7.2 Drill core MM190

In cluster 1 the minerals present strongly indicate hydrothermal alteration or retrograde metamorphism. Samples with chamosite indicate high iron concentrations while samples with clinochlore indicate higher magnesium concentrations. Prehnite and babingtonite indicate calcium-rich environments.

Cluster 2 could be divided into 2 smaller sub-clusters where 5 first samples have very clear signal and the latter 5 have weaker signal of plagioclase feldspars. The diffractogram peak profiles are mostly similar in the two sub clusters, but even small variations in the peak locations and heights strongly affect the suggested minerals by the software. The minerals present in this cluster suggest that the rocks in these samples are not as strongly affected by hydrothermal alteration as in the cluster 1.

Cluster 3 seems to only contain cordierite(-anthophyllite) rocks. Cordierite and anthophyllite suggest these rocks have formed from the metamorphism of magnesium- or iron-rich rocks in relatively high temperature but lower pressure. The minerals present are typical for contact-metamorphism halos, but also for regional metamorphism settings, which both match the known formation history of these rocks. Cordierite-anthophyllite rocks are typical indicators for nearby VMS ore formations (Beeson, R., 1988).

Cluster 4 contains basic metamorphic amphibole facies rocks that are not very important in terms of indicating ore presence. Some of the samples might contain cordierite, but the cordierite peaks do not match the peak profile perfectly or they share peaks with other present minerals.

Cluster 5 contains rocks with calcite and minerals that are typical for limestones. There are also some minor and uncertain signals of some sulphide minerals in the samples. The minerals in the samples of this cluster are potential for indicating ore presence nearby.

Samples MM190_225 and MM190_235 have not been clustered with other samples in this drill core. Both of the samples likely contain sulphides and the background is atleast partially low quality in both of the samples.

7.3 Drill core MM196

Cluster 1 only has two samples, and both have somewhat different mineral composition. It is not possible to make conclusions on the general type of this cluster other than it containing amphibolites.

The only conclusion that can be made of cluster 2 is that it contains samples with sulphides that are likely to affect the background of the diffractograms. Also, on both samples the diffractogram background rises at the lower angles and then slowly decreases towards higher angles. It would be useful to know if this phenomenon is exclusive to sulphide minerals, making it possible to be used for quickly detecting samples that possibly contain sulphides, or can other factors cause it as well.

Cluster 3 samples contain pyrite based on the analysis and although cordierite was not detected, they should contain it according to the logging report. The samples in this cluster are therefore likely near or within sulphide mineralization. The minerals present in MM196_123 suggest strong hydrothermal alteration, but the other samples do not have as strong signal for it.

In cluster 4 the main common factor is the strong present of quartz. Also, plagioclase minerals and micas are quite clearly present in most of the samples. The lack of cordierite detection in most samples could be just “bad luck” of no cordierite ending up in the samples, or the logging report is not detailed enough since it only shows vague depth ranges where the samples have been taken from. Based on the analysis results and the lack of anything particularly interesting in terms of ore geology, this cluster likely contains basic rocks not directly related to sulphide mineralizations. If cordierite is present in the samples, then this cluster could partially contain important rocks in terms of mineral exploration.

In cluster 5 both samples contain quartz and pyrite, so the samples are likely taken from or near sulphide mineralization. MM196_98_40 has been stated by the logging report to contain cordierite, but it was not detected.

In cluster 6 the samples seem to partially be missing the detection of typical “main minerals”, and the mineral content of each sample is very varying. Some of the samples seem to contain sulphides and almost all of the samples have quite clear signals of hydrothermal alterations so these rocks could be relatively near to potential ore mineralizations.

7.4 Drill core MM198

Cluster 1 contains amphibolite rocks with strong signals of hydrothermal alteration or retrograde metamorphism. The samples in this cluster could indicate nearby sulphide mineralizations, but sulphides were not reliably detected from the samples.

Based on the analysis results, cluster 2 contains quartz-rich rocks, and hydrothermal alteration minerals and sulphides were detected in some of the samples. Most of the samples have been taken from cordierite-bearing rocks according to the logging report, but cordierite was not detected in almost any of the samples. This cluster seems to mostly contain rocks that directly contain sulphide mineralizations or contain indicator minerals for VMS mineralizations.

Samples MM198_53 and MM198_73/ MM198_73b have not been clustered with other samples in the drill hole. Sample MM198_73 contains sulphides and MM198_53 contains calcite and dolomite based on the analysis, so both of the samples are interesting in terms of mineral exploration.

7.5 Drill core MM241

Cluster 1 contains over half of the samples in this drill core. It is challenging to make any clean conclusions of this cluster as it seems to contain both quartz rich schist rocks with no major signs of hydrothermal alteration, and amphibolites with minerals like epidote that could indicate hydrothermal alteration or retrograde metamorphism. Sulphides were detected only on MM241_5. The common feature is the presence of both quartz and feldspars.

It is challenging to make any important conclusions of cluster 2. Both of the samples contain plagioclase feldspars and amphibole minerals based on the analysis. Only MM241_15 possibly contains sulphide. MM241_105 contains micas while MM241_15 does not.

Samples MM241_45 and MM241_85 have not been clustered with other samples in the drill hole. Both are stated to contain skarns by the logging report, but only on MM241_85 the detected minerals fully match the stated rock type. Sulphides are not detected in either of the samples, but since calcite or dolomite is possibly detected in both samples, they could contain indicator rocks in terms of mineral exploration.

7.6 Clustering of all samples

7.6.1 Cluster 1 (red)

In this cluster the common feature is the dominating presence of quartz. Plagioclase feldspars and micas are present in majority of the samples. Other common minerals include amphiboles and pyroxenes. Epidote, chlorites and sulphides were detected in some of the samples, but the peaks are mostly low compared to the main minerals. According to the logging report, most samples in this cluster contain various schist, gneiss or amphibolite rocks. There are also some samples that are taken from skarn unit, but those samples seem to mainly contain quartz so they might have been taken from quartz veins.

Based on the analysis, about half of these samples contain basic rocks present in the environment that are not very important in terms of ore geology. Cordierite or minerals indicating possible hydrothermal alteration like chlorites and epidote were detected in about ¼ of the samples. Sulphides were detected in about ¼ of the samples. The cluster contains multiple samples which were stated to contain cordierite, but the software did not detect cordierite, making the samples seem barren based on the results. Of all the clusters, this cluster seems to contain the largest number of basic rocks, but sulphides and indicator minerals are present in multiple samples.

7.6.2 Cluster 2 (yellow)

In this cluster the common feature is the presence of cordierite and micas in all samples. Quartz is possibly present in most samples, but the peak is partially shared with other minerals. Anthophyllite, chlorites and sulphides are present in some samples. According to the logging report, all of the samples contain cordierite schist or gneiss, and the minerals detected match the stated rock type very well. These are almost the only samples where cordierite is both clearly detected and stated as a main mineral by the logging report.

Based on the analysis, these samples contain cordierite(-anthophyllite)-rocks that are typical indicator for VMS ore environment. Some of the samples also showed potential presence of sulphides. This cluster is very important in terms of mineral exploration.

7.6.3 Cluster 3 (green)

This cluster contains only two samples that are relatively close to each other and fit into the same logging unit. The rocks are stated as mica schist by the logging report. Both of the samples contain quartz and plagioclase minerals according to the analysis. One sample also contains micas, while the other sample possibly contains chlorite minerals. The cluster seems to contain basic rocks that are not very important in terms of mineral exploration.

7.6.4 Cluster 4 (cyan)

According to the logging report, this cluster contains various schists and possibly some skarn samples. Some of the samples are stated to contain visible sulphides as well. Based on the analysis, these samples contain rocks that are likely from the sulphide mineralizations. The common feature in this cluster is the clear presence of pyrite. Some of the samples contain other sulphides as well. Quartz, amphibole minerals and micas are present in atleast one of the samples, but the sample analyses barely show indications of minerals other than sulphides.

7.6.5 Cluster 5 (blue)

The common feature in this cluster is the presence of plagioclase minerals and amphibole minerals in all of the samples. Cummingtonite is detected in some of the samples. Cummingtonite often occurs in the footwall below VMS orebodies where hydrothermal alteration has removed calcium and increased the magnesium and iron content of the rock (Dreher et al. 2018; Evans & Ghiorso 1995). Quartz is present in most of the samples as well. Micas and chlorites are present in only couple of the samples and there is potential but uncertain signal of cordierite in some of the samples. No sulphides were detected in any of the samples. Based on the analysis, these samples likely contain basic amphibolite rocks present in the environment with not much interest in terms of ore geology. The analysis results and logging report information seem to match each other relatively well.

7.6.6 Cluster 6 (pink)

The common feature in this cluster is the presence of pyroxenes (diopside). 2/3 of the samples also contain plagioclase feldspars. Based on the analysis, all of the samples could potentially contain calcite or dolomite, but it's not certain. The cluster only has 3 samples and the results and stated rock types have some variation, so it is hard to make any certain conclusions from this cluster. Background on all of the samples is atleast somewhat bad and some of the peaks are hard to match to logical minerals, so they could also contain sulphides or have bad measurement quality. Based on the results, the samples in this cluster could be relevant in terms of indicating nearby sulphide mineralizations but would need more detailed analysis.

7.6.7 Cluster 7 (orange)

This cluster only has 2 samples. Both of the samples contain pyrite and are stated to be cordierite schist by the logging report, but they share no other common features. Cordierite was not detected in either of the samples. Both samples are likely from sulphide mineralization.

7.6.8 Cluster 8 (light green)

This cluster only has 2 samples. Both of the samples are stated to contain tremolite skarn by the logging report. Both contain amphiboles and chlorite based on the analysis. Both are stated to contain sulphides, but sulphides were detected only on MM190_235. This cluster is small but based on the results the samples are likely from or near sulphide mineralizations.

7.6.9 Cluster 9 (cyan green)

This cluster only has 2 samples. The only common feature in this sample is the presence of chlorite. In addition to chlorite, MM196_93 contains micas and MM198_4 contains prehnite. Both of the samples have signs of chloritic and hydrothermal alteration, but sulphides were not detected in either of the samples. Cordierite was not detected on MM196_93 although the logging report states it to contain cordierite. This cluster is potentially important in terms of mineral exploration.

7.6.10 Cluster 10 (light blue)

The common feature in this cluster seems to be that all of the samples have atleast somewhat bad background indicating presence of sulphides, or bad measurement. All of the samples also seem to contain chlorite minerals. The rock type stated by the logging report varies. Cordierite was not detected in samples stated to contain cordierite by the logging report, but the sample MM196_51_20 potentially contains cordierite based on the analysis. This cluster contains rocks that are important for mineral exploration. The software not detecting cordierite in most of the samples could make the samples seem somewhat less relevant for indicating ore presence than they actually are based on the logging report.

7.6.11 Cluster 11 (purple)

The common feature in this cluster is the presence of calcite. Dolomite, pyroxenes, amphibole minerals and chlorite minerals are also present in atleast half of the samples. There are potential signals for sulphides in most of the samples, but the signals are not very reliable. The rock types stated by the logging report include limestones, skarn and amphibolite with calcite zones. Based on the stated rock types and the analysis results, this cluster contains calcite rich rocks that are likely at or near skarn and contact metamorphism zone. These rocks are important for mineral exploration, especially as the analysis shows potential presence of sulphide minerals in the samples.

7.6.12 Cluster (deep pink)

This cluster only has 2 samples, but both of them contain sulphides based on the analysis. The backgrounds have low quality in both samples, but especially on 196_100_30 so it was challenging to match other minerals than sulphides to the peak profile. Based on the analysis results this cluster contains samples directly from ore mineralizations. Cordierite was not detected in either of the samples although both should contain cordierite according to the logging report.

7.7 Comparing drill core clustering and sample clustering

Generally, the clustering seems to work similarly with specific drill core sample sets and with all of the samples (AS) in one dendogram. However, in some cases, samples from a single drill core cluster are separated into two or more clusters in the dendogram with all samples. Usually, the samples end up in clusters that are near each other with only relatively small

dissimilarity in the dendogram. Cluster 4 of drill core MM196 seems to be the most divisive drill core cluster as the samples are spread across multiple clusters in the dendogram (AS), even so that the clusters have very high dissimilarity.

Cluster 1 of the dendrogram with all samples contains the same samples as cluster 1 & 2 from drill core MM190. Cluster 1 (AS) also contains all of the samples from cluster 2 of drill core MM198 and cluster 1 of drill core MM241. Cluster 1 (AS) also contains some samples from cluster 4 of drill core MM196. Cluster 2 (AS) contains all of the samples from the cluster 3 of drill core MM190 and the sample MM196_113 from cluster 4 of MM196. Cluster 3 (AS) contains two samples from cluster 4 of drill core MM196. The first 3 clusters (AS) are relatively close to each other in the dendogram in terms of dissimilarity and cluster 1 (AS) and cluster 3 (AS) also have quartz as the dominating mineral. However, the cluster 2 (AS) samples do not contain quartz as clearly and the samples contain cordierite(-anthophyllite) rocks so I would not combine the 3 clusters together.

Cluster 4 (AS) has samples from cluster 3 and 5 of drill core MM196, but not all of the samples from those clusters. Also, the sample MM198_73, that has no drill core cluster, is included. They all contain pyrite based on the pXRD analysis, but not all pyrite containing samples are in this cluster.

Cluster 5 (AS) contains all of the samples from cluster 4 of drill core MM190 and cluster 2 of drill core MM241. It also contains sample MM196_003 from cluster 1 of drill core 196, but the other sample MM196_013 is in cluster 6 (AS) instead. In addition to MM196_013, cluster 6 (AS) contains MM241_45 which has no drill core cluster. It also contains MM198_15 from cluster 1 of drill core MM198, but the other sample MM198_4 is in cluster 9 (AS). Clusters 5 & 6 are relatively close to each other in dissimilarity in the dendogram and well separated from other clusters.

Cluster 10 (AS) only contains samples from cluster 6 of drill core MM196. All other samples are in this cluster except MM196_93, which is in cluster 9 (AS).

Cluster 11 (AS) contains all of the samples from cluster 5 of drill core MM190, and the sample MM198_53 from cluster 4 of drill core MM198.

7.8 Mineral observations

It was possible to make some observations on specific minerals and mineral groups that are important in mineral exploration in this deposit type. These include sulphides, VMS-specific indicator minerals like cordierite and hydrothermal alteration related minerals like chlorites, micas and pyroxenes which can indicate the presence of nearby sulphide mineralizations.

7.8.1 Cordierite observations

Cordierite was detected only on couple samples where cordierite was stated to be present by the logging report. Because cordierite tends to appear as porphyroblastic grains in metamorphic rocks (Schneiderman & Tracy, 1991), it is possible that cordierite is simply not present in the spot the sample has been taken from even if the drill core logging unit contains cordierite. Cordierite also easily alters to pinite, which consists of micas and chlorite minerals (Ogiermann & Kalt, 2000). Majority of the samples that should contain cordierite contain either micas or chlorites or both based on the analysis. Without further analysis it is not possible to make conclusions on whether the cordierite in these samples have fully altered to pinite or if the cordierite is simply absent from the sample, but it is possible that some cordierite has altered to pinite. Cordierite was also detected on some samples on which the presence of cordierite was not mentioned by the logging report.

7.8.2 Pyroxene observations

Some of the samples are classified as diopside amphibolite by the logging report, but pyroxenes were detected only in half of those samples. Pyroxenes are also detected in some samples that are not mentioned to contain pyroxenes by the logging report. Pyroxenes often transform into amphiboles or chlorites during metamorphic alterations. Talc, epidote or micas are also possible alteration results and those have been detected in multiple samples (Plimer, 1993; Patterson et al., 2021). Prehnite is also possibly related to alteration of Ca-rich pyroxenes and is present in some of the samples based on the software analysis (Azer et al., 2018). Based on the results, all of the samples that are classified as diopside amphibolite also contain minerals that could have formed as a result of diopside alteration.

7.8.3 Chlorite, mica and clay observations

Chlorite and mica minerals are present in large numbers of the samples, likely indicating hydrothermal alteration. Chlorite minerals were detected in most of the samples that are stated

to contain chlorites by the logging report. In most cases the software is not able to clearly distinguish chlorites of different compositions from each other.

The software suggests clinochlore, the Mg-rich end member chlorite, in many samples. The concentration of Mg-rich chlorite compared to Fe-chlorite increases near the ore mineralizations and skarn units in this deposit, probably due to Mg-Fe-metasomatism (Siira 2021). According to Siira (2021) the appearance of Mg-chlorite is also connected to the clay mineral montmorillonite. In many of the samples there were strong peaks at the left side of the diffractogram, which typically indicates presence of clay minerals. The software does not find any minerals to those peaks in most cases, so it is not possible to tell which clay minerals are present by using pXRD data only. The Fe-rich end member chamosite was detected only on very few samples. Siira (2021) also observed that chamosite was not detected as often as clinochlore. According to Siira, it is possible that the database used has more examples of clinochlore peak patterns than chamosite, which is why it is able to detect clinochlore more often than chamosite.

7.8.4 Sulphide observations

In most cases if the logging report mentions possible presence of sulphides in the logging unit the sample has been taken from, it was also possible to detect some sulphides. In some cases, the detected sulphide minerals and logged sulphide minerals were not the same. In multiple samples sulphide minerals were detected even though the logging report does not mention sulphides. The logging report notes are very relatively vague, so it is challenging to make any reliable conclusions on how well the logging observations and pXRD analysis results match each other.

In multiple sulphide-bearing samples the background is very high, messy or spiky, making it challenging to detect minerals reliably. The background does not have low quality in every sample with sulphides detected, however. It has been noticed in previous studies (Siira, 2021; Sarala & Koskinen 2018) that sulphides tend to elevate the background, especially galena. This happens likely because of fluorescence caused by Cu anode in samples with Fe-containing sulphides, but the elevated backgrounds also happen with the Co anode used in this study.

Rocks where sulphides were detected are mostly stated to contain skarns, limestone, cordierite schist or other schists by the logging report. Some sulphide bearing samples contain quartz

feldspar schist and only few contain amphibolites. Sulphides themselves seem to not be a major factor in formation of the clusters in most cases. However, since the sulphides seem to be present mainly in the samples with specific rocks and minerals, the clustering of the samples somewhat follows the presence of sulphides.

7.9 Usability of pXRD and clustering methods in mineral exploration

Portable XRD's ability to detect various minerals, possible causes of errors and sample procedures have been explained in more details by Siira (2021). Also, Sarala & Koskinen (2018) have done detailed research on pXRD's ability to detect specific minerals and comparison between pXRD and laboratory XRD. They used XPowder software instead of DIFRRAC.EVA which was used in this study.

pXRD analysis seems to be capable of detecting both sulphide minerals and various ore indicating hydrothermal alteration and metamorphic alteration related mineral groups. The reliability and accuracy of the analysis is very sensitive to measurement quality. Also, sulphides and any possible other causes often make the background higher or spiky, making it challenging to reliably detect minerals present in the sample. Low quality samples or measurements with high or spiky background easily cause errors as the software might suggest minerals that are not actually present. Samples with low quality background should be measured again with longer measurement time to see if that results in better quality measurement. Based on the couple samples measured twice in this study, re-measuring samples might make the results better, but not certainly. In some cases, it is not possible to detect minerals that should be present according to the logging report. The database used in the software can also strongly affect the results.

The results suggest that the clustering method is able to separate barren samples of basic rocks from samples that contain sulphides or VMS indicator minerals like cordierite, anthophyllite or hydrothermal and chloritic alteration minerals (Taylor et al. 1995). Clustering works relatively well on drill core specific smaller clusters, but there are some clusters where samples do not fully match each other. In the cluster 1 (AS), almost half of the samples could be classified as barren in terms of mineral exploration. Cluster 3 (AS) only contain basic barren rocks based on the analysis. Cluster 5 (AS) contains basic rocks mostly without anything important in terms of mineral exploration. Other AS clusters seem to contain samples that either contain sulphides or indicator minerals. Being able to spend less time on large number of samples could potentially decrease the workload of the research project.

Since the samples in this study are taken from a VMS deposit of highly altered, metamorphosed and deformed rocks, a very large portion of the samples contain atleast some alteration minerals that are typical indicator minerals. It could be useful to test the clustering method with a sample set that has been taken from another deposit type where the mineralization and alteration zones have more defined borders to see how well the clustering is able to separate ore indicating samples from barren samples.

As mentioned in the chapter 3.4, the alterations near VMS deposit tend to be zoned so that the promixal zone is characterized by higher concentrations of Fe-chlorite, quartz and possibly talc. The chlorite becomes more Mg-rich, and sericite (phengite) becomes more abundant further away from the core (Galley et al. 2007). This seems to conflict with Siira's (2021) observations of Mg-rich chlorite becoming more abundant near the ore minerals in this deposit. Since the software is usually not able to distinguish chlorites of different composition from each other, it is not reliably possible to make interpretations on the effectiveness of clustering to detect different alteration zones on chlorite alone. Other methods like imaging spectroscopy can be used together with pXRD to identify the specific compositions of solid solution minerals like chlorite to get better information on the alteration zones (Siira 2021). Although the software can distinguish biotite and phlogopite from muscovite and phengite, there doesn't seem to be much of any specific correlations in the clustering results. In most cases, micas and chlorites are not minerals that are the main factor in how the clusters form. Quartz on the other hand is more or less present in almost all of the samples that the lack of presence is more noticeable. Talc is detected only in very few samples. Since the samples are from a VMS deposit that has gone through deformation after the formation, the alteration zones might not be as clearly defined as in non-deformed VMS deposits.

Portable XRD, however, is very dependant on the quality and amount of the samples included and requires atleast well-made logging reports to compare the analysis results with. Good logging reports are required, for example to solve the problem of pXRD not detecting cordierite or other minerals that do not appear evenly in the rock. Since the samples have been taken from a certain spot within the logging unit which can be tens of meters long in some cases, it is very likely that some minerals mentioned in the logging report are simply not present in the exact spot the sample has been taken from. Same applies to any possible veins present in the sample. The software inability to detect cordierite in samples where it should be present is the single largest problem based on the results in terms of mineral exploration usefulness, but it doesn't seem to affect the clustering itself much. Vague and low detail

logging report in this study made it significantly more challenging to be certain of some results given by the pXRD analysis. Another question is whether then minerals that can work as indicator minerals have formed during the ore forming process, or if they were already present in the rock or have formed afterwards. Simply detecting relatively common mineral like chlorites in the sample does not automatically mean that the sample is located near sulphide mineralization. Therefore, it is important to know the geological history of the study area to be able to reliably analyze the clustering results.

The results also show that if the number of samples is relatively small, the clustering method is unable to group some samples into clusters and they remain alone. Usually, these samples seem to have bad background, or they contain sulphides or other uncommon minerals or mineral combinations that are not present in most samples. The clustering method seems to be somewhat able to separate barren basic rocks from ore indicating rocks even with just 10-15 samples, but the resulting smaller clusters do not provide much information themselves usually. Having atleast 20-25 samples makes the clustering results more useful. The 10 meters sample interval in this study is the bare minimum to get enough informative results, especially on deformed deposit type like in this study where changes in the rock type can be quick in small distances. Smaller interval would increase the amount of information, but also increase the time required to make and analyze the samples. Samples should also be taken from any interesting parts of the drill core based on the logging of the core in addition to having samples from certain intervals.

Previous studies on the usability of pXRD clustering method on mineral exploration are limited, but some research has already been done by Makvandi et al. (2023) for example. Their study included 24 samples from epithermal and telescoped porphyry-epithermal deposits from Greece. The measurements took 7 minutes and the as a result, the samples were clustered into 5 clusters and 5 samples ended up without clusters. They found that the clustering method was a cost- and time-efficient method for sample selection for further, more detailed studies. Their observations match the observations made in this study.

Based on this study, the most effective way to analyze pXRD results is to first make clustering of the samples and then do detailed mineralogical sample specific analyses based on the resulted clusters. The clustering method does not rely on a database so only the samples are needed to make it. The clustering tool automatically gives a suggested cutline for the clusters, but in this study, it was found that usually it should be lowered a bit to get better

clusters. After the suitable clusters have been made, it is easy to make sample specific mineralogical analyses from each cluster. Often it is possible to just visually check the diffractograms in the cluster to see that they are likely to contain similar mineralogical compositions.

8 Conclusions

In this study the pXRD mineral analysis and clustering methods were tested with data from Metsämonttu VMS deposit to see if they could have potential for mineral exploration usage. The pXRD mineral analysis was proven to be able to detect sulphide minerals and alteration minerals related to ore mineralization. The clustering method was proven to be partially capable of separating ore mineralization related samples from samples containing basic barren rocks in this deposit type. The clustering of the samples also makes it easier to do sample specific mineralogical analyses for large number of similar samples as the samples in one cluster often have almost identical diffractograms, making it possible to determine majority of the mineral compositions visually.

The reliability and accuracy of pXRD mineral analysis results are limited, however. While it can indeed detect sulphide minerals and hydrothermal alteration and metamorphism related minerals, the results are very sensitive to measurement quality and possible effects affecting the background of the diffractograms. The method can be used to detect the presence of certain mineral groups but most of the time it is unable to distinguish which minerals from the group are actually present. Therefore, it is possible to detect if minerals related to VMS alteration zones are present, but it is challenging to determine which alteration zone the sample is from with only pXRD data. Other analysis methods like geochemical analysis would have to be done to get detailed information of specific mineral compositions.

The clustering method was found to be relatively easy and quick way to separate most of the ore mineralization-related and indicator minerals bearing samples from barren basic rock samples. However, the clustering did not work well on giving information on distal or proximal alteration zones, atleast not from a highly deformed deposit like this. Also, the usefulness and reliability of the clustering method decrease with smaller number of samples. It was found that clustering samples from a singular drill core with just around 10 samples does not give as much useful information as having 20+ samples in the clustering data set.

Further investigation could be done by comparing pXRD mineralogical analysis and clustering results with geochemical or other more detailed data from the samples to see how well the results correlate. Portable XRD and clustering method could also be researched using samples from other ore deposit types to see if the method is able to separate barren rocks from ore indicating rocks in other deposit types as well. It would be useful to test if the clustering

method is able to separate distal and proximal alteration samples from each other in deposits where the alteration zones are more distinct. Also, more research should be done on the cause of the higher background on some sulphide bearing samples and why does the background get bad only in some cases and not in every sulphide bearing sample. Some research could be done on potential differences between different XRD analysis softwares like DIFFRAC.EVA and XPowder, and different databases to see how much the software and available database affect the results.

Acknowledgements

I would like to thank my supervisor professor Esa Heilimo from the University of Turku for all your professional and academic advice and for finding this subject. I would also like to thank my second supervisor, researcher Irmeli Huovinen from the Geological Survey of Finland (GTK) for all of your academic, technical and practical advice for this study.

References

Azer, M. K., Gahlan, H. A., Asimow, P. D. & Alfaifi, H. J. (2018). Prehnite as an indicator mineral in the Wadi Nasb uralitized gabbro, South Sinai, Egypt. *Journal of Asian Earth Sciences* 160: 107–117.

Barr, G., Dong, W. & Gilmore, C. J. (2004). High-throughput powder diffraction. II. Applications of clustering methods and multivariate data analysis. *Journal of Applied Crystallography* 37: 2, 243–252.

Beeson, R. (1988). Identification of cordierite-anthophyllite rock types associated with sulphide deposits of copper, lead and zinc. Transactions of the Institution of Mining and Metallurgy, Section B. *Applied Earth Science* 97: 108–115.

Bogdanova, S., Gorbatschev, R., Skridlaite, G., Soesoo, A., Taran, L. & Kurlovich, D. (2015). Trans-Baltic Palaeoproterozoic correlations towards the reconstruction of supercontinent Columbia/Nuna. *Precambrian Research* 259: 5–33.

Booysen, R., Gloaguen, R., Lorenz, S., Zimmermann, R. & Nex, P. A. M. (2021). Geological Remote Sensing. *In*: Alderton, D. & Elias, S. A. (eds). *Encyclopaedia of Geology*, 2nd ed, 301–314. Elsevier.

Burkett, D. (2018). Portable X-ray diffraction for unconventional and conventional petroleum exploration. *ASEG Extended Abstracts* 2018: 1, 1–4.

Cervantes, G. A. (2016). *Technical Fundamentals of Radiology and CT*. IOP Publishing, Bristol. 321 pp.

Bruker AXS GmbH. (2014). *DIFFRAC.SUITE: DIFFRAC.EVA Cluster analysis user manual*. Bruker AXS GmbH, Karlsruhe. 113 pp.

COM. (2023). Regulation of the european parliament and of the council establishing a framework for ensuring a secure and sustainable supply of critical raw materials and amending Regulations (EU) 168/2013, (EU) 2018/858, 2018/1724 and (EU) 2019/1020. COM/2023/160 final.

Dreher, A. M, Tavares, F. & Oliveira, J. K. (2018). Wall rocks and hydrothermal alteration associated with the Pojuca and Furnas deposits, Carajás province. *Anais do 49º Congresso Brasileiro de Geologia*: 724.

Eilu, P., Ahtola, T., Äikäs, O., Halkoaho, T., Heikura, P., Hulkki, H., Iljina, M., Juopperi, H., Karinen, T., Kärkkäinen, N., Konnunaho, J., Kontinen, A., Kontoniemi, O., Korkiakoski, E., Korsakova, M., Kuivasaari, T., Kyläkoski, M., Makkonen, H., Niiranen, T., Nikander, J., Nykänen, V., Perdahl, J.-A., Pohjolainen, E., Räsänen, J., Sorjonen-Ward, P., Tiainen, M., Tontti, M., Torppa, A. & Västi, K. (2012). Metallogenic areas in Finland. *Geological Survey of Finland Special Paper* 53: 207–342.

Ermrich, M. & Opper, D. (2011). *X-Ray powder diffraction: XRD for the analyst: Getting acquintanced with the principles*. PANalytical GmbH, Kassel. 94 pp.

Etter, M & Dinnebier, R. E. (2014). A Century of Powder Diffraction: a Brief History. *Zeitschrift für anorganische und allgemeine Chemie* 640: 15, 3015–3028.

Evans, B. W. & Ghiorso, M. S. (1995). Thermodynanics and petrology of cummingtonite. *American Mineralogist* 80: 7-8, 649–663.

Franklin, J. M., Gibson, H. L., Jonasson, I. R. & Galley, A. G. (2005). Volcanogenic Massive Sulfide Deposits. *Economic Geology 100th Anniversary Volume*: 523–560.

Galley, A. G., Hannington, M. D. & Jonasson, I. R. (2007). Volcanogenic massive sulphide deposits. *In*: Goodfellow, W. D. (eds). Mineral deposits of Canada—A synthesis of major deposit-types, district

metallogeny, the evolution of geological provinces, and exploration methods. *Special Publication* 5: 141–161. Geological Association of Canada, Mineral Deposits Division.

Groves, D. I., Goldfarb, R. J., Gebre-Mariam, H., Hagemann, S. G. & Robert, F. (1998). Orogenic gold deposits: A proposed classification in the context of their crustal distribution and relationship to other gold deposit types. *Ore Geology Reviews* 13: 1–5, 7–27.

Haapala, I., Rämö, O. T. & Frindt, S. (2005). Comparison of Proterozoic and Phanerozoic rift-related basaltic-granitic magmatism. *Lithos* 80: 1–4, 1–32.

Hamilton, W. B. (1995). Subduction systems and magmatism. *In*: Smellie, J.L. (eds). Volcanism associated with extension at consuming plate margins. *Special Publications* 81: 3–31. Geological Society of London.

Hannington, M. D., Galley, A. G., Herzig, P. M. & Petersen, S. (1998). Comparison of the TAG mound and stockwork complex with Cyprus-type massive sulfide deposits. *In*: Herzig, P.M., Humphris, S.E., Miller, D.J., & Zierenberg, R.A. (eds.). *Proceedings of the Ocean Drilling Program: Scientific Results* 158: 389–415.

Hokka, J., Leväniemi, H. & Leskelä, T. (2024). Hydrothermal alteration and geochemical proximity indicators to ore at the Metsämonttu Zn–Pb–Cu–Au–Ag deposit, Uusimaa belt, southern Finland. *Journal of Geochemical Exploration* 262: 107491.

Koskinen, H. (2018). Kannettavan XRD-analysaattorin soveltuvuus kriittisten mineraalien tunnistamiseen kentällä. Unpublished M.Sc. Thesis. University of Oulu. 77 pp.

Kähkönen, Y. (2005). Svecofennian supracrustal rocks. *In*: Lehtinen, M., Nurmi, P. A. & Rämö, O. T. (eds). *Precambrian geology of Finland - Key to the evolution of the Fennoscandian shield*, 343–406. Elsevier, Amsterdam.

Lahtinen, R., Korja, A. & Nironen, M. (2005). Paleoproterozoic tectonic evolution. *In*: Lehtinen, M., Nurmi, P. A. & Rämö, O. T. (eds). *Precambrian Geology of Finland - Key to the Evolution of the Fennoscandian Shield*, 481–532. Elsevier, Amsterdam.

Latvalahti, U. (1979). Cu-Zn-Pb ores in the Aijala-Orijarvi area, southwest Finland. *Economic Geology* 74: 5, 1035–1059.

Lavina, B., Dera, P. & Down, R. T. (2014). Modern X-ray diffraction methods in mineralogy and geosciences. *Reviews in Mineralogy & Geochemistry* 78: 1, 1–31.

Leväniemi, H., Hokka, J., Hulkki, H., Huovinen, I., Karjalainen, J., Kaunismäki, J., Kuikka, J., Sandström, J., Stenberg, R. & Vuohelainen, J. (2020). Tiedonkeruukäytännöt Aijala-Metsämonttu projektin kairasydänmittauksissa 2019–2020. *Työraportti*: 39. Geological Survey of Finland

Leväniemi, H & Hokka, J. (2021). Petrophysical target characterization with lithogeochemical clustering: The Metsämonttu Zn–Pb–Cu deposit, southern Finland. *Near Surface Geophysics* 20: 6, 637–660.

Lydon, J. W. (1984). Ore deposit models – 8. Volcanogenic Massive Sulphide Deposits Part I: A Descriptive Model. *Geoscience Canada* 11: 4, 195–202.

Makvandi, S., Cauzid, J., Tarantola, A., Melfos, V. & Voudouris, P. (2023). XRD clustering and quantitative analysis as a fingerprinting technique to study ore deposits. *17th SGA Biennial Meeting Proceedings* 3: 280–283.

Mineral deposits and exploration. (2026). Geological Survey of Finland. Page visited: 15.6.2026. <*https://gtkdata.gtk.fi/mdae/index.html*>

Mutanen, T. & Huhma, H. (2003). The 3.5 Ga Siurua trondhjemite gneiss in the Archaean Pudasjärvi Granulite Belt, northern Finland. *Bulletin of the Geological Society of Finland* 75: 1–2, 51–68.

Nironen, M. (2017). Bedrock of Finland at the scale 1:1 000 000: Major stratigraphic units, metamorphism and tectonic evolution. *Geological Survey of Finland Special Paper* 60: 41–76.

Ogiermann, J. & Kalt, A. (2000). Chemical characterization of cordierite breakdown products in gneisses and migmatites of the Schwarzwald and the Bayerische Wald. *Journal of Conference Abstracts* 5: 2, 752.

Ohmoto, H. (1995). Formation of volcanogenic massive sulfide deposits: The Kuroko perspective. *Ore Geology Reviews* 10: 3–4, 135–177.

Patterson, S. N., Lynn, K. J., Prigent, C. & Warren, J. M. (2021). High temperature hydrothermal alteration and amphibole formation in Gakkel Ridge abyssal peridotites. *Lithos* 392–393: 106107.

Plimer, I. R. (1993). Epidote and ore deposits. *Abhandlungen der Geologischen Bundesanstalt in Wien* 49: 27–32.

Puustinen, K. (2003). Suomen kaivosteollisuus ja mineraalisten raaka-aineiden tuotanto vuosina 1530–2001, historiallinen katsaus erityisesti tuotantolukujen valossa. *Arkistoraportti M*: 10.1/2003/3. Geological Survey of Finland.

Robb, L. (2005). *Introduction to ore-forming processes*. Blackwell Publishing, Malden. 373 pp.

Sarala, P. & Koskinen, H. (2018). Application of the portable X-Ray Diffraction (pXRD) analyser in surficial geological exploration. *Geologi* 70: 3, 58–68.

Sarala, P., Taivalkoski, A., Huovinen, I., Kalliosalo, H., Karinen, J., Koskinen, H., Lehtonen, M., Lukkari, S., Strand, K., Toppila, R., Joutsenvaara, J. & Valkama, J. (2019). Indikaattorimineraalien automatisoitu tunnistaminen kriittisten mineraalien etsinnässä - Indika: Loppuraportti. *Työraportti*: 47. Geological Survey of Finland.

Sarrazin, P. C., Blake, D. F., Feldman, S., Chipera, S. J., Vaniman, D. & Bish, D. L. (2005). Field deployment of a portable XRD/XRF instrument on Mars analog terrain. *Advances in X-ray Analysis* 48: 194–203.

Schneiderman, J. S. & Tracy, R. J. (1991). Petrology of orthoamphibole-cordierite gneisses from the Orijärvi area, southwest Finland. *American Mineralogist* 76: 5-6, 942–955.

Siira, S. (2021). Hydrothermal alteration of medium-grade metamorphic rocks of Metsämonttu VMS deposit, southern Finland: A comparative portable XRD and near-infrared spectroscopy analysis. M.Sc. Thesis. Maantieteen ja geologian laitos, Turun Yliopisto. 116 pp.

Taylor, C. D., Zierenberg, R. A., Goldfarb, R. J., Kilburn, J. E., Seal, R. R., II, & Kleinkopf, M.D. (1995). Volcanic-associated massive sulfide deposits. *In*: du Bray, E.A. (eds). Preliminary compilation of descriptive geoenvironmental mineral deposit models, 137–144. *Open-File Report* 95-831. U.S. Geological Survey.

Väisänen, M. & Mänttäri, I. (2002). 1.90–1.88 Ga arc and back-arc basin in the Orijärvi area, SW Finland. *Bulletin of the Geological Society of Finland* 74: 1–2, 185–214.

Warma, A. (1975). Outokumpu Oy:n Aijalan ja Metsämontun kaivosten vaiheita. *Vuoriteollisuus* 33: 2, 94–98.

Ziegler, P. L. (1992). Plate tectonics, plate moving mechanisms and rifting. *Tectonophysics* 215: 1–2, 9–34.

Appendices

Appendix 1. Picture of the sample MM196_133 drill core

One of the cordierite schist samples where cordierite was not detected.

Appendix 2. Picture of the sample MM190_195 drill core

One of the cordierite samples where cordierite was detected.

Appendix 3. Picture of the sample MM190_225 drill core

One of the samples where sulphide minerals were detected but not mentioned in the logging report.

Appendix 4. Picture of the sample MM196_51_20 drill core

An example of skarn rock sample.

Appendix 5. Picture of the sample MM196_73 drill core

One of the sericite schist / quartzite samples.

Appendix 6. Picture of the sample MM196_100_30 drill core

One of the samples where sulphide minerals were both detected by the analysis and noted in the logging report.

Appendix 7. Picture of the sample MM198_14 drill core

One of the diopside amphibolite samples.

Appendix 8. Picture of the sample MM198_34 drill core

Appendix 9. Picture of the sample MM198_43 drill core

Appendix 10. Picture of the sample MM198_73 drill core

One of the quartz feldspar samples.

Appendix 11. Picture of the sample MM198_103 drill core

A sample which has been logged as cordierite schist / gneiss, but quartz is dominating on the diffractogram.

Appendix 12. K-feldspars

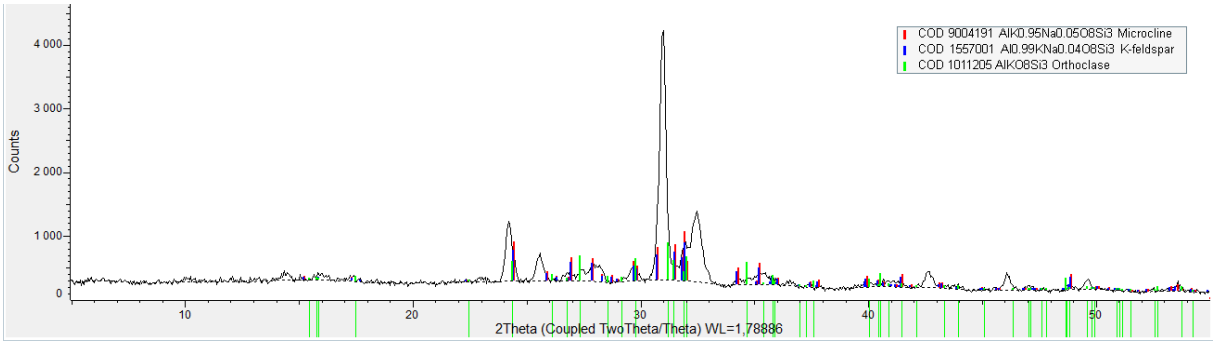

The sample MM241_25 diffractogram with various suggested K-feldspars selected.

Appendix 13. Plagioclase feldspars

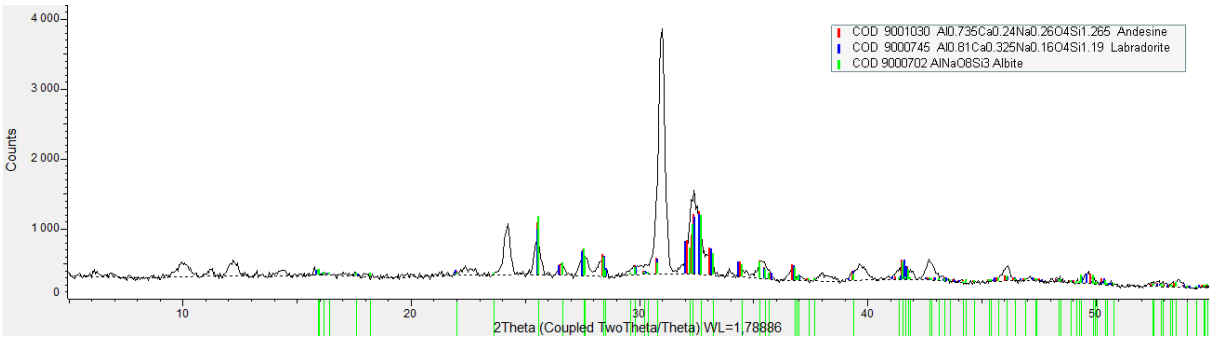

The sample MM190_15 diffractogram with various suggested plagioclase feldspars selected.

Appendix 14. Biotite and phlogopite

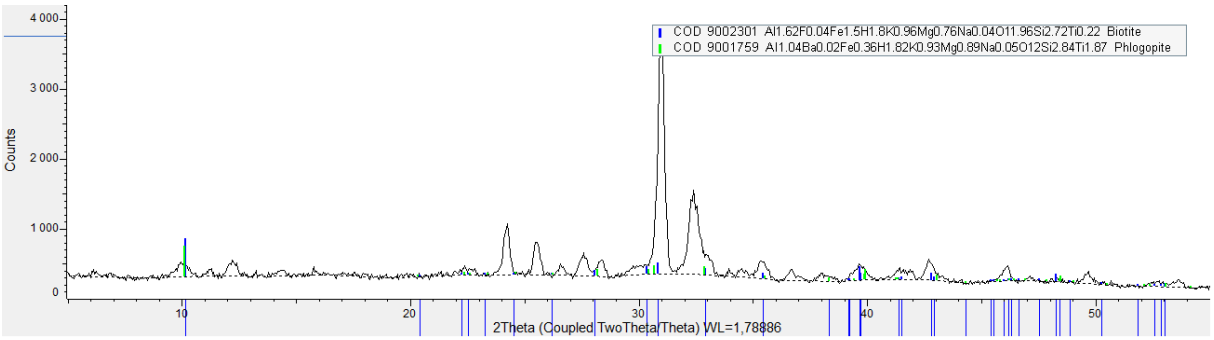

The sample MM190_15 diffractogram with biotite and phlogopite selected.

Appendix 15. Amphibole minerals

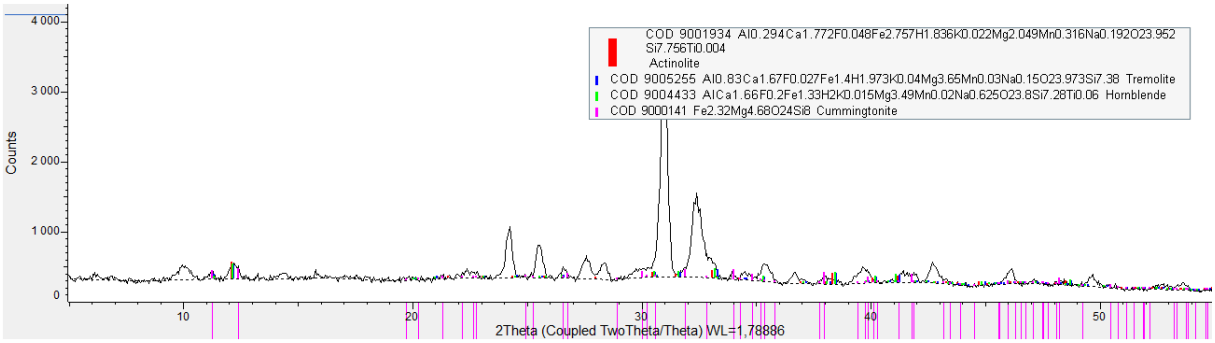

The sample MM190_15 diffractogram with various suggested amphibole minerals selected.

Appendix 16. Chlorite minerals

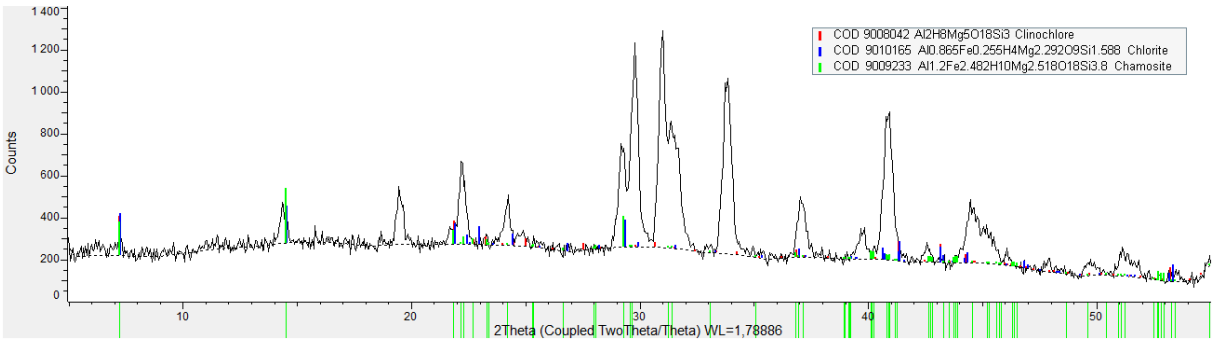

The sample MM190_135 diffractogram with various suggested chlorite minerals selected.

Appendix 17. Pyroxene minerals

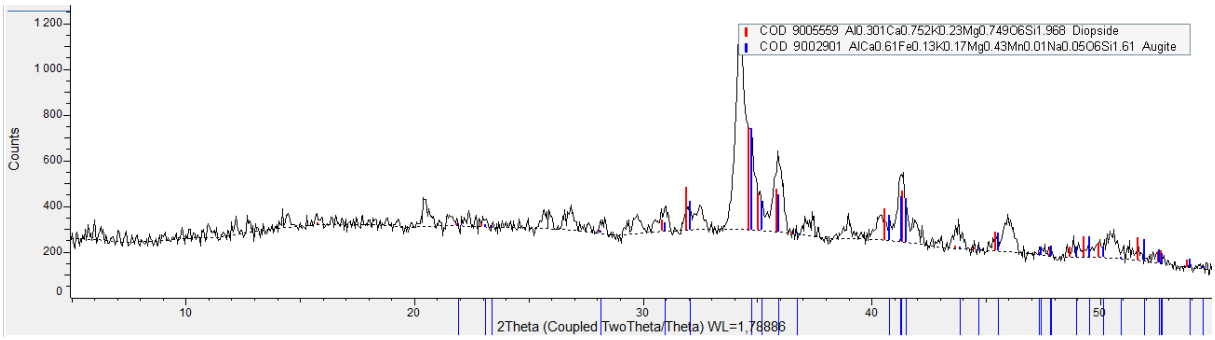

The sample MM190_85 diffractogram with suggested pyroxene minerals selected.